The Joining Development, Metallurgical Study and Characterisation Approach of Brazed Joints Between Tungsten and Fusion Related Materials for Divertor Applications

PhD Thesis

Yuxuan Zhang

Department of Mechanical and Aerospace Engineering

University of Strathclyde, Glasgow

May, 2021

Declaration of authenticity and author's rights

'This thesis is the result of the author's original research. It has been composed by the author and has not been previously submitted for examination which has led to the award of a degree. '

'The copyright of this thesis belongs to the author under the terms of the United Kingdom Copyright Acts as qualified by University of Strathclyde Regulation 3.50. Due acknowledgement must always be made of the use of any material contained in, or derived from, this thesis.'

Signed:

Date:

Abstract

The design of brazed joints between tungsten to other fusion related materials is a significant challenge in developing fusion reactors, largely due to the dissimilar physical metallurgy of the materials to be joined. Under extreme thermal loading and plasma irradiation conditions, selecting suitable materials is very restricted and poses a significant challenge to the design. The candidate brazing filler materials for fusion related materials are often unconventional and lack material data and design experience. The work presented in this thesis focuses on the design and fabrication of dissimilar brazed joints between tungsten and fusion relevant materials with novel gold-based fillers. Vacuum furnace brazed joints of tungsten-tungsten, tungsten-Eurofer 97, tungsten - copper and tungsten-SS316L are successfully joined with a novel gold-based Au80Cu19Fe filler. Metallurgical and interfacial studies have been carried out for each brazed joint to understand their microstructural properties, and nanoindentation testing was performed at the joints to generate mechanical properties of the brazed layers. Optimised brazing procedures for vacuum furnace brazing and induction brazing were developed to limit the defects within the brazed layers with an equivalent Au80Cu20 filler. The brazing developments showed that the gold-based fillers could be used to fabricate qualified brazed joint between tungsten and the dissimilar materials considered. The brazing process design has been used for the proof-of-concept study of divertor mock-up fabrications, and the findings have contributed to the limited test data on fusion relevant materials. Finally, due to the substantial procurement costs of the gold-based filler material and the inability to generate macro scale properties from the braze layer, the use of conventional Cu60Zn40 fillers allowed a casting and brazing process methodology to be developed to correlate the in situ mechanical properties within the brazed layer to the properties generated by macro-level mechanical testing. The findings showed that this methodology could be used for predicting the mechanical properties of the brazed layer by the cast and heat-treated macro-level filler metal specimens, which are applicable to brazed joints in a range of applications.

Acknowledgements

Table of Contents

List of Figures

List of Tables

List of Symbols

T_{braze}	brazing temperature
T_{lq}	liquidus temperature
γ_{SL}	surface tension between solid and liquid
γ_{SV}	surface tension between solid and vapour
γ_{LV}	surface tension between liquid and vapour
Θ	contact angle of the liquid droplet on the solid surface
e_o	gap clearance
P_c	capillary pressure
P_{ext}	external pressure
$\varnothing$	diameter
σ_0	yield strength
σ_{UTS}	ultimate tensile strength
τ_{max}	maximum shear stress
τ_0	shear yield strength
τ_{USS}	ultimate shear strength

Abbreviations

HHF	High Heat Flux
UTS	Ultimate Tensile Strength
OFHC	Oxygen-Free High Thermal Conductivity
JET	Joint European Torus
ITER	International Thermonuclear Experimental Reactor
DEMO	Demonstration Power Plant
PFC	Plasma-Facing Components
CFC	Carbon Fibre Composite
DBTT	Ductile Brittle Transition Temperature
HIP	Hot Isotactic Pressed
dpa	displacements per atom
RAFM	Reduced Activation Ferritic-Martensitic
ODS	Oxide Dispersion Strengthened
HEMJ	Helium-cooled Modular Divertor with Jet Cooling
HEMS	Helium-cooled Modular Divertor with Integrated Slot Array
fcc	face-centred cubic
CTE	Coefficient of Thermal Expansion
FEA	Finite Element Analysis
XRD	X-ray Diffraction
SEM	Scanning Electron Microscope
EDS	Energy Dispersive X-ray Spectroscopy
IIT	Instrumented Indentation Testing
CSM	Continuous Stiffness Measurement
LSC	Local Stress Concentrations
DSC	Differential Scanning Calorimetry
NDT	Non-destructive testing
SAM	Scanning Acoustical Microscope

1 An overview of joining technologies and selection of material in thermonuclear fusion reactors

1.1 Introduction

Nuclear fusion energy, released from the joining of light nuclei of hydrogen into the heavier nuclei of helium, is the most promising carbon-free energy source of the future [1]. The temperatures required for fusion reaction are hundreds of millions of degrees Centigrade and no currently available material can be used as a container. Hence, magnetic fields have been used as the primary force to contain reacting fusion fuel [1]. To capture the energy from fusion, the hydrogen isotopes are heated to high enough temperatures (approx. 150,000,000°C) until they are ionized and become plasma. The most promising device to confine the plasma is the tokamak, which serves to control and contain the plasma within a torus-shaped chamber by the aforementioned magnetic fields. This ring-shaped fusion system was developed by scientists in the U.S.S.R around 1960, and it was called Tokamak, an acronym in Russian for toroid-chamber-magnet-coil [2].

A number of Tokamaks have been built at research facilities around the world. The Joint European Torus (JET) at the Culham Centre for Fusion Energy at Abingdon, UK, currently houses the largest tokamak. JET achieved a breakthrough in late 1997 in fusion energy release by ultimately generating 21 MJ of fusion energy, a peak power of 16 MW, and a ratio of fusion power to input power of 0.65 [2]. The International Thermonuclear Experimental Reactor (ITER) was proposed in 1985, and the construction of facilities was started in 2007. As JET's successor, ITER is a large-scale scientific experiment reactor, shown in Figure 1-1, which aims to deliver ten times the power it consumes, from 50 MW of input power to produce 500MW of fusion power [3]. The Demonstration Power Plant, DEMO for short, is a proposed fusion power plant that follows ITER. It is intended to be comparable in output to current fission power plants, producing net electricity and being able to breed tritium to self-sufficiency generate fuel [2], [4].

In tokamak reactors, directly plasma-facing components (PFC), i.e. divertor and blanket, shown in Figure 1 and Figure 2, are the most critical and technologically challenging due to direct exposure to the high heat flux (HHF) and fast neutrons from the plasma and have very demanding design requirements [5].
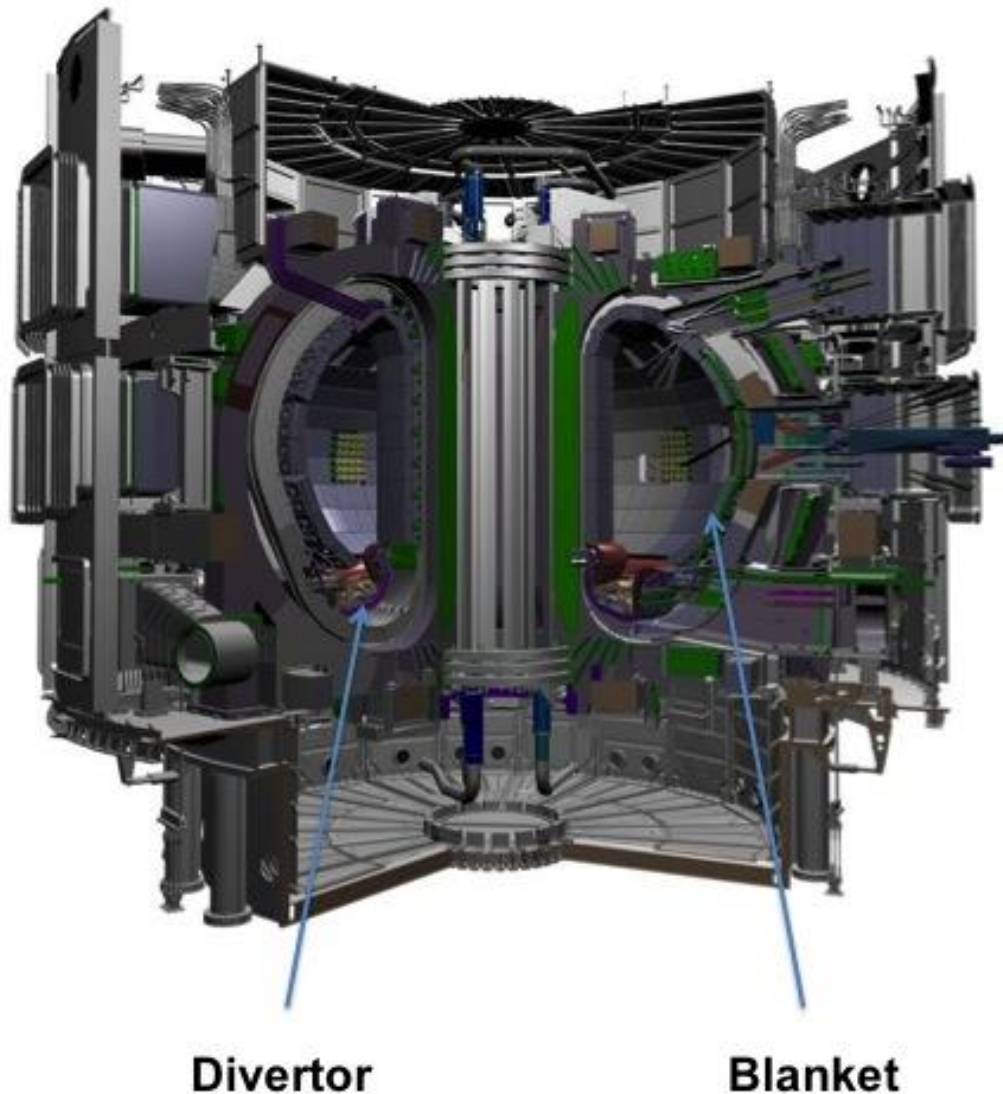
Figure 1- 1: Cross-section view of ITER tokamak [3]

The divertor labelled 2 in Figure 1-2, located at the bottom of the plasma chamber, is one of the critical components in the tokamak reactor and has the function of exhausting extract heat, helium ash and impurities from the plasma. The divertor is

the highest thermally loaded components, it serves as a shield for the magnetic coils behind it, and it is designed to remove nearly 15% of the fusion thermal power and to withstand a high surface heat flux of up to 20 MW/m^2 in addition to 3000°C surface temperature [3], [4], [6], [7]. To achieve continuous operation, the hydrogen isotopes, helium (exhausted from nuclear fusion) and particles from PFC have to be cleaned from the plasma. Tokamak uses the magnetic fields lines, labelled 3 in Figure 1-2, to redirect these unwanted ions from burning plasma to the divertor. The ions recombine to neutral atoms during or briefly before the impact on the divertor and then will be removed from by vacuum pumps [7]. Therefore, the plasma-facing divertor parts also have to withstand the sputtering erosion caused by energetic ions and neutral atoms from the plasma [8]. Helium produced in neutron-irradiated materials causes swelling, which can accelerate surface erosion and induce additional stresses leading to a reduced component lifetime [8].
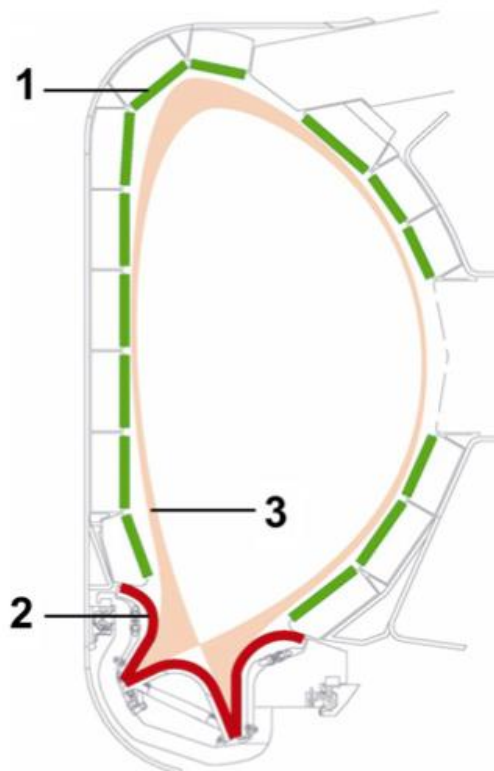
Figure 1- 2: The illustration shows the cross-section of the torus of a tokamak. (1) The blanket first wall (2) the divertor (3) The magnetic field lines which direct exhaust particles to the divertor [7]

Tungsten is one of the primary candidate materials for use in nuclear fusion plasma armour applications because it possesses a high melting point, high thermal conductivity, high ultimate tensile (UTS), yield and shear strength [7], [9]. In the developing fusion reactors, the design of joints between tungsten and other fusion related materials is a significant challenge as a result of the dissimilar physical metallurgy of the materials to be joined [10].

This thesis focuses on the design and fabrication of dissimilar brazed joints between tungsten and fusion relevant materials such as reduced activation ferric-martensitic (RAFM) steel EUROFER 97, oxygen-free high thermal conductivity (OFHC) Cu and SS316L in which gold-based brazing foils Au80Cu19Fe1 and Au80Cu20, in wt.% were used as the brazing materials.

Firstly, this work develops the initial vacuum furnace brazing procedures with the Au80Cu19Fe1 filler for dissimilar joining of tungsten to other fusion compliant materials to create successfully brazed joints for characterisation. Metallurgical and mechanical studies are performed with the specimens to advance the understanding of the interfacial regions of these dissimilar brazed joints. Based on these investigations, an optimised vacuum furnace brazing procedure and an induction furnace brazing procedure are then developed to create sound quality dissimilar brazed joints with the Au80Cu20 filler. The work then investigates a method of correlating the mechanical properties measured by micro/nanoindentation within the real brazed joints and the mechanical properties of the casting brazing filler metal specimens generated by standard tensile testing. Due to the high cost of gold-based filler and the large amount required for development, this investigation also employed the use of conventional Cu60Zn40 brazing filler.

The current study forms part of a series of separate works between the University of Strathclyde and Culham Centre for Fusion Energy for proof-of-concept study of small scale divertor mock-up fabrications. In this regard, several parallel studies broadly focused on fatigue testing of dissimilar brazed joints and the analysis of residual

stresses within dissimilar brazed joints [11], [12] although, these parallel studies are not reported herein.

1.2   Thesis layout

The thesis is structured to present the experimental work that created brazed joints for candidate divertor designs and investigations to understand the interfacial properties of the brazed layers. In this chapter, the material selections strategies relating to the designs of divertors for nuclear fusion reactors are discussed in detail. The selection of brazing filler material for fusion applications and the challenges of fabricating brazed joints between tungsten and dissimilar materials are reviewed and discussed. A literature review of the background information on brazing is reported to build the fundamental knowledge to help design the brazing procedures. As both metallurgical and mechanical properties of these brazed joints are used for experimental input to the numerical studies in the research collaborations, a literature review of the failure assessment methods of brazed joints is also included.

Chapter 2 discusses the design of vacuum furnace brazing processes to fabricate specimens to be used for the metallurgical characterisation and the techniques used for qualifying and investigating the brazed joints. Considering the diversity of material combinations, experimental setups and analysis methods that were studied, Chapter 2 is restricted to the experimental methods that are referred to throughout. The experimental and characterisation processes specifically used are reported as they appear in each chapter.

Chapter 3 presents the first stage experimental investigation of four different butt-type brazed joints for divertor applications created with novel gold-based filler. For each material combination, microstructural examinations were performed, and in-situ mechanical properties were determined to assess the quality of brazed joints and interfacial metallurgical properties to validate the feasibility of using gold-based filler in concept divertor designs.

Based on the results from Chapter 3, Chapter 4 reports on an optimised furnace brazing procedure with gold-based filler to limit the defects in brazed joints and

fabricate qualified specimens that could be used for fatigue testing development within the research group. An induction to the brazing process for fabricating well-aligned brazed specimens was developed and explained in Chapter 4.

Chapter 5 presents a design methodology using the copper-based filler for validating the in situ mechanical properties, measured by nanoindentation, in the brazed layer with mechanical properties generated by standard mechanical testing from specimens manufactured from as-cast filler metal. This investigation was to build up more faith for the designers to use the data measured directly at brazed layers. As this approach was a theoretical development for assessing generic dissimilar brazed joints, a more cost-effective binary CuZn alloy was used as the filler metal. Finally, Chapter 6 summarises the key findings in this thesis and future research opportunities lead by this thesis.

1.3   A review of material selection in divertor applications

The current example of an actual divertor is the ITER divertor which is a water-cooled type using tungsten (W), carbon fibre composite (CFC) and beryllium (Be) as the reference plasma-facing material [13]. W has been used for the divertor baffle area and CFC for the strike point region locating at the lower part of the divertor vertical target [14]. W and CFC are joined onto the water-cooled heat sink components made from precipitation hardened copper chrome zirconium alloy, CuCrZr [13]. Since the divertor baffle area has a high concentration of neutral particles, W has been selected as the armour material due to it having a low erosion rate [13]. Standard powder metallurgical sintered W grade (99.94% W) is the present reference material in ITER. The design of using small tiles of W minimised the effect of radiation-induced embrittlement due to the shift of the ductile to brittle transition temperature (DBTT) of W [15]. Cast W armour tiles with a Cu interlayer are brazed or hot isotactic pressed (HIP) onto CuCrZr heat sink components [6]. A reference design of the ITER W divertor mock-up is shown in Figure 1-3 [14].
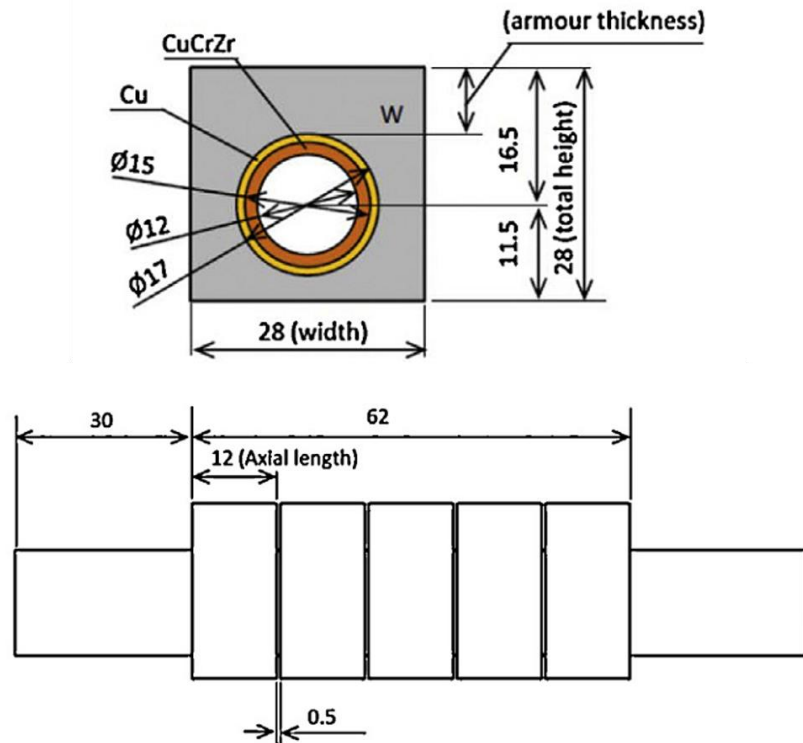
Figure 1- 3: A reference design of small-scale ITER divertor mock-up [14]

CFC is selected due to the absence of melting during plasma disruptions [13], [15]. Pure Cu is cast onto laser-textured CFC armour tiles with a Ti coating that aids wetting. The pure copper is then joined to the CuCrZr heat sink by means of brazing, HIP or electron beam (EB) welding [6], [16].

The divertor used for DEMO (beyond ITER) operates under more extreme working conditions due to higher neutron loads (ITER: 0.37-0.47 MW/m^2, DEMO 1.8-2.4 MW/m^2) [17]. W and W alloys have been considered as the primary candidate materials for the DEMO divertor due to the high temperature strength, good thermal conductivity and low sputter rates [7], [18], [19]. W and W alloys are designed to be used for two different applications, plasma-facing armour components and structural components. W is suitable for the armour material due to the highest melting point of all metals and high temperature strength. However, the use of W as a structural material has to limit the operating temperature window at the lower end by the DBTT and on the upper end by the recrystallisation temperature or the loss of creep

strength. The inherent brittleness of W is also a disadvantage for structural materials [17]. However, the design of the DEMO divertor has not been selected formally, and the operation requirements are not yet available [10] and future design of these critical components are subject to change, so material selections vary with the divertor design concepts based on different coolants. The current divertor concepts under development can be distinguished between water-cooled, gas-cooled or liquid metal types. For the near-term DEMO, the ITER generic type low-temperature (100-200 °C coolant) water-cooled divertor concept and high-temperature (more than 600 °C coolant) helium-cooled divertor concept are the reference choices [9].

A conceptual design of a water-cooled divertor monoblock is shown in Figure 1-4 [20]. Pressurised water with swirls flows through the pipes joined with the plasma-facing material to remove the heat. The pressurised part of an ITER divertor is made of a CuCrZr pipe, and this setup can remove $20MW/m^2$ [16]. Under the more extreme DEMO operation conditions, CuCrZr pipes have to be replaced after neutral irradiation damage of about 10 displacements per atom (dpa), which leads to a shortened lifetime for the water-cooled divertors. Reduced activation ferritic-martensitic (RAFM) steel, typically Eurofer steel 97 or oxide dispersion strengthened (ODS) Eurofer, is the preferable material for DEMO divertors due to the higher durability and the excellent swelling behaviour under neutron irradiation [4], [21]. The impact properties of Eurofer steel are strongly degraded after a 70 dpa neutron irradiation at 300 °C, but after 3 hours post irradiation heat treatment at 550 °C with helium, these properties will be recovered [17]. Along with Eurofer, which is specially designed for DEMO, austenitic steel, such as SS316L is another option for DEMO [4], [17]. Although the austenitic steel (SS316L) has a shorter service life, it is has been extensively used in fission reactor technology and has been well used in the nuclear industry [22]. SS316L was selected as the primary structural material for ITER [23] and also a candidate to be used in the vacuum vessel, divertor and blanket designs [4], [15], [24].

However, the use of RAFM steel reduces heat removal capability because steel has a lower thermal conductivity compared with Cu and Cu alloys. Steel pipe can only remove 10 MW/m^2 heat instead of 20MW/m^2 that can be removed by CuCrZr pipework [17]. Therefore, as a consequence of their excellent thermal conductivity and heat removal capacity, Cu and Cu alloys are still considered as the preferred candidate heatsink materials in the future improved water-cooled divertor design [17].
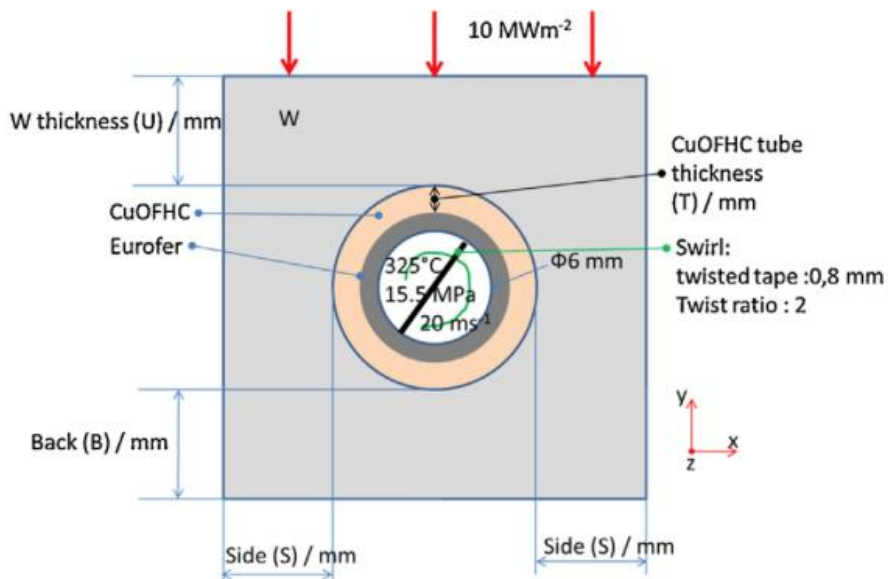
Figure 1- 4: A conceptual design of DEMO water-cooled divertor monoblock [20]

For DEMO He-cooled divertor concepts, the design requirement is to remove a high heat load of at least 10 MW/m^2. Helium-cooled modular divertor with jet cooling (HEMJ) is the reference design along with Helium-cooled modular divertor with integrated slot array (HEMS) as a backup design. Figure 1-5 shows the cooling finger designs for HEMJ and HEMS. Both designs use W tiles, about 5 mm thick, as the thermal shield and sacrificial layer. The tiles are brazed to thimbles made of tungsten alloy such as W-1% La$_2$O$_3$ (WL10) and form a cooling finger unit. The cooling finger unit is then brazed or mechanically locked to the supporting structure that is made of ODS steel, e.g. ODS Eurofer [25]. The DEMO HEMJ divertor will consist of 200,000-500,000 cooling finger units. In order to achieve high thermal energy conversion

efficiency and heat removal capacity, the fingers are cooled with helium jet impingement at 10 MPa and the inlet/outlet temperature is 600/700°C, as shown in Figure 1-5. However, helium jet impingement can achieve a heat transfer coefficient of av. 34kW/m^{2}K, which is three times smaller than the coefficient of the water-cooling concept [26].
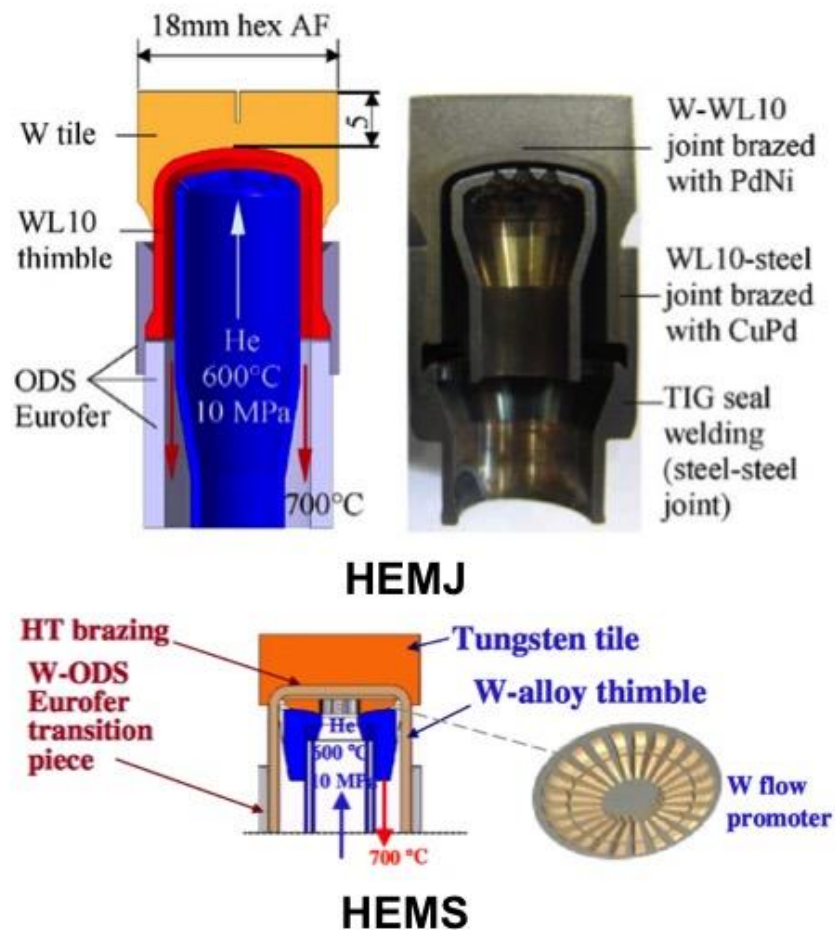
Figure 1- 5: DEMO reference concept: He-cooled modular divertor with multiple jet cooling (HEMJ) cooling finger and backup concept: He-cooled modular divertor with integrated slot array (HEMS) cooling finger [25], [27]

The material selection for DEMO divertors is still under assessment and varies with divertor concepts. At the current stage, some candidate materials for DEMO have been proposed and discussed in the nuclear fusion research communities. These materials are list below.

- Plasma facing armour materials:

Pure W and W alloys

- Structural materials:

Pure W and W alloys

RAFM steels like Eurofer 97 and ODS Eurofer

Austenitic stainless steel like 316LN IG, a reduced activation type developed for ITER

Oxygen free high conductivity (OFHC) copper and copper alloys

As all the design concepts of DEMO divertors require a large number of physical joints between these materials, it is evident that the success of future reactors is dependent on the fabrications of reliable dissimilar material joints between these specialized materials. Hence, this research focused on the study of the joints between some of the materials under consideration for DEMO, namely, pure W, Eurofer 97, AISI SS316L and OFHC Cu.

1.4 Brazing dissimilar nuclear fusion materials

The methods for joining solid materials can be classified as mechanical fastening, adhesive bonding, brazing/soldering, fusion welding and solid state joining. As described in section 1.3, for both ITER and DEMO divertors, there are still so many uncertainties for the design and material selection. In all the proposed plans, fabricating reliable joints between the candidate materials has brought up significant challenges that have to be conquered because the development of DEMO relies on the success of developing joining techniques. Joining W divertor components to other structural materials is critical, and high temperature brazing has been chosen as one of the suitable joining technologies [17], [27]. From the joining point of view, one of the main issues of manufacturing high heat-flux components is the large thermal expansion mismatch between the armour, heat sink and structural components. In this section, brazing and other joining suitable technologies are assessed based on the requirements for DEMO divertors.

1.4.1 Advantages of brazing towards DEMO divertor applications

Brazing is a process for joining two or more parent materials with a filler material by heating them to the brazing temperature T_{braze}, which is the liquidus temperature T_{lq} of the filler material and below the solidus of the base materials [28]. Brazing can use various heat sources such as the furnace, torch, induction, chemical reaction and infrared and can be performed in different environments – air, inert gases and vacuum [28], [29]. When the parts are heated to brazing temperature, the filler metal melts and spreads over the surfaces of the parent materials by capillary action. Then the filler metal solidifies and creates a metallurgical bond between the parent materials. Brazing uses metallic filler materials with T_{lq} above 450 °C, while soldering uses filler materials with T_{lq} not exceeding 450 °C [28], [29]. Furthermore, brazing can also be performed at temperatures approaching the semi-solid temperature range of filler materials which is lower than T_{lq} [30]. Semi-solid brazing has been developed to reduce T_{braze} to limit the reaction between parent materials and filler metal [31].

At present, the DEMO divertor designs are still conceptual, and many uncertainties are standing in the way, including the joining method. As described in section 1.3, most of the joints between DEMO divertor components are dissimilar joints, and some of them are between metallic and non-metallic materials. Some of the candidate materials used in DEMO divertor are extraordinary or of specialised design, like W, W alloys, ODS metals and RAFM steels. Both water-cooled and He-cooled DEMO divertors require reliable joints between W to WL10, Cu, RAFM steel or austenitic steel, and the joints between W and other materials are primarily considered in this study.

Welding techniques, including electron beam (EB) welding, tungsten inert gas (TIG) welding and laser welding, are conventionally used to join structural materials like austenitic steels and also have the potential to join RAFM steels. Yapp et al. [32] reported that the solidification structure of tungsten resulting from melting has very low ductility and may crack during cooling due to the residual stresses. Therefore,

welding is not suitable for joining many DEMO candidate materials due to the melting of the parent materials.

For joining the W block to the CuCrZr pipe and the W block to the W/Cu laminate pipe in both water-cooled and helium-cooled divertor concepts, direct bonding processes such as diffusion bonding produced by HIP or Hot Radial Pressing (HRP) along with brazing can be used and may achieve good joining quality [33].

For joining the W block to RAMF or austenitic steel pipe, the diffusion bonding process is not recommended because W and Fe can form intermetallic compounds such as Fe_7W_6, FeW, Fe_2W, which has to be avoided under any circumstances in the transition area between W and steel. Therefore, brazing is preferred for this joining task [17].

Due to the fact that the parent materials do not melt or plastically deform during brazing processes, brazing has many distinct advantages compared with other welding processes [34]. Thus, brazing is a popular joining process in the fusion research community. Some of the benefits of brazing are very attractive for divertor applications:

- Ability to join dissimilar metals
- Ability to join non-metals to metals
- Ability to join cast materials to wrought metals
- Ability to preserve special metallurgical characteristics of metals
- Ability to preserve protective metal coating or cladding
- Capability for precision production tolerance
- Joint temperature capability approaching that of base metal

1.4.2 Selection of brazing filler for divertor components

The selection of brazing filler materials has not currently been agreed for fusion applications, and this remains a significant challenge in the fusion research

community [17]. However, the ASME III NB-4512 code states the requirements for the brazing filler material and fluxes in nuclear components as follows:

(a) The filler material used in brazing shall be a nonferrous metal or alloy with a solidus temperature above 425°C and at least 260°C above the highest temperature of the joint in service.

(b) The filler material shall melt and flow freely by capillary action within the desired temperature range and in conjunction with a suitable flux or controlled atmosphere. The filler material shall wet and adhere to the surfaces to be joined.

(c) Fluxes that are fluid and chemically active at the brazing temperature shall be used, when necessary, to prevent oxidation of the filler metal and the surfaces from being joined and to promote free-flowing of the filler material.

Another brazing material selection criterion is defined by the brazing temperature window. For joints between W and its alloy, the working temperature of the brazing filler has to comply with the temperature window of divertor components. The liquidus temperature should be higher than the divertor operating temperature, which is 100-200°C for water-cooled type and 600°C for He-cooled type, and lower than the recrystallisation temperature of W, about 1400°C [9]. For joints between W and EUROFER steel, the brazing temperature should be higher than the operating temperature of 600°C and lower than the grain growth temperature of steel, which is 1100°C. Figure 1-6, reproduced from [29], shows the principal brazing metal families and their melting ranges. Considering the brazing temperature requirements stated above, the most suitable metal families can be summarised, as shown in Table 1-1.
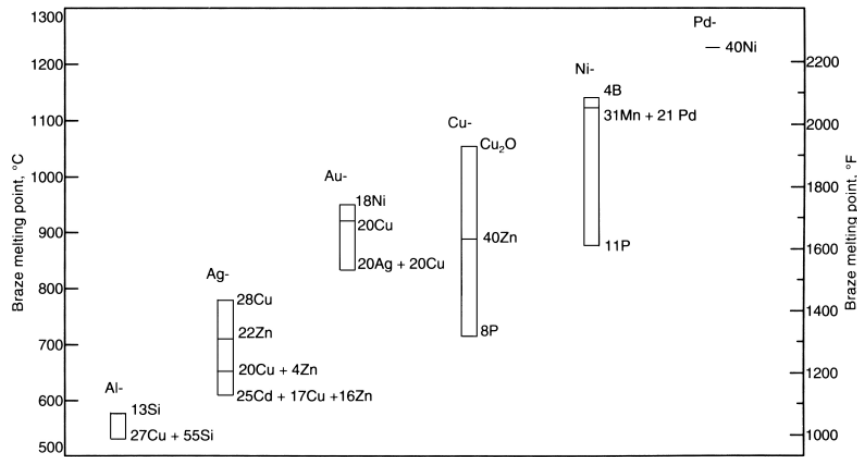
Figure 1- 6: Principal brazing alloy families and melting ranges [29]

Table 1- 1: Suitable metal families for divertor applications

W-W joint

Application	Temperature window	Suitable metal families
Water cooled	460°C <T_{braze}<1400°C	Ag, Au, Cu, Ni, Pd
He-cooled	860°C <T_{braze}<1400°C	Au, Cu, Ni, Pd

W-Steel joint

Application	Temperature window	Suitable metal families
He-cooled	860°C <T_{braze}<1100°C	Au, Cu, Ni

Joining of tungsten to tungsten and tungsten to steel by brazing has been achieved in divertor concepts, and a number of fillers have been reported in the literature with Pd, Ni, Ti and Cu based alloys. In previous studies [18], [27], Pd60Ni40 (liquidus temperature T_{lq} = 1238 °C) was used for brazing W-WL10 and Pd18Cu82 (T_{lq} = 1100 °C) was used for WL10-steel using the vacuum furnace brazing method. In both cases, successful brazed joints were achieved. However, in the W-WL10 joint with PdNi filler, significant diffusion of tungsten was observed in the brazed layer. In work from Rieth et al. [19], pure titanium, TiFe and TiCrFe were used for creating brazed joints of W-W in a vacuum furnace, and the best joints were obtained with Ti-86Fe and Ti-46Fe fillers. Various defects were detected in these joints: pores, dissolution of W in the

filler, partial dissolution of the W grain boundaries and formation of brittle intermetallic compounds.

Kalin et al. [35] used a nickel-based filler STEMET ®1309 (Ni_{bal}-15Cr-4Mo-4Fe-(0.5-1.0)V-7.5Si-1.5B) to join martensitic steel EP-450 to two grades of tungsten. Both joints were brazed with 0.5mm Fe50Ni50 spacers to reduce residual stresses. Kalin et al. [36] later tested a Ti-based filler (Ti_{bal}-22.5Cr-7.5V-3Be) and a Fe based filler (Fe_{bal}-18Ta-8Ge-2Si-2Pd-3.5B) to braze monocrystalline tungsten to polycrystalline tungsten. Norajitra et al. [37] used a Co-based filler on the HEMJ design for Eurofer sleeve to WL10 thimble joint. For brazing the WL10 thimble to pure tungsten tile, Ni-based STEMET®1311 and 66CuNi44 were used. Norajitra et al. [27] later changed to use Pd60Ni40 to improve the quality of W-WL10 joints, and the braze filler for WL10—Eurofer joint was Cu82Pd12 filler. Munez et al. [38] used Ni55Ti45 alloy filler wire for joining W–Ti–Y2O3 alloy and EUROFER steel by means of laser brazing, and it was found that NiTi filler showed low brazeability. Cracks caused by residual stresses initiated from the brazed layer and extended to the parent materials. Energy dispersive X-ray spectroscopy (EDS) analysis showed that elements of tungsten alloy and NiTi filler diffused into each other after brazing. Furthermore, Ehrlich [22] detected nickel alloys with significant embrittlement effects after neutron loading testing (c. 150 dpa) and indicted a reduction of performance.

Prado et al. [39] used Cu80Ti20 as the brazing filler material for the W-Eurofer97 joint and found the presence of an intermetallic Cu_3Ti transition phase between tungsten and brazed layer. Prado et al. [40] then performed shear testing to these joints in which all observed fractures propagated through the W-braze interface. It was reported that the combined effects of the intermetallic compound and the accumulation of residual stresses caused by the mismatch in the coefficient of thermal expansion (CTE) explained the fracture mechanism [39]. Bachurina et al. [41] used copper-based STEMET ®1203 (Cu50Ti50) brazing alloys in rapid quenching ribbon form for joining tungsten to RAFM steel RUSFER EK-181 and intermediate

phases $TiCu$ and Ti_2Cu, and TiC was formed both as individual crystals and as continuous layers on the steel side.

Although alloying between brazing filler and the parent material can improve the wettability, Reiser et al. [17] noted that the brazed joint of W to dissimilar materials is a critical area when exposed to cyclic thermal load and reported that brittle intermetallic compounds should be avoided under all circumstances and W solid solution should be avoided if possible.

Another important consideration in filler metal selection is that of irradiation behaviour. Figure 1-7, reproduced from [42], shows the Clearance Indices of the following brazing base metal elements: Ni, Au, Ag, Pd, Cu and Ti. The Clearance Index of a material determines if the material can be disposed of without special precautions according to IAEA guidelines. Activation calculations were performed using the three neutron spectra for the European power plant conceptual study (PPCS), the spectrum calculated for the JET experimental device and the International fusion materials irradiation facility (IFMIF) high flux region. In each graph, the solid dark blue curve represents the data produced from irradiation of the element with the first wall spectra. The dash-dotted blue curve and the dotted red curve represent results for the blanket and shield spectra, respectively. The purple dash-dot curve represents the results for IFMIF irradiation. The solid green curve represents the results of calculations, with the spectrum representing the average flux over the vacuum vessel wall on the inboard side of JET. Each graph is a log-log plot of the activation property as a function of decay time following irradiation. The decay time ranges from 10^{-6} to 10^6 years. A brown line indicating a Clearance Index of 1 is provided on the graphs. If the Clearance Index is less than 1, then the material can be disposed of as if it were non-radioactive [43]. Figure 1-7 shows that after 100 years, Au and Ti are the least active, Cu and Pd are in the middle, while Ni and Ag are the most active.
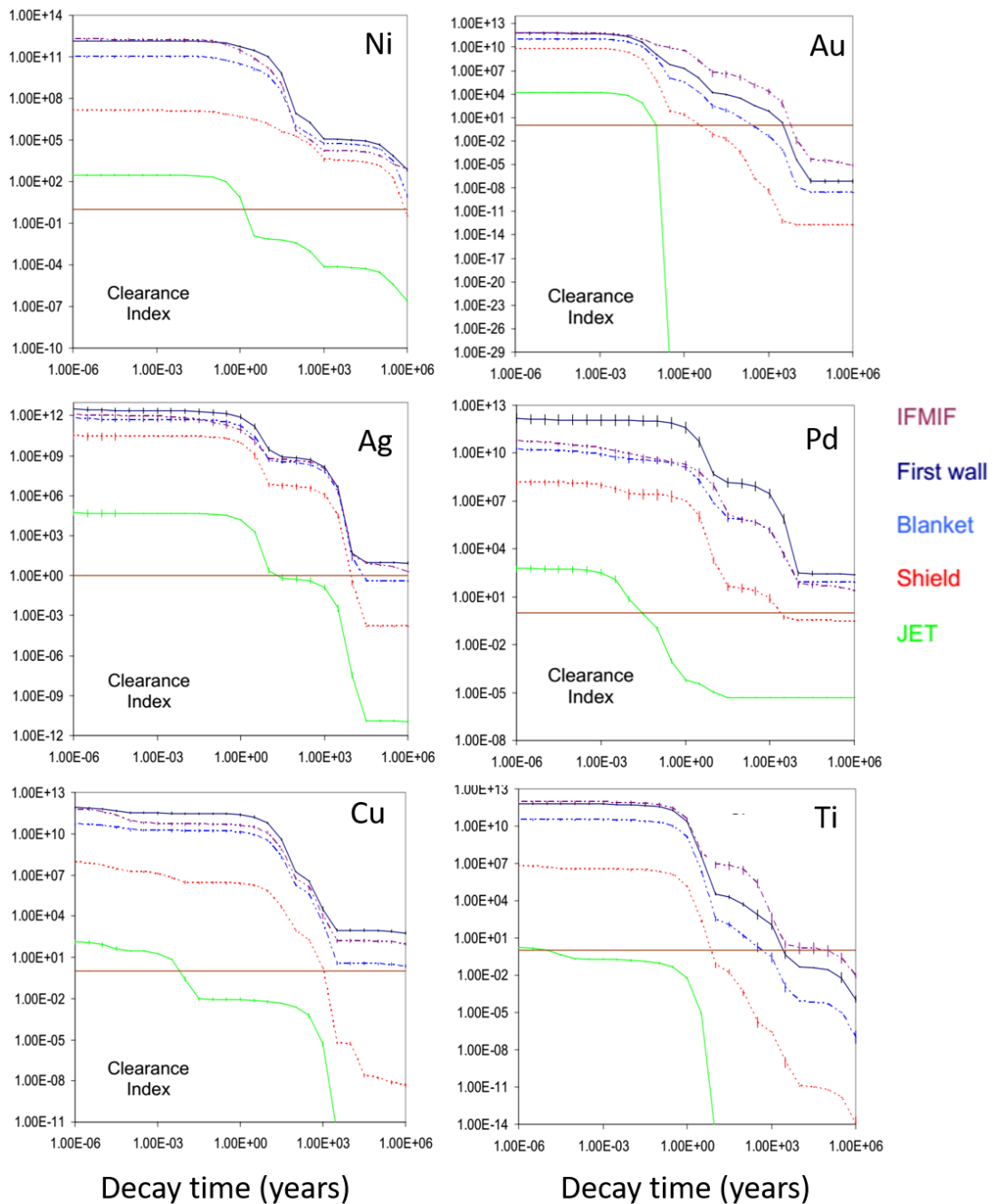
Figure 1- 7: Activation graphs for base metal of typical braze fillers, reproduced from [42]

After the review of previous works, to the best of the author's knowledge, there is no industrially or commercially developed filler fulfilling all the crucial requirements of divertor design. Current approaches of experimental validations have no choice but to use available filler metals that have sound brazeability without considering the irradiating behaviours. As researchers have believed that the first priority is to create

sound and reliable brazed joints with these candidate materials so that components can be tested experimentally and numerical design works can be validated. The results obtained by approaches ignoring the irradiating behaviours of the filler metal are inaccurate and are likely to lead to a serious failure. However, there are no better approaches at the current stage of research. At the time of this work, no mention of joining tungsten and steel using gold-based filler could be found in the literature. Considering the promising irradiation characteristics of gold, this thesis focuses on an approach based on generating knowledge of using two commercial-quality gold-based alloys, Orobraze 910 (Au80Cu19Fe1) and Orobraze 890 (Au80Cu20) (in weight %) as new filler selections for brazing W and other divertor candidate materials.

Figure 1-8 shows a modified phase diagram of the Au–Cu system [44]. In this case, for Au80Cu20 and Au80Cu19Fe1, solidification started from a disordered face-centred cubic (fcc) structure (Au, Cu). This structure transferred into a long period ordered structure AuCu II. AuCu II then transferred to a face-centred tetragonal structure AuCu I, which is stable at low temperatures [45], [46]. Gold-based alloys are recognised as providing good wettability on tungsten, good resistance to oxidation and corrosion at high temperatures, and can create ductile joints without excessive inter-alloying/erosion of the parent metals [47]. The Au80Cu20 and Au80Cu19Fe1 fillers used in this work are equivalent alloys. The small quantity of iron added to the Au80Cu19Fe1 is to retard the ordering transformation, which takes place in the Au80Cu20, and accompanied by volume changes that cause difficulties in the fabrication of this material and may affect the properties of joints it produces.
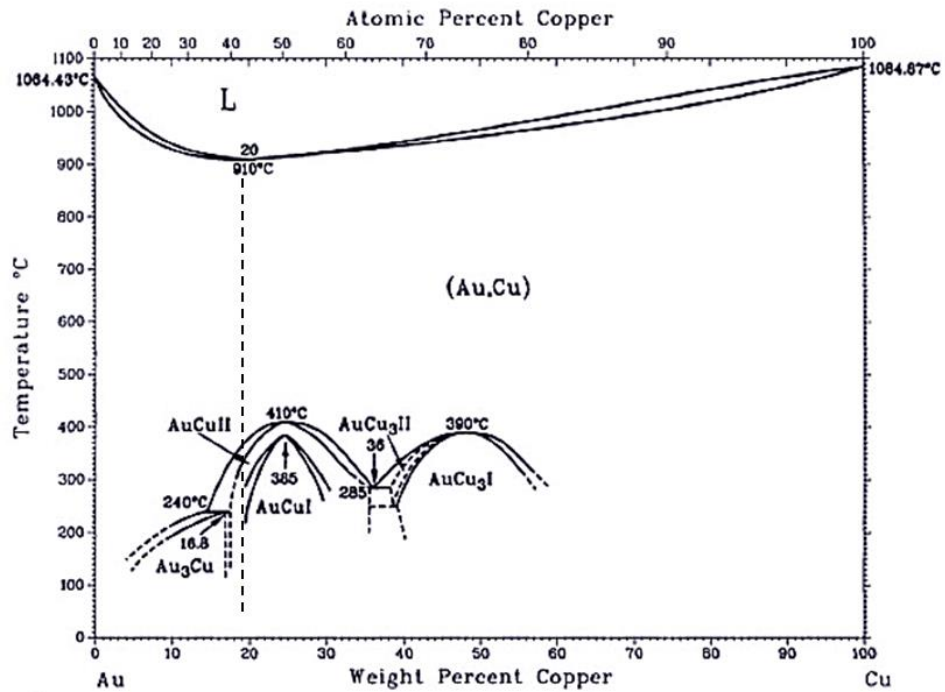
Figure 1- 8: Au-Cu phase diagram, modified from [44]

1.5 Background of brazing and failure assessment of brazed joints

Brazed joints are mostly used for constructing structural components and tend to be used at temperatures usually below half the melting temperatures. The principal failure modes of brazed joints tend to be fatigue, stress overload, and corrosion [29]. Brazed joints subject to mechanical stress will often result in brittle failure. However, as introduced in section 1.3, in DEMO divertor applications, brazing is under development for connecting structural parts and also performing as the sealant of cooling components. The brazed joints in divertor components should be functional with sound lifetime and operating temperature range in severe working environments whilst maintaining structural integrity under both mechanical/thermal and irradiation loadings.

Mechanical testing of brazed dissimilar joints is challenging the knowledge of engineering designers. The brazed joints are heterogeneous and composed of parent materials with very thin brazed layers between them. The final formation of a brazed

layer is very sensitive to the brazing design and production processes. The brazed layer can have complex microstructures with diffusion regions at the interfaces between both parent materials. Its geometry can introduce localised stress concentrations and even stress singularities. There are many challenges existing in assessing the failure of brazed joints due to the lack of knowledge. The presence of residual stresses is one of the most critical problems in manufacturing and the failure of dissimilar joints. This section reviews the key parameters of brazing and the knowledge relating to design the brazing process for dissimilar brazed joints.

1.5.1 The aspects of brazing

The wetting in brazing

Wetting and capillary action are the two key parameters for creating brazed joints. Wetting is the ability that the molten filler metal can adhere to a solid surface and make a strong bond with the solid. The classical model of wetting is defined by the behaviour of a liquid droplet drop on a flat solid surface. The liquid drop will spread over a solid surface under the effects of three surface tensions forces are in balance, as shown in Figure 1-6. The sessile drop technique is widely used for testing wetting as the experiment procedures are well developed and easy to perform. After cooling, the sessile drop specimen can be easily used for characterising braze/solid reactivity by microscopy.
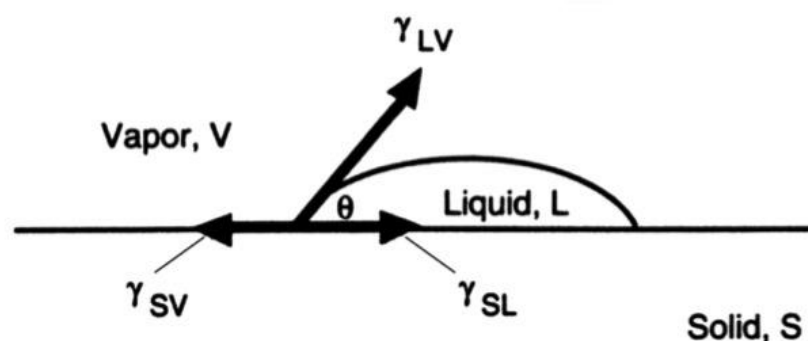
Figure 1- 9: Classical model of contact angle [29]

21

The wetting equation, Equation 1-1, is derived according to the balance of forces. In this equation, γ_{SL} is surface tension between solid and liquid, γ_{SV} is surface tension between solid and vapour, γ_{LV} is surface tension between liquid and vapour, and Θ is the contact angle of the liquid droplet on the solid surface.

$$\gamma_{SL} = \gamma_{SV} - \gamma_{LV} \cos \theta$$

Equation 1- 1

As shown in Figure 1-6, the contact angle $\theta < 90°$ represents the condition $\gamma_{SV} > \gamma_{SL}$, and the imbalance between surface tensions provides the driving force for spreading liquid over the solid surface. Thus, the contact angle θ is the measurement of wetting, as shown in Figure 1-7: a liquid droplet will wet and spread on the substrate if $\theta < 90°$ and the area this droplet can spread increases if θ decreases; if $90° < \theta < 180°$, some wetting can occur but the liquid droplet will not spread on the substrate surface; if $\theta > 180°$, de-wetting occurs and the liquid will keep the droplet form on the substrate surface.
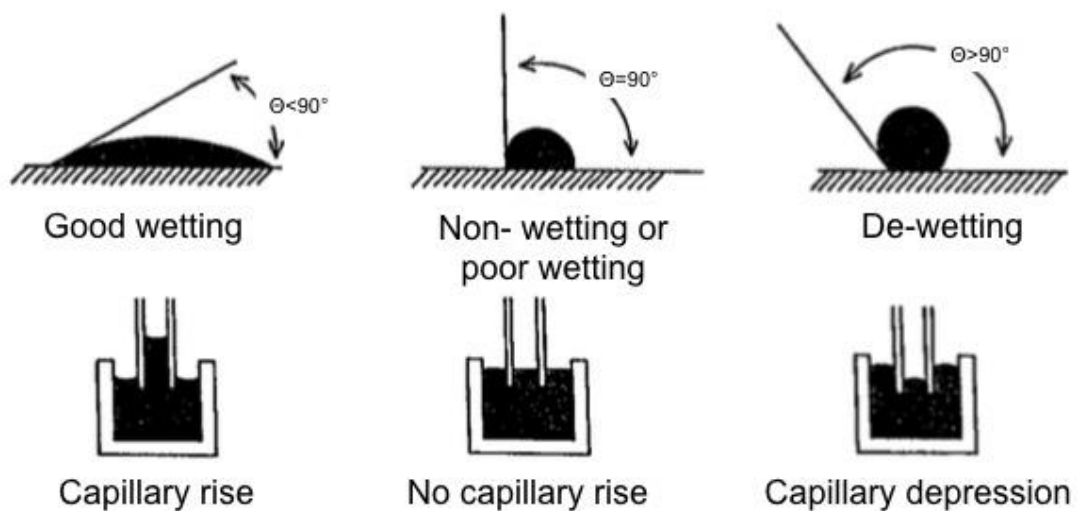
Figure 1- 10: Schematic shows relations between wetting, contact angle and capillary actions, modified from [28]

It has to be emphasised that there are major differences between sessile drop experiments and brazing tests. In brazing, size effects can be observed because brazing involves particularly low values of braze volume per unit area of the

solid/braze interface. However, size effects cannot be observed in sessile drop experiments. When two dissimilar materials are brazed, the information obtained from two individual wetting experiments is not sufficient [48]. Furthermore, in some circumstances of brazing, even liquid metals can wet well on the solid substrates. The wetting under real brazing conditions can be led to non-wetting contact angles. This is often due to a skin formation on the surfaces of solid substrates, which tends to act as wetting barriers. Eustathopoulos et al. [49] summarised that stainless steels are resistant to oxidation because the surface is covered by tenacious oxide layers. However, the adverse aspect of these films is they are also a barrier to wetting and brazing by liquid metals and alloys. In the cases of brazing stainless steel, wetting temperature is an important technical parameter because good wetting and brazing can be achieved by heating stainless steels in a high vacuum above a specific temperature but not too high to affect the microstructure and properties of the steel [50].

The classical wetting equation 1-1 is used for describing the wetting of solids by non-reactive liquids. Wetting of ceramic by a liquid metal can be assisted by reactive wetting, which can be achieved by forming continuous layers of a new compound wetted better than the initial substrate [48]. In the circumstances of reactive wetting, the contact angle varies between the initial contact angle θ_0 and the final contact angle θ_F. θ_0 is the contact angle on the unreacted substrate S ($\theta_0 = \theta_S$), and θ_F is the contact angle on the reaction product P ($\theta_F = \theta_P$). The reaction product can be either better wetted or worse than the initial substrate [51], [52]. Thus, the wetting process in real brazing conditions is very complicated. Considering the complex situations of wetting, properties generated from sessile drop experiments are useful, however limited.

Capillary action in brazing

Capillary action is the major physical phenomenon that ensures the molten filler distributes over the gap between the parallel surfaces to be brazed. In a properly designed joint, the molten filler metal can be drawn through the joint area and

creates voids or gaps free joint [28]. The relations between wetting, contact angle and capillary action are as shown in Figure 1-7. Depending on various setup procedures, brazing can be distinguished as two configurations, so-called the 'sandwich' or the 'capillary' [48], as shown in Figure 1-8. Capillary brazing is more frequently encountered in the industry. However, in this work, all the brazed specimens are created by sandwich brazing.

Kozlova [53] observed and Hausner and Wielage [48] summarised four different wetting configurations of sandwich brazing depending on the contact angle θ. They are defined as θ ≫ 90°, θ > 90°, 45° < θ ≤ 90° and θ < 45°.
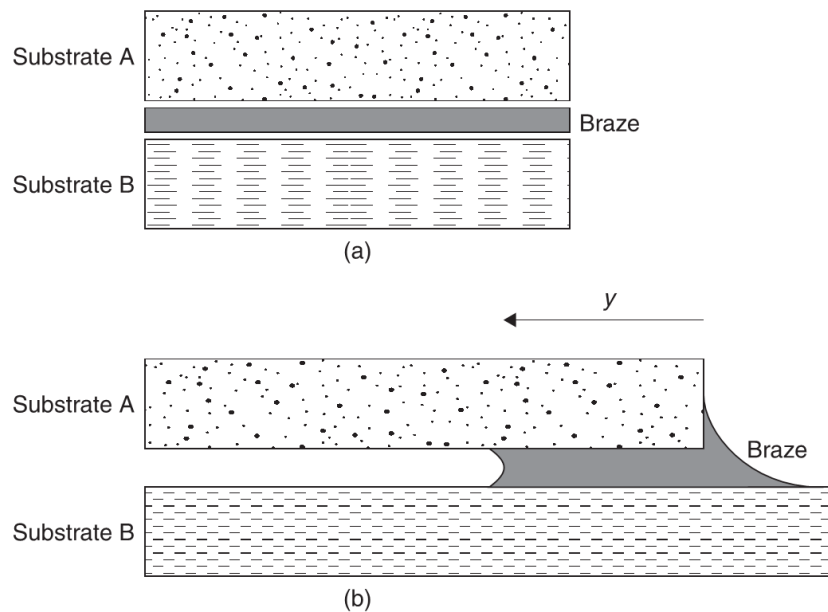
***Figure 1- 11: Schematic of brazing: (a) 'sandwich' configuration; (b) 'capillary' configuration** [48]*
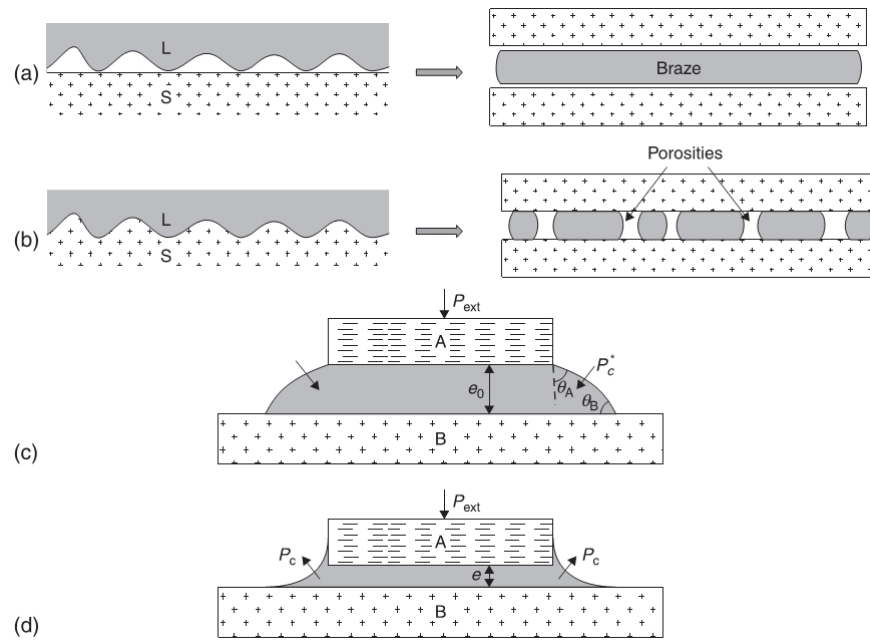
Figure 1- 12: Four configurations of sandwich brazing and the brazing results they lead to: (a) ϑ ≫ 90°, (b) ϑ > 90°, (c) 45° < ϑ ≤ 90°, (d) ϑ < 45°[48]

Figure 1-9 [48] explains the brazing results created by these four configurations. It was noted by Eustathopoulos et al. [48] that the configuration of $\theta \gg 90°$ leads to wetting shown in Figure 1-9 (a), and even small stresses generated during cooling can result in detachment of the brazed layer.

For $\theta > 90°$, braze and solid substrates can contact intimately, as shown in Figure 1-9 (b). However, de-wetting is likely to exist in the joint during solidification and lead to the solidified brazed layer with porosities and bubbles, as shown in Figure 1-9 (b).

For $45° < \theta \leq 90°$, braze can wet the solid well on interfaces and form sound brazed joints, as shown in Figure 1-9 (c). Hausner noted that in the case of $\theta > 45°$, the values of P'_c are positive and acting against the external pressure P_{ext}. The liquid braze is retained inside the braze gap unless an additional external pressure higher than the capillary pressure P'_c is applied. It was also noted that brazed joints created under this configuration are the most desirable because the action of positive P'_c is able to keep the gap clearance e_o by retaining the filler material inside braze interfaces.

For θ < 45°, braze can contact the substrates intimately across the brazing gap. However, meniscuses are formed at the edges of the brazed layer as shown in Figure 1-9 (d), if θ < 45°, the capillary pressure P_c is negative and acting in the same direction as the external pressure P_{ext}. This phenomenon results in the formation of meniscuses and a decrease in the thickness of the brazed joint [48], [53].

1.5.2 Factors affecting the mechanical properties of brazed joints

Considering the nature of the metallic bond, a brazed joint can have high strength if it is properly designed and made. The brazed joints can have strength equal to or greater than the as-brazed parent metal [28]. A brazed joint is a heterogeneous body, including different materials with different mechanical, physical and chemical properties. A brazed joint will consist of filler and parent metals and alloying phases at the interface between filler and parent metals due to diffusion processes. In the case of dissimilar brazing materials, the joint will be more complex. There are so many variables to be considered in fabricating brazed joints. The properties of brazed joints are strongly affected by joints design, filler/parent metal, heating processes, and brazing techniques. These factors have major effects on the geometries and microstructures of brazed joints, hence, their properties [28].

As discussed in sections 1.3 and 1.4, the selection of materials used in fusion reactors remain unclear, and the proposed candidate materials are limited. Suppose the filler/parent metals have been specified. In that case, the strength of the joint varies with the joint clearance, degree of filler metal-base metal interaction (diffusion and solution of base metal), the presence of defects, and the specific design [54].

Joint clearance has a significant effect on the mechanical performance of a brazed joint, including all types of loading (i.e. static, fatigue, impact, etc.) and all joint designs [54]. The effects of joint clearance on mechanical performance include (1) the purely mechanical effect of restraint to plastic flow of the filler metal by the greater strength of the base metal, (2) the possibility of flux entrapment, (3) the

possibility of voids, and (4) the relationship between joint clearance and capillary force which accounts for filler metal distribution [54].

Figure 1-13 shows the relationship of shear strength to the joint thickness in induction butt brazed drill rod using pure silver filler. The curve in Figure 1-13 indicates that the shear strength decreases with joint thickness increases. The increase of shear strength tends to be greater if the joint thickness is smaller than 0.001 inch.
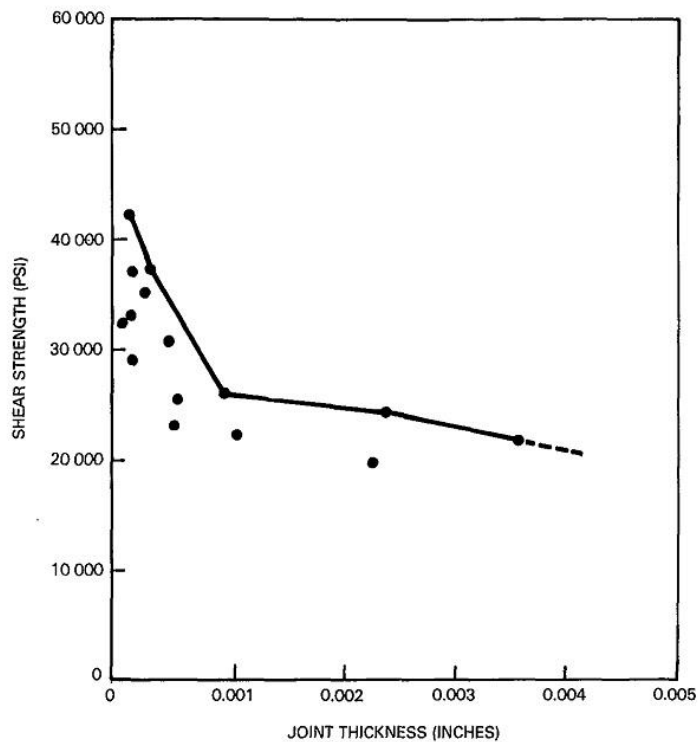
Figure 1- 13: Relationship of shear strength to joint thickness for induction butt brazed Ø0.5 inch drill rod with pure silver filler [54]

Figure 1-14 shows the relationship between tensile strength and joint thickness in butt brazed 0.5 inch diameter 4340 steel with silver filler. It was noted that these data were obtained with nonstandard test specimens. The imperfect samples show some variations, and a curve was created with the results obtained from joints without defects. The curve shows that the tensile strength increases with joint clearance decreases and can reach a peak around when thickness/diameter= 10^{-4}. It worth to

be noted that the tensile strength of the specimen drops when the joint clearances are extremely small.
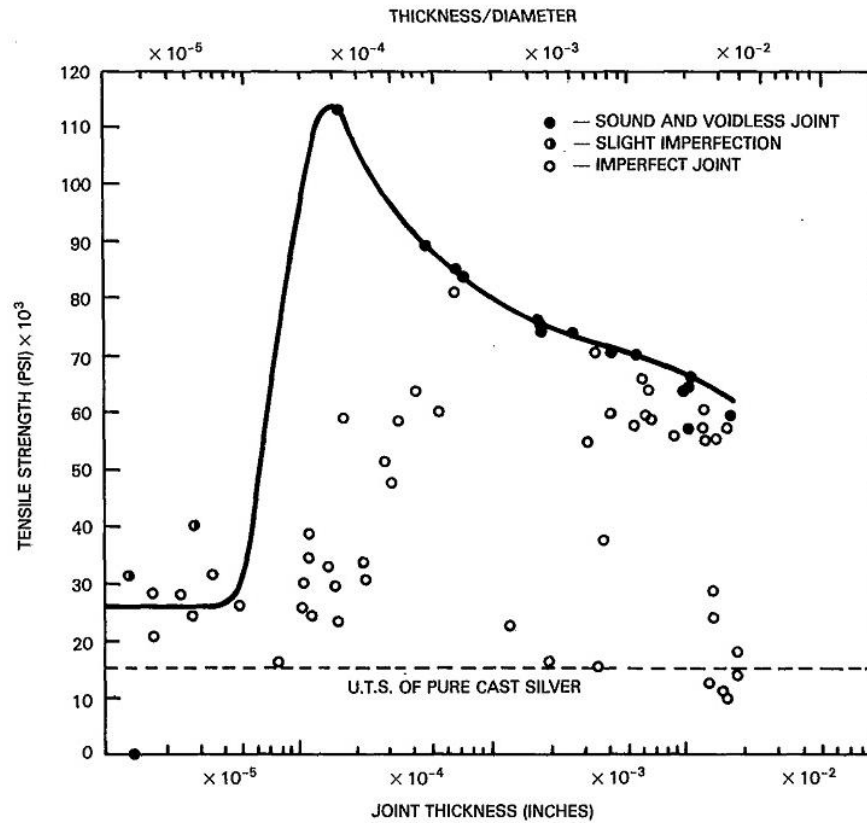
Figure 1- 14: Relationship of tensile strength to joint thickness for butt brazed Ø0.5 inch 4340 steel with silver filler [4]

In practice, small joint clearances should be used because the small clearance can prevent the presence of extensive alloying and dissolution between filler and parent materials which results in a reduction of parent material thickness [55]. It is also better for the filler metal spreading throughout the joint area and preventing the formation of defects like voids, shrinkage and cavities in the solidified filler metal [28]. As shown in Figure 1-13 and 1-14, if the clearance is not extremely small, the brazed joints can have high shear and tensile strength as the filler metal and even higher. Generally, sound brazed joints should have clearances ranging from 0.03 to 0.08mm (0.0012 to 0.003 in.) so that they can have the best capillary action and the greatest joint strength [28]. Table 1-2 shows recommended joint clearances for different filler metal systems. When designing a dissimilar brazed joint, which is a common

application in the DEMO divertor, the clearance should be calculated at the brazing temperature. As dissimilar materials have different coefficients of thermal expansion, the joint clearance set at room temperature can dramatically change at brazing temperature and can lead to defects and even the failure of the joint. Furthermore, residual stress will be generated during the cooling from the brazing temperature to room temperature. In the solidified dissimilar brazed joint, at least one of the parent materials, filler metal or an added layer of ductile base metal must yield during cooling. Thus, when brazing dissimilar materials, the clearance should be designed so that any residual stresses do not add to the stress imposed during service [54].

Table 1- 2: Preferred joint clearances for different brazing filler metal systems [28]

Brazing filler-metal system	Joint clearance, mm (in.)
Al-Si alloys (a)	0.15–0.61 (0.006–0.024)
Mg alloys	0.10–0.25 (0.004–0.010)
Cu	0.00–0.05 (0.000–0.002)
Cu-P	0.03–0.13 (0.001–0.005)
Cu-Zn	0.05–0.13 (0.002–0.005)
Ag alloys	0.05–0.13 (0.002–0.005)
Au alloys	0.03–0.13 (0.001–0.005)
Ni-P alloys	0.00–0.03 (0.000–0.001)
Ni-Cr alloys (b)	0.03–0.61 (0.001–0.024)
Pd alloys	0.03–0.10 (0.001–0.004)

(a) If joint length is less than 6 mm (0.240 in.), gap is 0.12 to 0.75 mm (0.005 to 0.030 in.). If joint length exceeds 6 mm (0.240 in.), gap is 0.25 to 0.60 mm (0.010 to .024in.). (b) Many different nickel brazing filler metals are available, and joint-gap requirements may vary greatly from one filler metal to another.

1.5.3 The effect of residual stresses in dissimilar brazed joints

One of the most critical problems when joining dissimilar materials, like W and steel, is the large mismatch in thermal expansion coefficients of W (4.2×10^{-6} 1/K at RT) and RAFM steel (ca. 12×10^{-6} 1/K at RT) [17]. Other dissimilar material properties such as Young's moduli and yield stress, in combination with the mismatch in thermal expansion coefficient, will result in high residual stresses in the joint regions as a result of the joining process [56], [57]. Under the severe DEMO divertor working conditions, the brazed joints are critical as a result of being exposed to thermal cyclic loads in both water-cooled and he-cooled divertor applications [17]. Kalin et al. [35] developed a brazing process to join W to a ferritic/martensitic steel for use on He-cooled divertors and other plasma-facing components. It was found that cracks initiated in W at a small distance away from the brazed layer, which showed that the residual stresses created by the joining process are highly significant. Under cyclic loading, these joints can fatigue and fail. Norajitra et al. [27] developed cyclic high-heat-flux tests on the W to EUROFER97 steel joints and found that cracks initiated and propagated through the brazed joints as a result of significant residual stresses. Hence, the presence of residual stress is known to be detrimental to the fatigue life of the brazed joint and should be considered in the design of a component.

Residual stresses will always be present in parent materials as residual stresses can be induced by most of the manufacturing processes, including removal of materials, plastic deformation and non-uniform cooling. Further residual stresses will develop during the joining processes in dissimilar material joints. Moreover, the residual stresses in dissimilar joints may not be reduced by stress relief. The residual stresses will be either detrimental or beneficial to the performance of dissimilar joints under operation conditions depending on whether they are tensile or compressive [12].

In this work, dissimilar brazed joints are created between a brittle material W and ductile materials, i.e. Eurofer 97, SS316L and OHFC. The brittle W will develop tensile axial and hoop residual stresses, while the ductile materials will develop compressive axial and hoop residual stresses. The large tensile residual stresses in the brittle

material are undesirable and can reduce the fatigue and ultimate strength of the joint [35], [58].

1.5.4 Challenges in generating material properties in dissimilar brazed joints

Brazed layers are difficult to be directly characterised due to their extremely small thickness (30-100 μm thick) and complex microstructures. In previously reported work [48], [59], [60], tensile testing of brazed butt specimens and shear testing of lap brazed specimens showed similar stress-strain behaviour as the parent materials up to the point of failure of the brazed joints. It was noted that during uniaxial tension of a brazed butt joint, the mechanical constraint provided by the parent material could develop a high triaxial tensile stress state within the brazed layer, and even ductile filler metal will fail without plastic deformation [48]. Under quasi-static loading, the triaxial stress state will strongly influence the joint performance and result in a decreased effective (von Mises) stress and an increased yield and tensile strengths of the brazed joint in comparison with the filler metal in the bulk form [48], [61]–[63]. Under the multiaxial stress conditions, the brazed filler metal will fail in a different way comparing the homogenous tensile or lap-shear specimens, and even a very ductile filler metal will fail in a quasi-brittle manner [64]. Therefore, it is challenging to identify the stress-strain curve of brazed joints with standard tensile testing as brazed joints fail in a quasi-brittle manner without large plastic deformation.

Previous groups [65]–[67] have shown that yield and plasticity properties of the filler metal are the key properties relating to the development of residual stresses. Research on assessing residual stresses has been carried out with three modelling approaches. For example, by modelling the brazed layer as a homogenous material, Chehtov [68] used finite element analysis (FEA) to predict the stress distribution in a Eurofer 97/WL10 brazed joint with a nickel-based filler. Two thin diffusion regions are detected within the brazed joints adjacent to both W and Eurofer 97. These diffusion regions are very complex and certainly will affect the properties of the brazed layer. However, they are ignored in this analysis. The brazed joint is assumed as a homogenous material with uniform bulk material properties for predicting the stress

distribution due to cooling from an assumed stress-free brazing temperature. However, this is an approximation, and in reality, brazed layers are inhomogeneous materials with varying compositions, microstructures and properties, without considering the effect of residual stresses. Hamilton et al. [57], [69] reported that temperature-dependent material properties data for the braze layer is sparse, and any material property characterisation is likely to be based on the as supplied condition rather than in brazed condition. This fails to account for the effect of the diffusion of elements from the parent materials into the filler and different cooling rates which can affect grain size, microstructure and yield stress, which has an important effect on the performance of the joint. Hence, the analysed results based on these properties are not accurate and reliable. This issue is widely existing in the approaches to assessing brazed joints. In order to create an accurate FE model and assess the integrity of a brazed joint, the properties of a brazed layer in a real brazed condition need to be characterised. This is a considerable challenge and one of the hot topics in the FEA designer community.

Nanoindentation is one of the very few convenient techniques that can measure the elastic and plastic properties of very small volumes of materials [70], [71]. Nanoindentation can be applied to the brazed layer and diffusion regions to generate properties such as Young's modulus, hardness, fracture toughness, creep, and residual stress [72]. However, the reliability of these data is influenced by the complexity of the braze microstructure and the chemistry of the diffusion regions. This indicates that nanoindentation tests on different microstructure, different phases in an alloy and even in the same phase but penetrate into a completely different microstructure from the surface will produce different results. Nanoindentation is useful and convenient to generate in situ material properties at nano and micro levels. However, it has difficulties to predict the average properties on the macro level. Hardie [70] has developed a comprehensive study of characterising mechanical properties of irradiated Fe-Cr alloys by in situ nanoindentation and micro-mechanical testing methods. Hardie also performs micro-cantilever testing with depths of hundreds of nanometres. This work

demonstrates that these methods can generate mechanical properties, yet the data is unconventional and difficult to be applied to various failure mechanisms for fusion reactor design codes. Further development needs to be carried out for the validation and standardisation of these methods.

1.6   Summary

This chapter reviewed the selection of materials in water-cooled and helium-cooled DEMO reactor concept design and reported on the joints between some of the materials under considerations, i.e. pure W, Eurofer 97, AISI SS316L and OFHC Cu. Considering the suitable brazing temperature range and promising irradiation characteristics of gold, this work focuses on an approach based on generating knowledge of using two gold-based alloys, Orobraze 910 (Au80Cu19Fe1) and Orobraze 890 (Au80Cu20), as new filler selections for brazing W and other divertor candidate materials.

Although brazing has been used for a very long time in human history, it is usually used as a technique that relies on experience. The technology and applications of brazing are well developed in the industry. However, based on the review of the author, research works contributing to the failure of brazed joints are very limited. Although there is plenty of research works analysing different types of brazed joints, the properties of the brazed joints still cannot be clearly measured. Reported approaches are avoiding the properties of the brazed layer by predicting the behaviour of a brazed joint as a whole part. How to correctly assess the strength of a brazed joint remains a challenge for the designers.

Brazed joints assessed by standard tests fail in a quasi-brittle manner without large plastic deformation before failure due to the nature of mechanical constraints within brazed joints. It is difficult to identify the stress-strain of brazed joints, hence the yield and plasticity properties of the filler metal, which are the key properties relating to the development of residual stresses in dissimilar brazed joints. The thin brazed layer with complex microstructures and unknown material properties in a brazed joint brings many challenges in the numerical studies of brazed joints.

Consequently, the brazed layer's material properties are the heart of any procedures to assess the failure of brazed joints. The primary objectives of this work are fabricating and assessing the dissimilar brazed joints with DEMO divertor candidate materials and generating material properties of the brazed layers in these joints.

As described in section 1.4.2, the use of gold-based alloys for joining DEMO divertor components is a new approach. In order to generate the basic knowledge of these dissimilar brazed joints, this work is aiming to develop brazing procedures to create sound and defects free brazed joints for characterisation and mechanical testing. The design of experiments and characterisation methodology are reported in Chapter 2. Brazed joints are created between W and dissimilar materials, i.e. pure W itself, EUROFER 97, AISI SS316L and oxygen-free high thermal conductivity (OFHC) Cu, to assess the brazing quality and applicability of the gold-based fillers. The experimental work, including fabrication, metallurgical assessment and instrument tests, i.e. micro/nanoindentation of the brazed joints using these fillers, are reported in Chapter 3 and 4. In order to justify the mechanical properties of brazed layer generated in Chapter 3 and 4 by nanoindentation to be feed into design work, Chapter 5 is an investigation of developing a casting procedure that towards generating sub-sized test specimens in the 'as cast' condition that have a similar microstructure and chemical composition as the real brazed layer developed in practice. In this way, the specimen can be tested on the macro level and correlated with properties generated by nanoindentation. The preferred gold-based filler materials already used in Chapter 3 and 4 are uneconomic to make standard sized casting test specimens for the generation of mechanical properties. Therefore, Chapter 5 used a binary Cu60Zn40 filler material as the raw material for the development.

2 Brazing experiment design and characterisation techniques

2.1 Parent and filler materials

Parent materials used for brazing were commercially pure W, OFHC copper, AISI316L in the cylindrical butt form with dimensions of Φ12.7mm × 10mm and Eurofer 97 with dimensions of Φ10 mm × 10 mm. Figure 2-1 shows the prepared parent materials in cut and polished state before brazing. Eurofer97, OFHC Cu and SS316L were machined on a CNC lathe to ensure a consistent surface finish. While W was cut by wire EDM process and no polishing was carried out. The nominal chemical compositions of the parent materials are shown in Table 2-1. Table 2-3 listed the material combinations of interest and their relevant divertor design applications.

The dissimilar samples were brazed in butt joint form with the filler 'Orobraze 910', supplied by Johnson Matthey. The chemical compositions of Orobraze 910 filler are 80% Au, 19% Cu and 1% Fe, in weight percentage, and the working temperature range is 908–910 °C. Braze filler supplied as foils of 0.0508 mm (0.002 inches) was utilised throughout the experiments.
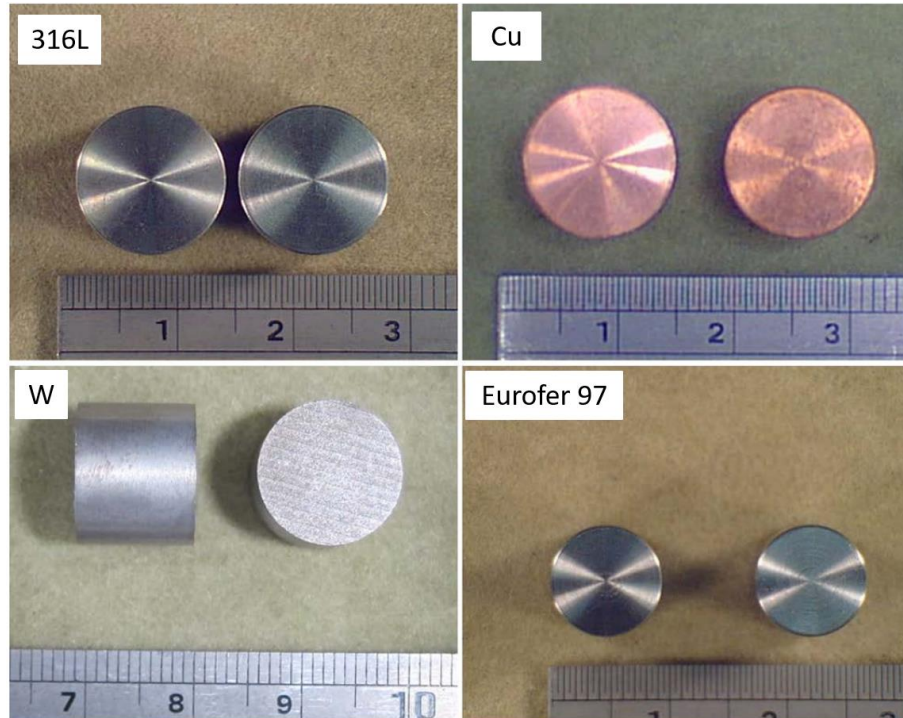
Figure 2- 1: Parent materials used for brazing characterisation specimens

Table 2- 1: Nominal chemical composition of the parent materials, wt% [34], [73]

	W	Cu	Fe	Cr	Ni	Mn	V	Ta	C	Si	Mo
W	≥98.7										
Eurofer 97	1.07		Bal	8.93		0.49	0.28	0.15	0.12		
OFHC Cu		≥99.99									
SS316L			Bal	16-18	10-14	2.00			0.03	1	2-3

Table 2- 2: Nominal mechanical properties of parent materials [74]–[76]

Metal	Elastic modulus (GPa)	Hardness (HV)	Melting point (°C)
Tungsten Annealed	405	>460	3420
Eurofer 97	208	210	1462
Copper	117	40-110	1083
SS316L	193	<226	1400

Table 2- 3: Material combinations of interest

Material combinations	Relevant divertor design
W-W	HEMJ/water-cooled
W-Eurofer 97	HEMJ
W-Cu	Water-cooled
W-316L	Water-cooled
Cu-316L	Water-cooled

2.2   Furnace brazing procedure

A vacuum muffle furnace was used to perform the brazed samples, and all the specimens were brazed in the same brazing run. The brazing filler was punched into Φ10 mm disks. Parent materials in the cut and polished condition were cleaned, assembled with brazing foil and loaded immediately into the brazing oven to minimise oxidation and other surface contamination. The joint clearance was set by the thickness of the filler metal disks, i.e. 0.0508mm, which complied with the recommended range of 0.03 - 0.13 mm for Au alloys as described in Section 1.5.2. A schematic of the butt joint and the jigging of pre-brazing specimens is shown in Figure 2-2. The parts were weighed down from the top to encourage the flow and spreading of the molten filler metal. Three carbon rods tied by molybdenum wire were used to keep the parts aligned during brazing.

The brazing was performed at a vacuum level of 5×10^{-6} millibar. As described in Figure 3-2, the furnace heating cycle of brazing was set to heat up by 10 °C/min to approximately 900 °C then dwell for 5 min then heated up by 10 °C/min to approximately 1000 °C followed by a dwell of 5 min. On completion of the brazing process, the furnace was switched off and the vacuum condition was maintained so that the samples could cool down very slowly to avoid thermal shock.
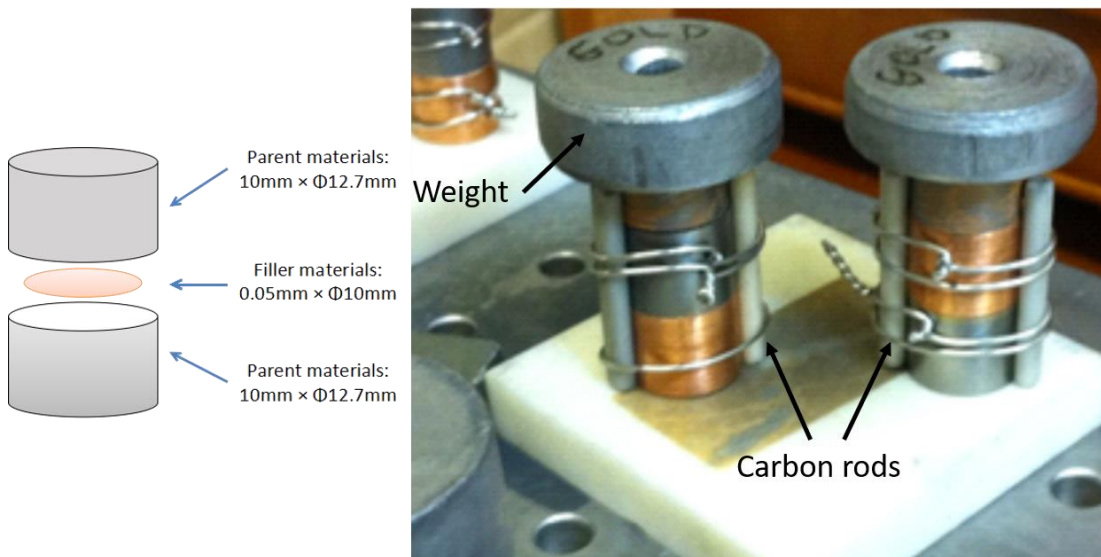
Figure 2- 2: Material dimensions and brazing jig setups
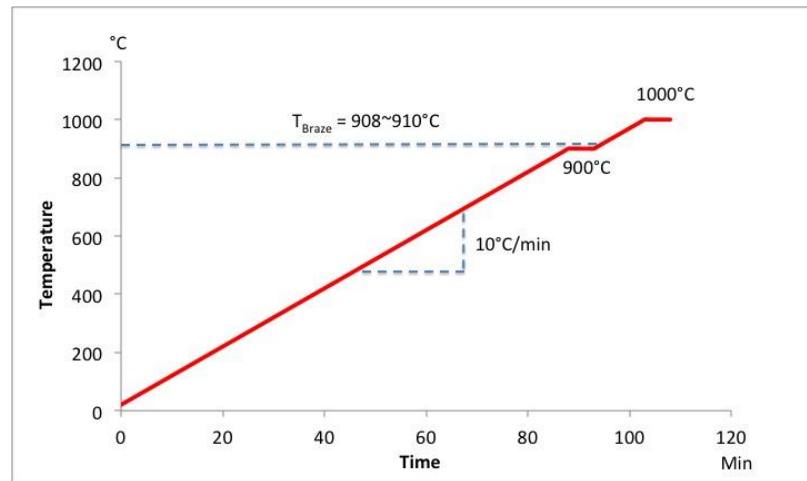
Figure 2- 3: Furnace brazing heating cycles

In this production run of brazing work, four sets of assembled parts were set in the furnace and fabricated for each material combination. Four successfully brazed specimens were obtained for W-W, W-SS316L, W-Eurofer97, while only three W-Cu specimens were successfully brazed. The brazed specimens are shown in Figure 2-4. Visual examinations were performed and found all the specimens showed regions of incomplete brazing. W-W and W-SS316 joints had overflow filler metals formed at the edge of the brazed joints. Figure 2-5 shows a reference W-SS316L specimen with these defects.
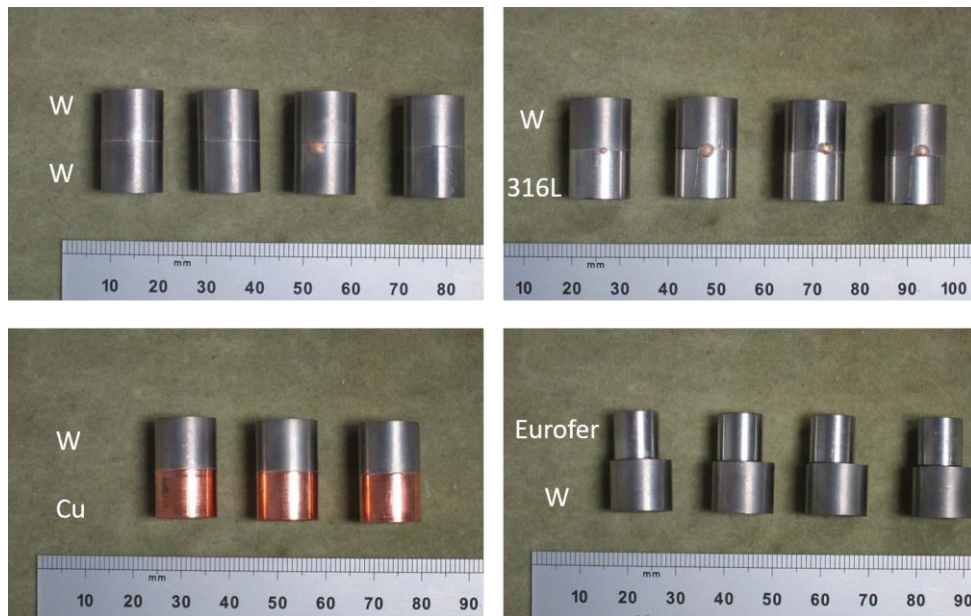
Figure 2- 4: Brazed specimens for characterisation

Figure 2- 5: W-SS316L specimen showing overflow of filler on joint edge and incomplete braze region by visual

2.4 Metallographic preparation

The basic aim of metallographic preparation is to obtain "The True Structure", which is an undisturbed material surface that can be analysed in an optical microscope or a scanning electron microscope (SEM). However, the preparation process always modifies the specimen surface, and the true structure without artefacts can never be obtained [77].

Vilella [78] and Samuels [79] defined the true structure as:

- No deformation—The plastically deformed layer created by the preparation should be removed or be negligible.

- No scratches—Scratches normally indicate a surface that is not yet sufficiently prepared, but small scratches might be allowed if they do not disturb the examination.

- No pull-outs—Especially in brittle materials, particles can be pulled out of the surface, leaving cavities that can be taken for porosity.

- No introduction of foreign elements—During the preparation process, abrasive grains can be embedded in the surface.

- No smearing—With certain materials, the matrix or one of the phases might smear (flow), resulting in a false structure or covering of structure details, or both.

- No relief or rounding of edges—Relief can develop between different constituents of the surface, caused by different hardness or other condition. Edge retention is important if the edge has to be examined.

The specimens being assessed in this thesis were prepared following the standard metallographic procedures. The post brazed samples were sectioned by Silicon Carbide (SiC) disks on a precision cut-off machine. In order to avoid excess heat produced during the cutting process, the feeding rate was set as 0.005 mm/s, and sufficient coolant was applied through the cut. The sectioned samples were then mounted in a conductive carbon material and prepared by mechanical grinding and polishing. The polished samples were then etched to show the microstructures. The etchants used throughout the thesis are listed in Table 2-4.

Table 2- 4: Etchant used

Material	Etchant
W	Murakami's regent
Eurofer 97	Kalling's regent
SS316L	Kalling's regent
Cu	FeCl$_3$ solution

The visual quality and microstructural properties were then assessed by use of a light optical microscope and SEM. A Hitachi 3700 W-filament SEM was used for imaging, and EDS was used to confirm the compositional variation. The analysis X-ray point has a minimum diameter of 1~2 μm.

2.5 Microindentation and Nanoindentation

Microindentation was developed to perform hardness measurements on very small objects, thin layers, surface treated materials or individual structure constituents [77]. Microhardness is the determination of hardness values with low test forces with the range between 9.8×10^{-3} and 9.8 N, which is very small compared to the macro hardness testing, and the indentations are correspondingly small. Vickers and Knoop

diamond indenters are successfully used in practice. The hardness error is directly proportional to the force error.

In order to perform precise microindentation, the specimen should be cleaned and polished. The prepared surface should be set up perpendicularly to the direction of indentation. The surface should avoid etching whenever possible because the smaller the test force and the indentation, the greater the influence of specimen preparation. For example, excessive polishing can cause cold work of the surface material. Vibrations and shaking of the machine must be avoided during measurement [77].

In this study, microindentation tests were performed on the parent materials of brazing. The microhardness values were measured at the parent materials as supplied condition and went through the same brazing heating cycles with the brazed samples. The results are correlated to the microstructure properties and reported in section 3.1.

Even using automatic machines with high-grade optical measurement systems, the classical microhardness testing with Vickers or Knoop indenter the diagonal length is recordable to at most 2-3 µm due to the limited resolution capability. In order to work with microcrystalline materials and extremely thin layers like brazed layers, a smaller indentation size was developed. The testing principle is Instrumented Indentation Testing (IIT) and so-called nanoindentation. For measurements in the nano range, a three faces Berkovich indenter is preferred. Figure 2-6 shows the size comparison of indents created by micro/nanoindentation and also the geometries of indents created by Vickers and Berkovich indenter.
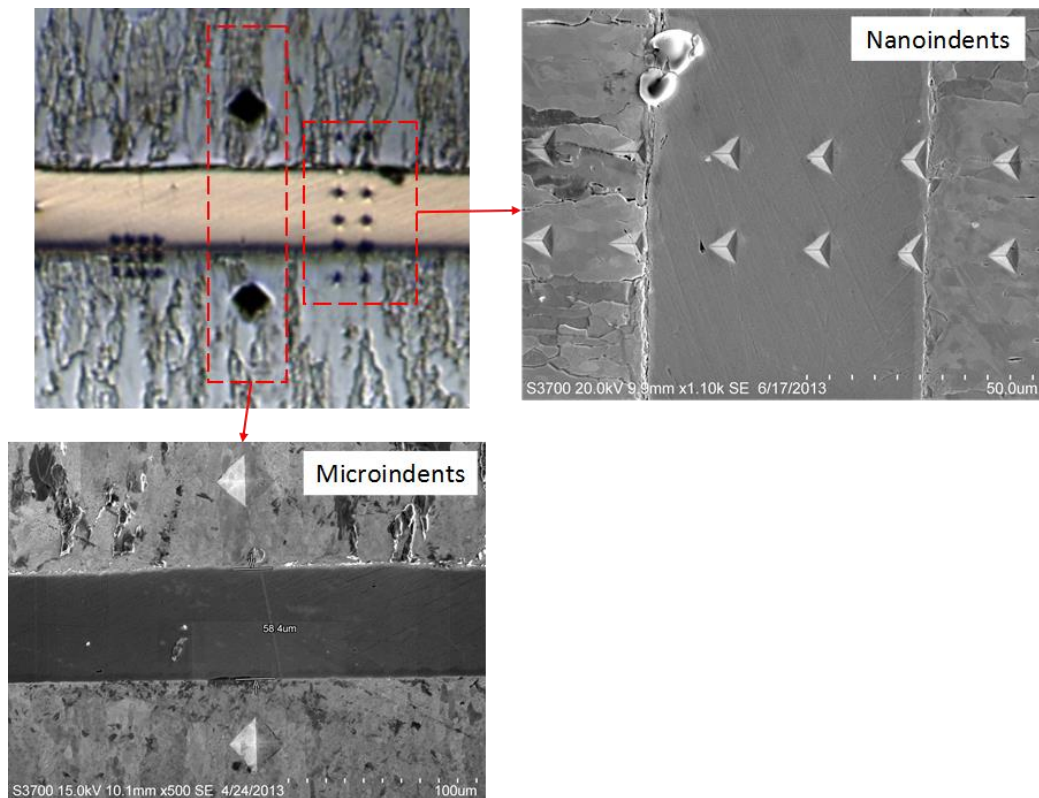
Figure 2- 6: Comparison of indents by micro/nanoindentation

An Agilent G200 nanoindenter fitted with Berkovich indenter was used for determining the hardness and elastic modulus values of the phases observed in the brazed joints. Nanoindentation measurements were also undertaken to generate local mechanical properties correlated to the interfacial reaction and diffusion phenomena due to the brazing procedures. The tests were performed at the interfaces of each material combination of interest. In this study, the continuous stiffness measurement (CSM) technique was used to study average elastic modulus and hardness values over an indentation range, as discussed in previous works [38], [80], [81]. Utilising the CSM module of the nanoindenter, average hardness and elastic modulus values over an indentation depth between 100 to 1000nm were analysed. In this thesis, the microstructures of brazed joints in different combinations of materials brazed to pure W were characterised and a CSM loading-unloading curve on W was shown as Figure 2-7. Additionally, interfacial reactions and elemental diffusion behaviour of each material combination have been analysed and discussed.
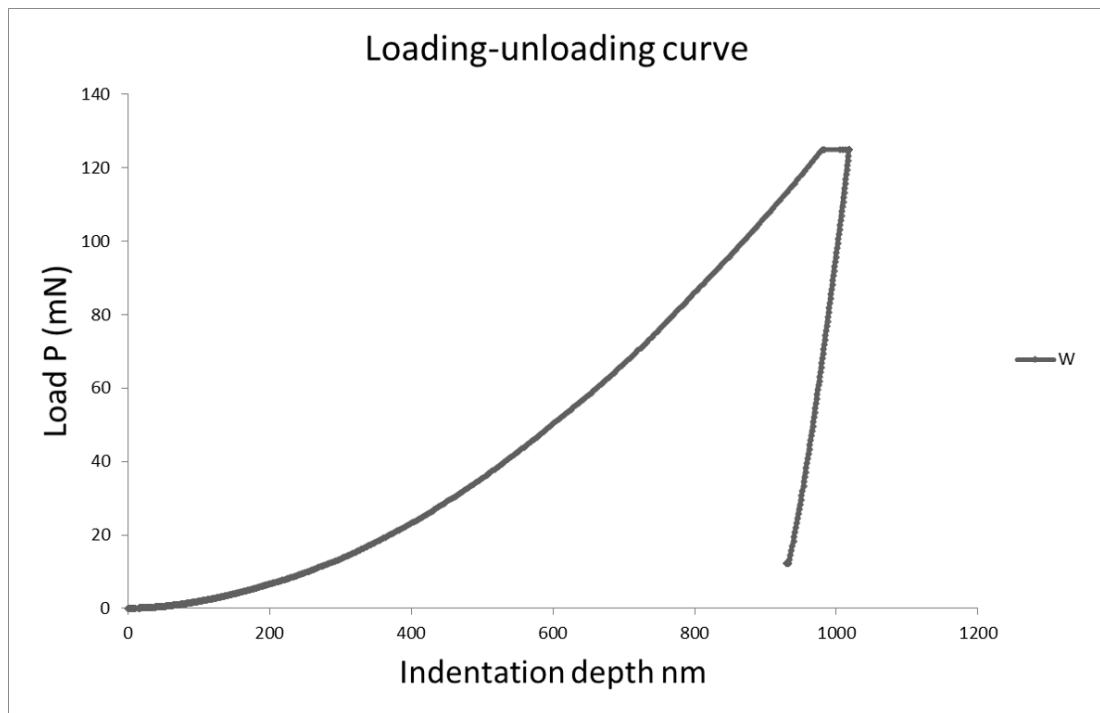
Figure 2- 7: A loading-unloading curve measured by nanoindentation on W using CSM

2.6 Qualification of brazing joints

A comprehensive microstructural analysis of the interfacial region of the brazed joints between the aforementioned materials has been undertaken. Flaws and imperfections were assessed for each brazed joint to ensure compliance with the classification of imperfections in the International Standard EN ISO 18279:2003 [82].

The braze quality showed a degree of uniformity in different material combinations. No cracks were detected after brazing, however various defects were detected, as shown in Figure 2-8:

(1) Bonding imperfection, as shown in the W-W joint.

Bonding imperfection leads to no bonding or inadequate bonding between the braze metal and the parent material.

(2) Recessed braze fillet, as shown in the W-Eurofer 97 joint.

43

Recessed fillet means the surface of the braze filler material in the brazed joint is below the required dimension. The recessed fillet indicated localised stress concentrations and a decrease in fatigue performance.

(3) Cavities and pores in the brazed layers, as shown in the W-Cu joint.

These cavities and pores were likely to be created by trapped gas. Small gas pores tend to be spheroidal, while large gas voids may be the width of the joint with an elongated shape.

(4) Filling imperfections, as shown in the W-SS316L joint.

The filler failed to fill the joint gap completely.

Besides these internal defects, excess braze metal solidified onto parent materials was observed outside the joint regions. Although all the materials combinations showed varying degrees of these defects, the successfully joined regions within the brazed joints were uniform.
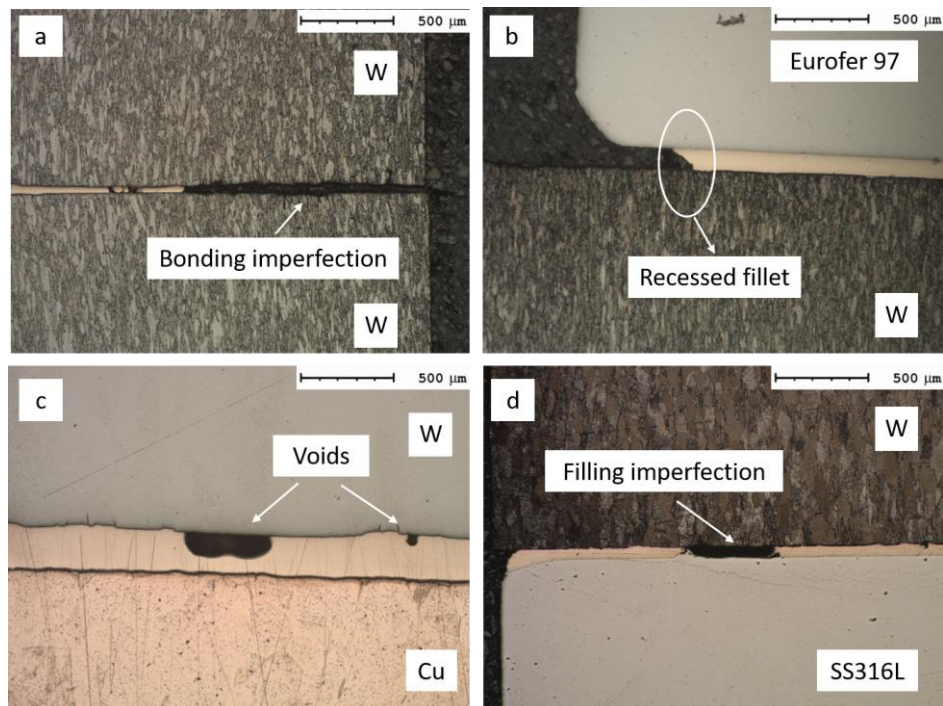
Figure 2- 8: Typical brazing defects and imperfections found in different joints: (a) Bonding imperfection (b) Recessed fillet (c) Voids (d) Filling imperfection

The ISO standard separates the acceptable limits for imperfections within different working environments into Moderate, Intermediate and Stringent. Fusion applications should be Stringent with the highest requirements due to the high loading and extreme working environment. The standard suggests cracks are not permissible. Cavities should not exceed 20% of the projected area. Bonding imperfection should not exceed 10% of the nominal brazed area. The filling should achieve 80% or more of the projected area with the braze metal. Recessed braze metal (recessed fillet) is permitted where the component function is not adversely affected. The ISO standard also suggested maximum permissible defects and imperfections may be defined for a particular application.

The ASME Boiler & Pressure Vessel Code and RCC-MR (Design and construction rules for mechanical components of nuclear installations) are widely used in fusion applications. ASME 2004 Section IX Welding and Brazing Qualification requires that the brazed specimens should be polished and examined with at least a four-power magnifying glass. The sum of the length of unbrazed areas on either side, considered individually, should not exceed 20% of the length of the joint overlap.

The brazed specimens were inspected under a microscope. The successfully bonded regions within the brazed joints are generally around 70% of the length of the joint, which is not acceptable according to the nuclear design code. This is likely due to the filler foil was punched into disks smaller than joint areas of parent material samples and resulted in the lack of filler metal. The reason for using a smaller filler disk was to prevent excess filler material from being squeezed out by the added weights and causing erosion on the surface of parent materials. A further optimised furnace brazing procedure was carried out in order to improve the quality of joints to an acceptable level and reported in Chapter 4.

2.5 Summary

This chapter discusses the design of brazing work and experimental methodology for characterising the brazed joints. Two equivalent gold-based fillers (Orobraze 910 and Orobraze 890) were used to fabricate brazed joints between 4 parent materials,

namely pure W, EUROFER 97, AISI SS316L and OFHC Cu. Vacuum furnace brazing processes were designed to fabricate sound quality brazed specimens. Characterisation experiments were performed to gain a better understanding of the quality of fabricated brazed joints for design reference. Micro and nanoindentation were performed to generate mechanical properties to be fed into parallel design work within the research group. The first batch of brazed specimens was created with Au80Cu19Fe filler and characterised. Detailed results are reported in Chapter 3. Due to the presence of defects, the second batch of brazed specimens with optimised brazing procedures was joined using Au80Cu20 to fabricate qualified joints. The W-Cu joints created with optimised furnace brazing were analysed and compared with W-Cu joints created by an induction brazing procedure. This work is reported in Chapter4.

3 Interfacial metallurgy study of brazed joints between tungsten and fusion relevant materials with Au80Cu19Fe1 filler using vacuum furnace brazing

Four different butt-type brazed joints were created and characterised, each of which was joined with the aid of a thin brazing foil (Au80Cu19Fe1 to ISO 17672:2010). The brazing procedures are reported and discussed in Chapter 2. Microstructures of the parent material were examined as supplied and after the brazing heat cycles to assess the microstructural changes related to mechanical properties and measured by microindentation tests. Microstructural characterisation and elemental analysis in the transition region of the joint were undertaken. The interfacial diffusion characteristics of each material combination were produced. Nanoindentation tests were performed at the joint regions and correlated with element composition information in order to understand the effects of diffused elements on mechanical properties. The experimental procedures of specimen fabrication and material characterisation methods are presented. The results of elemental transitions after brazing are reported. Elastic modulus and nano hardness of each brazed joints are reported.

3.1 Microstructural changes to the parent materials due to the brazing process

The microstructures and micro-hardness of the parent materials, W, Eurofer 97, OFHC Cu and SS316L, were assessed in the as supplied condition and after the brazing heat cycles. The samples used in this investigation were prepared with the same process as the parent materials used for brazing to keep the consistency. One sample of each parent material was set in the vacuum furnace along with the brazing samples to go through the entire brazing process.

According to the Hall-Petch relation, yield stress and hardness of polycrystalline metals can be increased by refining their grain size. Therefore, on the other hand, yield stress and hardness should decrease with the increase of grain size [83]. Because the post brazed parent materials went through the whole brazing heating

cycle, the brazing process could be considered as heat treatment, and the microstructures of the parent materials were likely to be changed due to this process.

3.1.1 Pure Tungsten (W)

Figure 3-1 shows the similar microstructures of W (a) as supplied (b) post brazing as grain growth of W starts from 1100 °C, which is higher than the brazing temperature. The similarity of microstructures indicates the mechanical properties of W should not change after the brazing, and the results of microindentation have confirmed this. Figure 3-2 shows the comparison of micro-hardness measured on the as supplied and post brazed specimens. Micro-hardness of W as supplied was 436 ± 5.29 HV, and post brazed was 438.3 ± 3.18 HV.
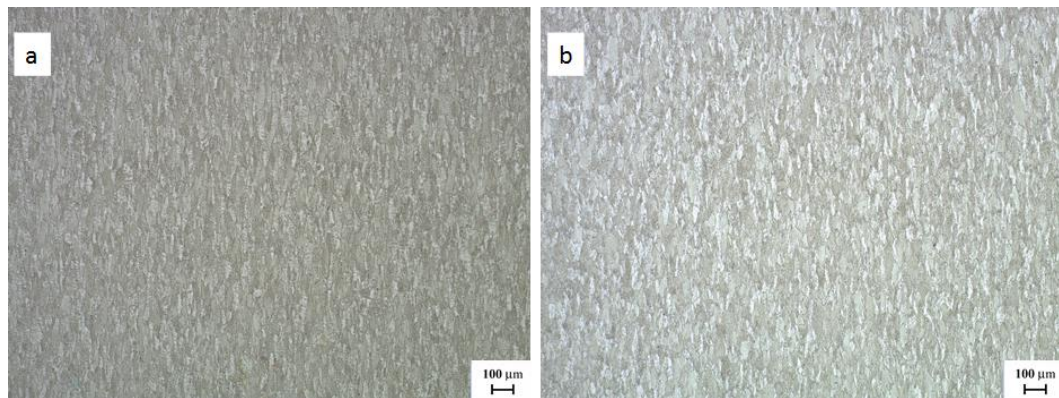
Figure 3- 1: Microstructure of W (a) as supplied, (b) post brazing
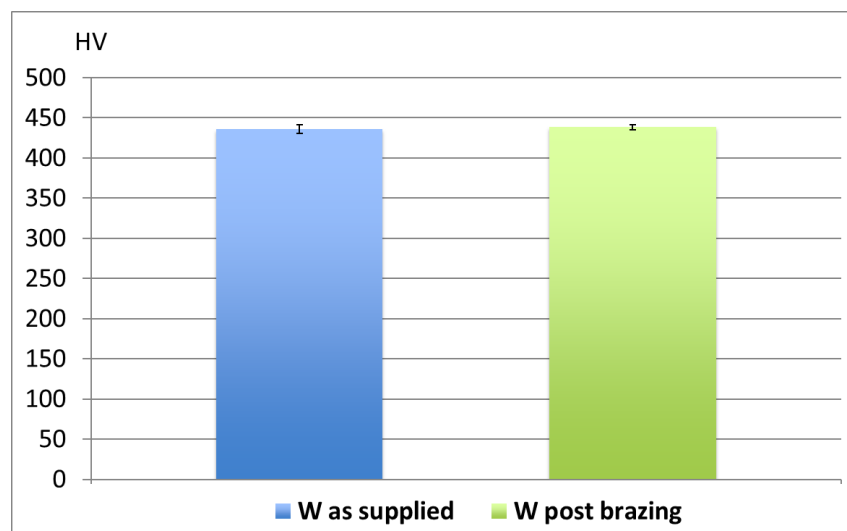
Figure 3- 2: Micro-hardness of W, as supplied and post brazing

3.1.2 Eurofer 97

Figure 3-3 shows the microstructure of the Eurofer 97 steel examined by light microscopy. As shown in Figure 3-3 (a) and (c), the steel showed a fully martensitic structure without ferrite, corresponding with its compositions. Figure 3-3 (b) and (d) shows the presence of precipitated phases observed in the post-brazed specimen.

Figure 3-4 shows the micro-hardness of Eurofer 97, as supplied was 216.3 ± 0.33 HV and post brazing was 382 ± 2.65 HV. Microindentation tests showed the hardness of Eurofer 97 was greatly increased post brazing. This phenomenon indicated that some microstructural changes contributed to the hardness increase of Eurofer 97.

In Lu's work [83], Eurofer 97 was normalized at 980, 1040, 1100, and 1150°C, followed by water quenching and air cooling. The grain size of Eurofer 97 increases with the increase of normalizing temperature, however the hardness also increased with the rise of temperature. According to the transmission electron microscope (TEM) work of Lu and other authors [38], [84], [85], the microstructure of Eurofer 97 after heat treatment is martensitic with $M_{23}C_6$, which is a Cr-rich carbide precipitated phase, and (Ta, V) C type Ta/V-rich carbides. Precipitation of $M_{23}C_6$ carbide occurs as a result of heating solution-annealed grades from 500 to 950 °C, and the fastest rate of precipitation takes place from 650 to 700 °C [86]. The presence of Ta-rich carbides contributes to the increase of hardness with temperature in the Eurofer 97. When hardenable parent metals are used in brazed joints, more complex metallurgical reactions between parent and filler metals will occur during brazing processes. These reactions can cause changes in the base-metal hardenability and can create residual stresses. Under these situations, the strength of the brazed joint will be less predictable [28].
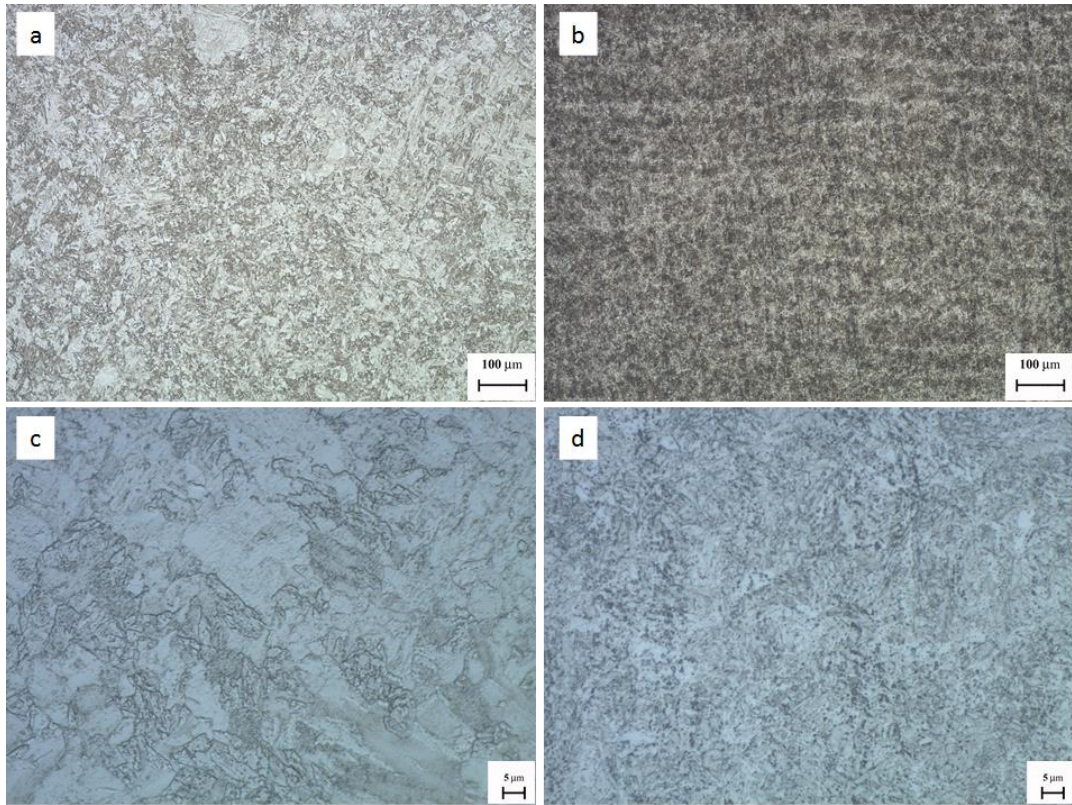
Figure 3- 3: Microstructures of Eurofer 97 (a) as supplied x100, (b) post brazing x100, (c) as supplied x 500, (d) post brazing x500
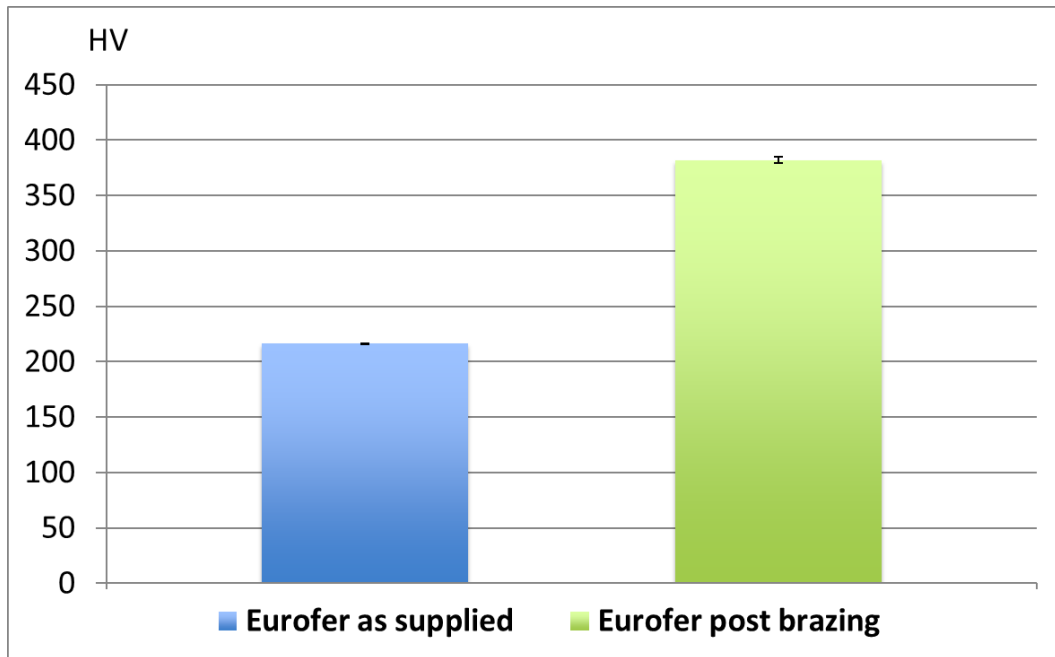
Figure 3- 4: Micro-hardness of Eurofer 97 as supplied and post brazing

3.1.3 Copper

Figure 3-5 shows the microstructures of Cu, (a) as supplied and (b) post brazing. Significant grain growth can be observed after the process, and this phenomenon indicates a significant reduction in hardness. Figure 3-6 shows micro-hardness measured on Cu as supplied was 89.6 ± 1.24 HV, and post brazing was 51.4 ± 1.52 HV. The hardness of Cu has been greatly reduced by the brazing heating cycle.
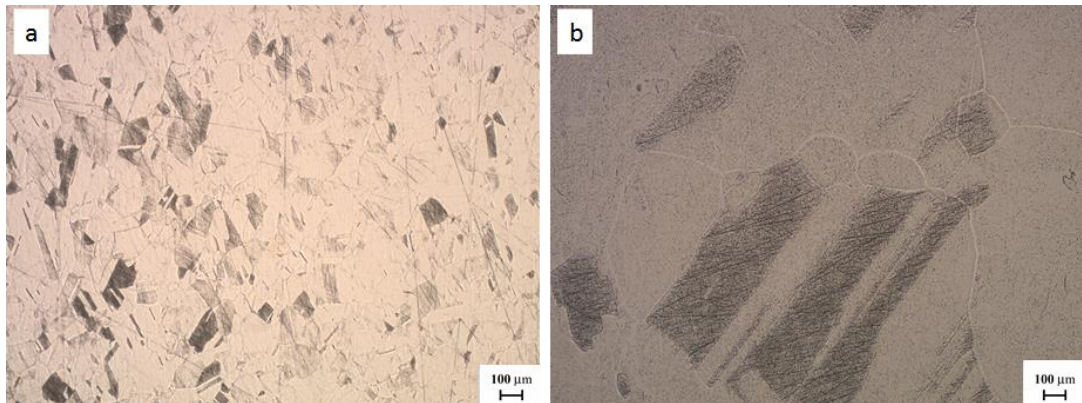
Figure 3- 5: Microstructures of Cu (a) as supplied (b) post brazing
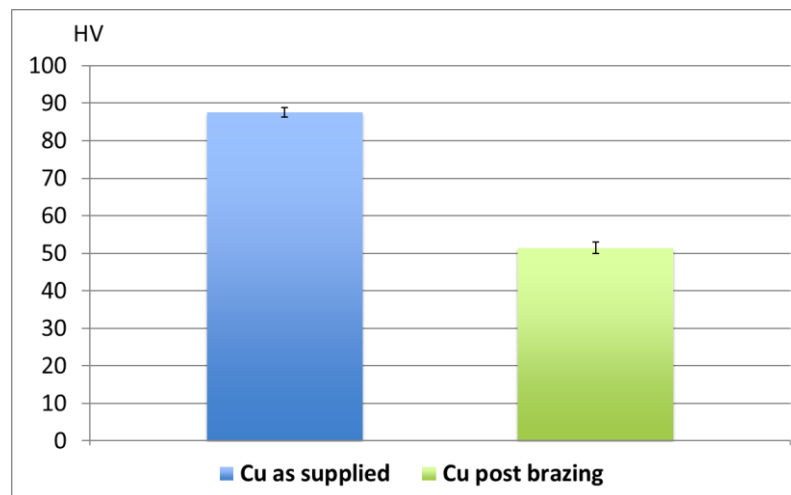
Figure 3- 6: Micro-hardness of Cu as supplied and post brazing

3.1.4 SS316L

Figure 3-7 shows the microstructures of SS316L, (a) as supplied and (b) post brazing. Recrystallized grains can be observed in the post brazing SS316L. Figure 3-8 shows the comparison of micro-hardness measured at SS316L as supplied was 237.3 ± 2.33

HV, and post brazing was 197.7 ± 1.76 HV. The reduction of hardness is known to be due to grain recrystallization and growth.
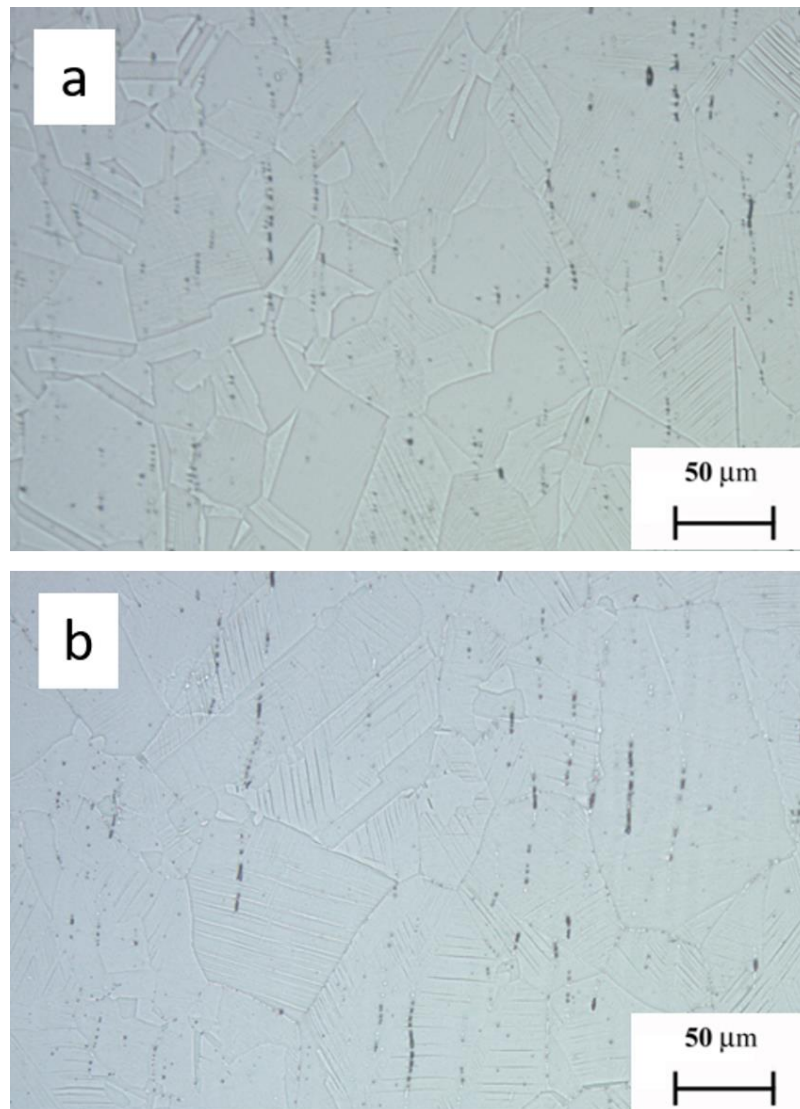
Figure 3- 7: Microstructures of SS316L (a) as supplied (b) post brazing
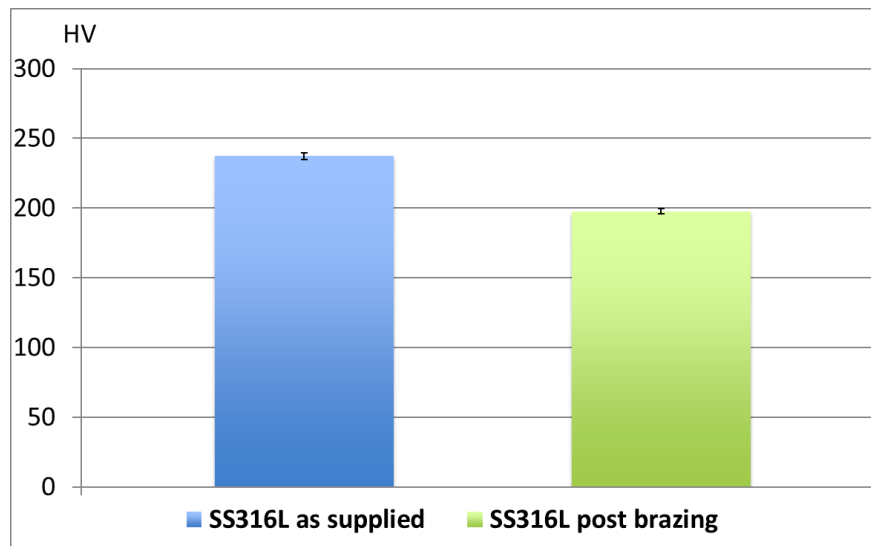
Figure 3- 8: Micro-hardness of SS316L as supplied and post brazing

3.2 W- W joint

Section 1.3 has reviewed the applications of different brazed joints. The DEMO He-cooled divertor concepts are designed to remove a high heat load of at least 10 MW/m^2. In the DEMO reactor, both HEMJ and HEMS divertor designs consist of cooling fingers formed by W tiles brazed to WL10 thimbles. During operation, the cooling fingers are cooled with helium jet impingement at 10 MPa and inlet/outlet temperature is 600/700°C. Norajitra et al. [6], [27], [87]], have performed three series of high heat flux tests on the W-WL10 brazed DEMO divertor components to simulate the challenging divertor working condition as described in Section 1.1. Different failures were detected in these tests after cyclic thermal loadings. Cracks in the tiles and thimbles propagated during the cyclic thermal loading due to high thermal stresses and/or poor production quality, and the tile and thimble were partially detached due to overheating in the brazed joint were detected.

In these applications, the brazed W-W component will have to withstand thermal cyclic loads during operation, and the brazed joint will be the most critical area. According to the observations of the W/AuCuFe/W brazed joint, the interfacial reaction is limited, and element transitions are within 1 μm, and the primary diffusion behaviour is grain boundary diffusion. The interfaces between W and the AuCuFe filler are the critical areas in the brazed joint due to the abrupt step change of

chemical compositions, mechanical and thermal properties. Temperature dependent mechanical and thermal properties of W have been studied by the Fusion community [73]. However, temperature dependent properties of the AuCuFe filler are very limited. Further work is ongoing trying to generate the properties of this filler in order to perform finite element (FE) analysis.

An SEM backscatter image of the brazed joint between pure W-W is shown in Figure 3-9 (a). As W has been etched, elongated grains of W can be observed. Nanoindentation tests take 12 measurements at different locations to generate mechanical properties across the W-W joint, with the indents spacing of 20 μm and a maximum depth of 1000 nm. The indent locations can be observed in Figure 3-9 (b). The elastic modulus and hardness values are calculated by CSM between the depths of 400 – 900 nm. For W, the mean value and standard deviation of E= 388 ± 32.91 GPa, and H = 6.72 ± 0.29 GPa. For AuCuFe, E = 154.68 ± 17.8 GPa and H = 4.54 ± 0.28 GPa.

The nano indents in Figure 3-9 (a) were also used to benchmark the regions where EDS analysis was performed. An EDS line scan analysis was developed by crossing the brazed joint to generate elemental transition information, with the results shown in Figure3-9 (b). The analysis performed 150 measurements through a distance of circa. 115μm with an accelerating voltage of 20 keV. The results of EDS analysis highlights that there is a step change of chemical compositions between W and the AuCuFe filler. No distinct diffusion regions are created at the AuCuFe/W interfaces, and the elements from W and AuCuFe filler do not diffuse into each other. Reiser [88] reported Cu and Au have no reaction with W thus, the diffusion of these elements into W can be nearly neglected. On the other hand, Fe can form intermetallic compounds with W, which is detrimental to the quality of the brazed joint.

There are a few measurements locating at the adjacent interfaces which consist of the elements from both parent and brazing materials, which indicates there might be some transitions or reactions in existence. Therefore, some further analyses were performed to confirm the conditions of the interfaces.
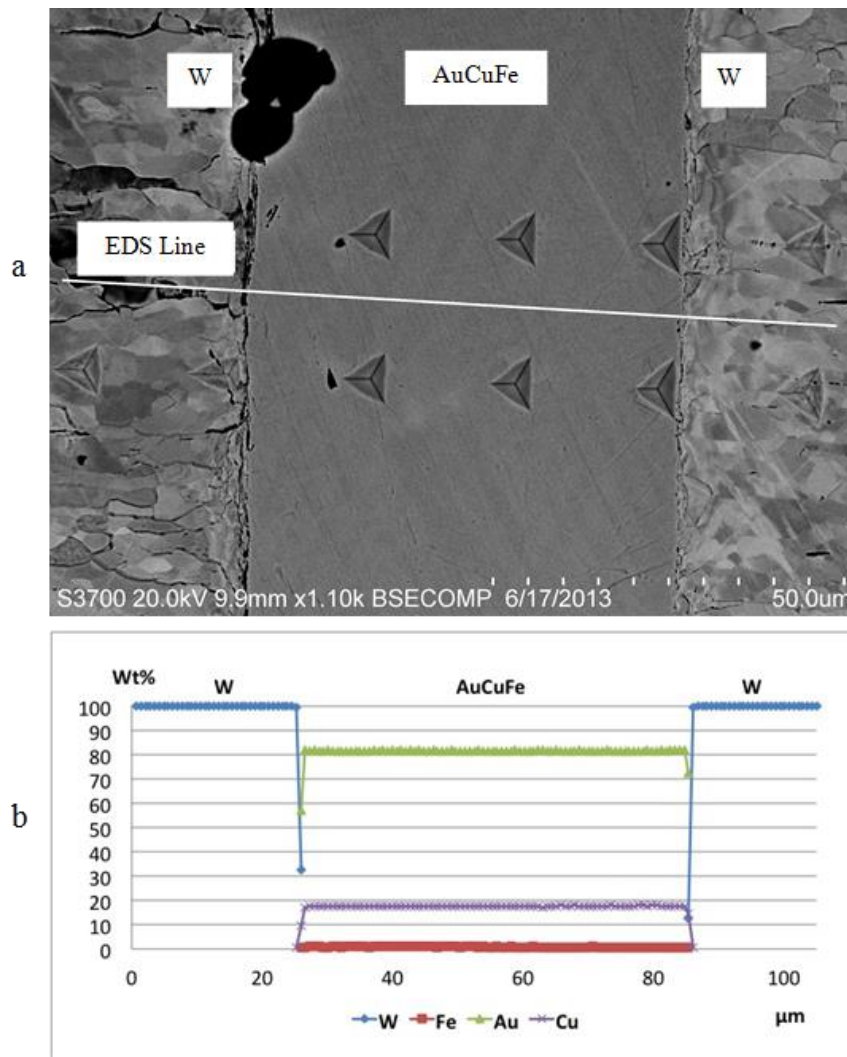
Figure 3- 9: (a) Backscatter SEM image of W/AuCuFe/W joint

(b) EDS analysis across the joint

Figure 3-10 is an optical microscope image captured at the AuCuFe/W interface in which filler material penetrations can be observed. This phenomenon is due to grain boundary penetrations, or micro-cracks on the W surface that hadbeen filled with braze material. In the presence of liquid filler metal during the brazing process, the alloying elements found in the filler metal may migrate into the base metal through solid-state diffusion or liquid metal grain boundary penetration. Furthermore, liquid penetration through grain boundaries may increase with decreasing mutual solubility [34]. As W has very low, or negligible, mutual solubility with Au and Cu, then grain

boundary liquid penetration is likely to be the primary interaction at the W/AuCuFe interface.
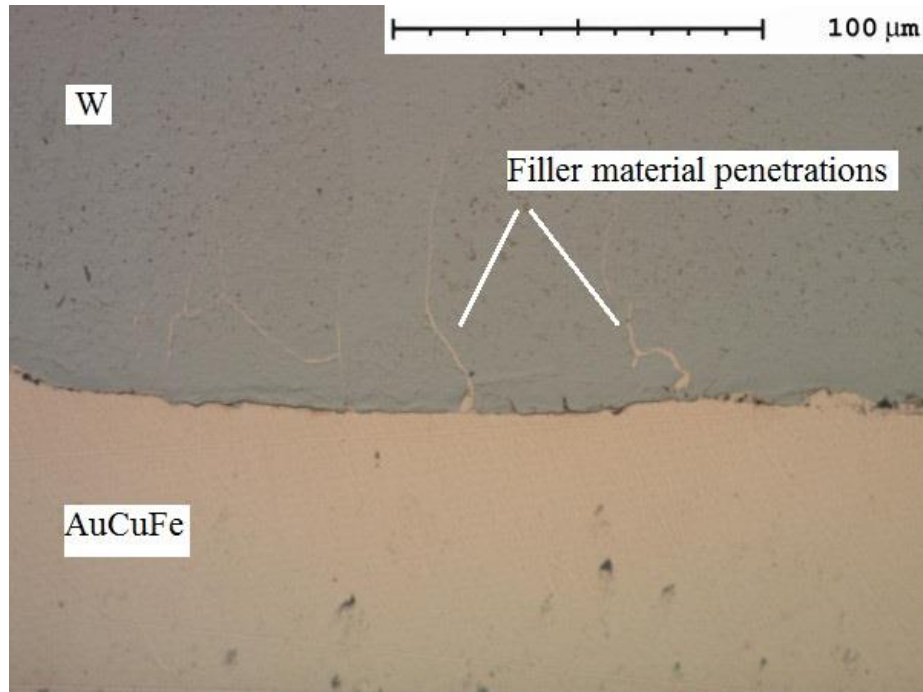
Figure 3- 10: Optical image shows the interface of W/AuCuFe

To confirm the step change of chemical compositions at the W/AuCuFe interface, further EDS analyses were performed at the W/AuCuFe interface at higher magnification, as shown in Figure 3-11. Four spectra were analysed at different locations shown in Figure 3d, and the results are shown in Table 3-2. Spectrum 1 and spectrum 3 were both approximately 1μm away from the brazed interface. Spectrum 2 and spectrum 4 were approximately 5μm away from the interface. However, the compositions shown in Table 3-2 confirmed that no diffused filler materials were detected on the W side. This is because the analysed region is relatively small, and the grain boundary diffused materials are randomly distributed along with the interface and, as a result, was not picked up by the measurement.
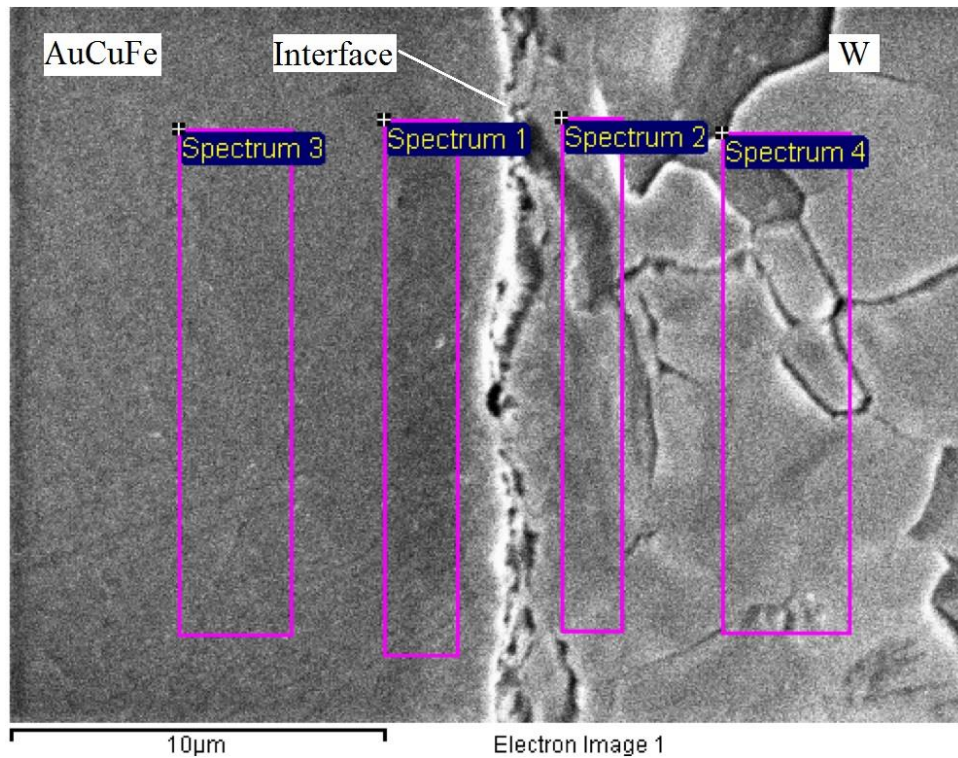
Figure 3- 11: SEM image with EDS analysis at the interface of AuCuFe/W

Table 3- 1: Elemental compositions measured at AuCuFe/W interface

	Au	Cu	Fe	W	Total Wt%
Spectrum 1	81.68	17.49	0.83		100
Spectrum 2				100	100
Spectrum 3	81.53	17.59	0.88		100
Spectrum 4				100	100

Figure 3-12 (a) shows an EDS line analysis performed at the W/AuCuFe interface at the same location in Figure 3-11. The study performed 25 measurements over 11 μm across the interface. Figure 3-12 (b) shows results over the distance of 11 μm across the W/AuCuFe interface, the abrupt change of chemical compositions can be confirmed, and this sudden change takes place within a distance as small as 1 μm. This abrupt change in chemical compositions will inevitably result in a change in the

mechanical and thermal properties of the joint. Furthermore, the change will result in stress concentrations along the interface under mechanical or thermal loadings and make the interfaces the critical areas within the brazed joint.

In the FE model of a butt brazed joint [57], analytical stress singularities exist at the free edge of the interface between dissimilar materials due to the abrupt changes in material properties. The stresses at the interface are theoretically infinite under an infinitesimally small mechanical or thermal load, which should result in failure of the joint. However, satisfactory dissimilar material joints with free edges can be created without failure. Therefore, in reality, the theoretical infinite stresses predicated by the elastic theory do not exist.

Previous researchers [57], [58] have summarised two reasons contributing to the above phenomenon, first is the linear elastic theory assumes a step-change in material properties. But in reality, this step change will never occur as there will be some form of grading at the interface, even over an extremely small scale. In this case, although the abrupt chemical composition changes were detected within 1 µm, there will still be an extremely small amount of some elemental transitions at the interface. Furthermore, the grain boundary diffusion of AuCuFe in W also disproved the step change of properties.

The second is analogous to the linear elastic fracture mechanics (LEFM) explanation which describes why sharp cracks in brittle materials do not fail under an infinitesimally small applied load but rather only if the applied load is raised to a critical value. In the analysis of dissimilar material joints, the theoretical infinite stresses predicted by the elastic theory do not exist at the interface due to plasticity effects in materials, even brittle materials, in this case W.
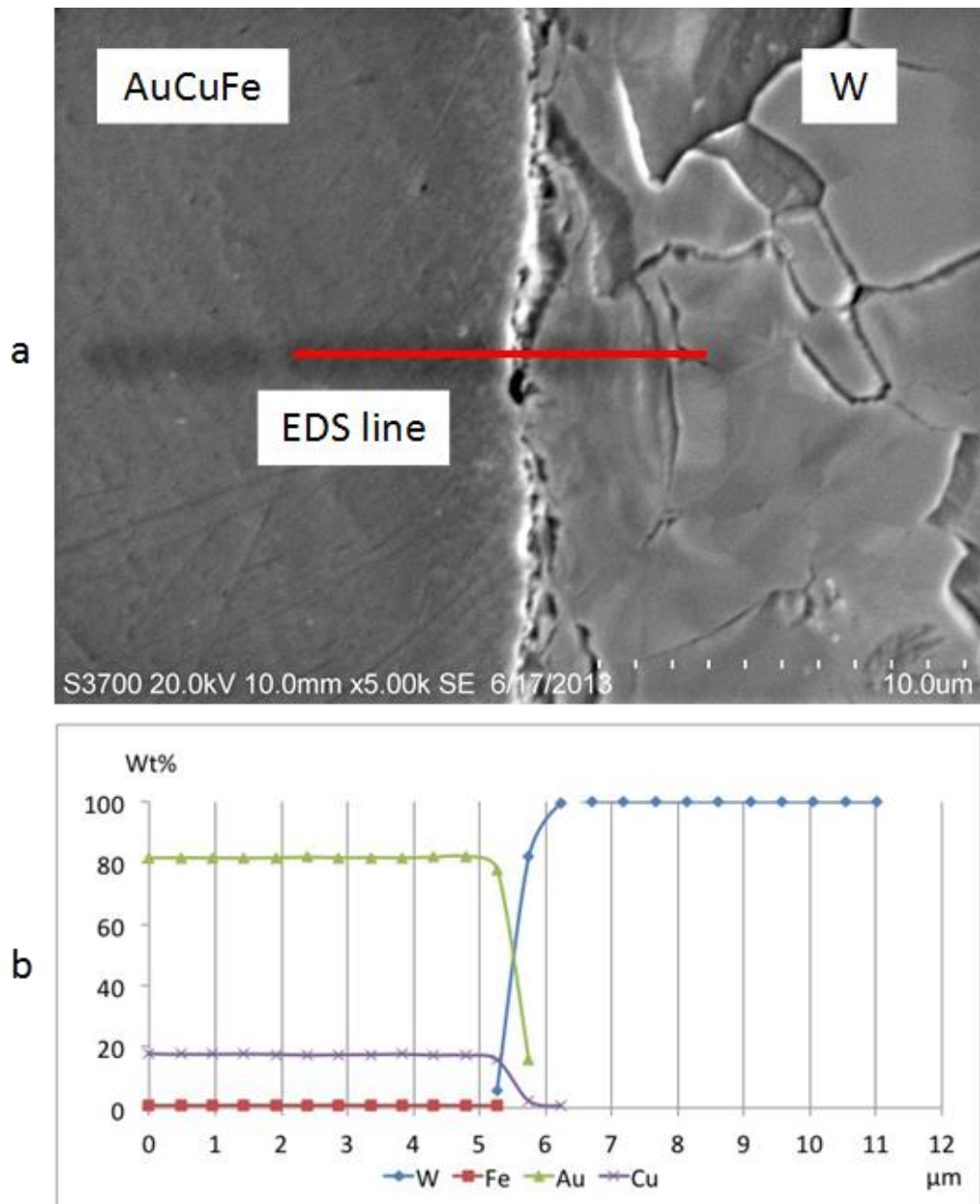
Figure 3- 12: (a) W-AuCuFe interface line scan

(b) Elemental transitions at the interface

Nanoindentation tests, shown in Figure 3-13 (a), were performed at the interface between the AuCuFe filler and W, and the maximum indentation depth was set as 1000nm. The indentation tests across the interface were numbered from 1 to 12, with an indent spacing of 10 μm, and both hardness and elastic modulus at each

indent location were calculated between the depths of 400 - 900 nm. Elemental compositions at each indent were analysed by EDS point scans with a radius of approximately 2 µm and an acceleration voltage of 20 keV. Figure 3-13 (a) shows the locations of indents left by the measurements, and the indents are numbered from 1-12 in order to be analysed separately. Figure 3-13(b) shows the variations in chemical compositions, where measurements 1-4 are located at the AuCuFe filler region and measurements 5-12 are located at the W region. Figure 3-14 shows the variations in elastic modulus and hardness measured by nanoindentation, and the results are presented with the numbering of the indents corresponding to those defined in Figure 3-13 (a), respectively. For the indents 1-4 at filler region, the mean value and standard deviation of E = 155.47 ±3.73 GPa, and H = 4.65 ± 0.13 GPa. For the indents 5-12 at W region, E = 405.55 ± 27.88 GPa and H = 7.21 ± 1.13 GPa. These results at the interface match well with previous results measured across the brazed joint, as showed in Figure 3-9 (a).

The modulus and hardness measured at the AuCuFe are constant as the solidified brazed layer is uniform, and no diffused phases were created during the brazing process. The results measured at W have relatively larger standard deviations due to the nanoindentation being affected by sample surface conditions. In this joint, W was polished and etched while the braze filler was polished and un-etched.
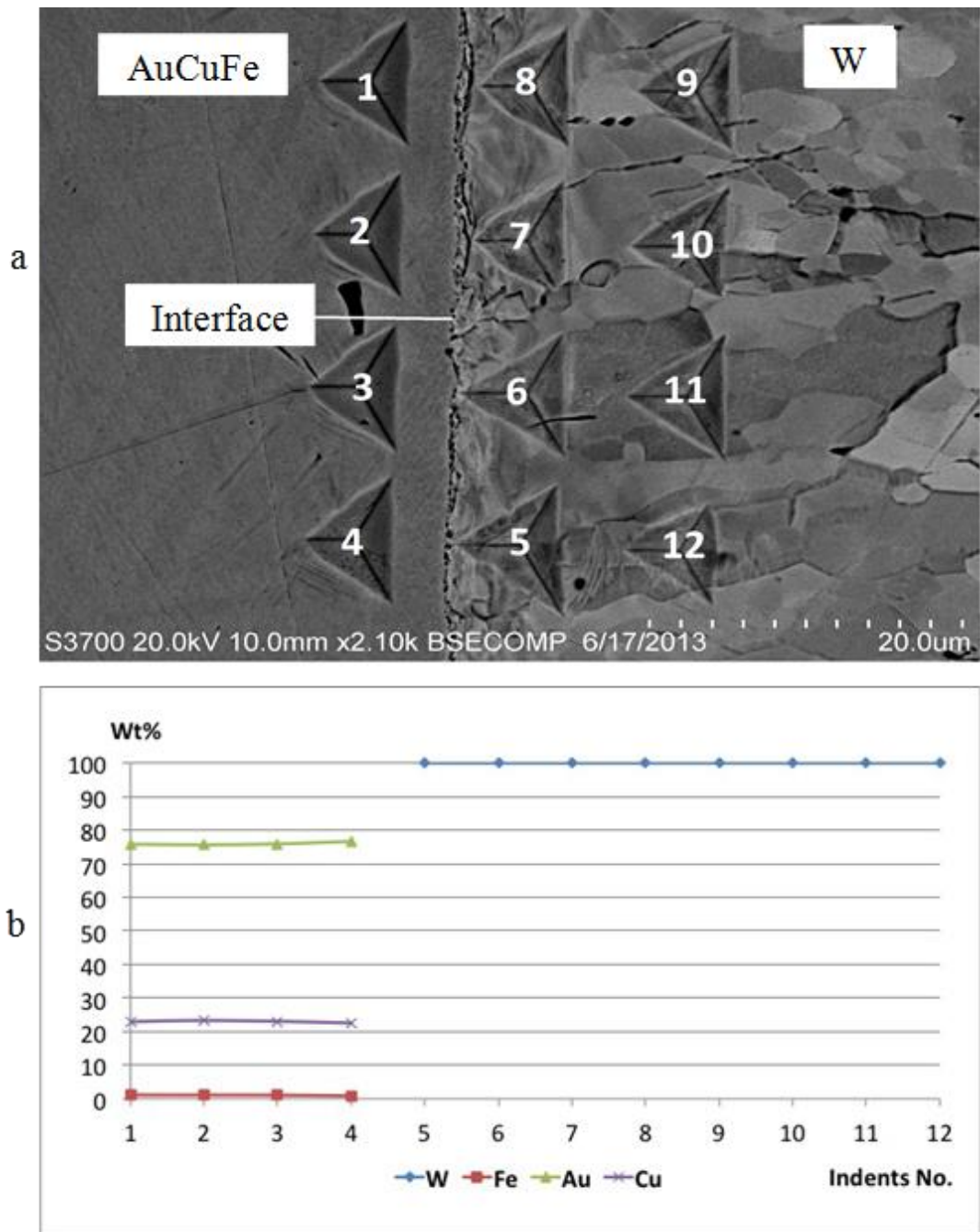
Figure 3- 13: (a) SEM image shows indentation locations

(b) Element compositions of indentations
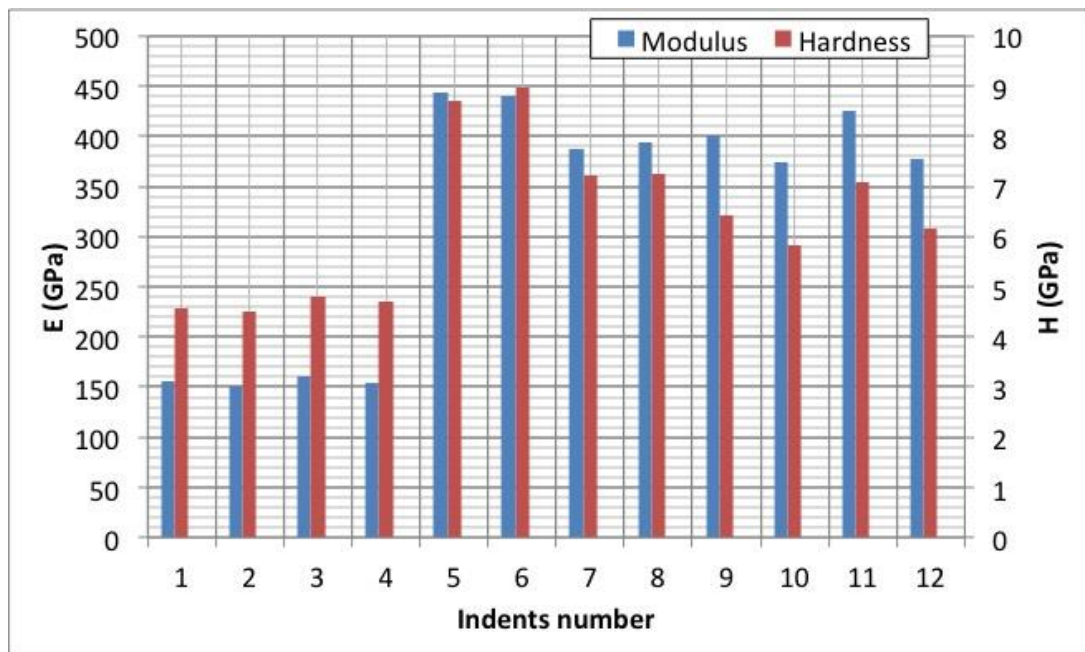
Figure 3- 14: Elastic modulus and Hardness measured by nanoindentation

3.3 W- Eurofer 97 joint

A number of W-Eurofer 97 brazing joints exists in both the He-cooled and the water-cooled DEMO divertor. One of the most critical problems when joining W-Eurofer 97 is the mismatch of thermal expansion coefficients, elastic modulus and Poisson's ratios resulting in residual stresses during cooling, which would lead to yield failure of the joint [35], [89]. Kalin [35] developed a brazed joint between W and a type EP-450 RAFM steel and found after 100 thermal cycles, heating to 700°C then air and water cooling, cracks propagated at in W along the brazed layer. The distribution of stresses was calculated and the normal stress perpendicular to the plate of a brazed joint has a maximum in the parent material with less plasticity that is located at some distance from the zone of brazing. The distance depends on the thickness ratio of brazed materials (χ = T_{Steel}/T_W). However, in Kalin's calculation, the brazed layer was ignored. It is also noted that, in reality, there is a temperature gradient along the component, with higher temperatures on the W side and lower temperatures on the Eurofer 97 side. However, thermal analyses showed that a relatively low temperature gradient (about 100K over joining area) appears at the joining area between the W

and the Eurofer 97, which would induce stresses much smaller than the stresses due to thermal mismatch between each material [26], [89].

The experiment setups for analysing the W-EUROFER 97 joint were the same as those used in the W-W joint. Figure 3-15 (a) shows the backscatter SEM image of the brazed joint. A diffusion region with complex microstructures at the interface between the AuCuFe filler and the EUROFER 97 can be observed. An EDS analysis was performed along the line shown in Figure 3-15 (a), and the results are shown in Figure 3-15 (b). The line analysis measured the composition at 150 points over a distance of 110μm. As shown from the EDS results, the diffusion region contains both diffused Fe and Cr. Diffusion of Fe and Cr reduces with the distance from the interface. Furthermore, Fe diffuses a further distance into the brazed joint than Cr but does not penetrate beyond the interface of W/AuCuFe. Neither Au nor Cu diffuses into the Eurofer steel, which is different from Fe and Cr.

Nanoindentation tests take 12 measurements to generate mechanical properties across the brazed joint, with the indents spacing of 20 μm and a maximum depth of 1000 nm. The indent locations can be observed in Figure 3-15 (a). The elastic modulus and hardness values are calculated by CSM between the depths of 100 - 400 nm. For W, the mean value and standard deviation of E= 430.2 ± 21.9 GPa, and H = 7.25 ± 0.31 GPa. For AuCuFe, E = 139.7 ± 11.1 GPa and H = 4.48 ± 0.23 GPa. For Eurofer 97, E = 243.5 ± 19.6 GPa and H = 4.51 ± 1.63 GPa.
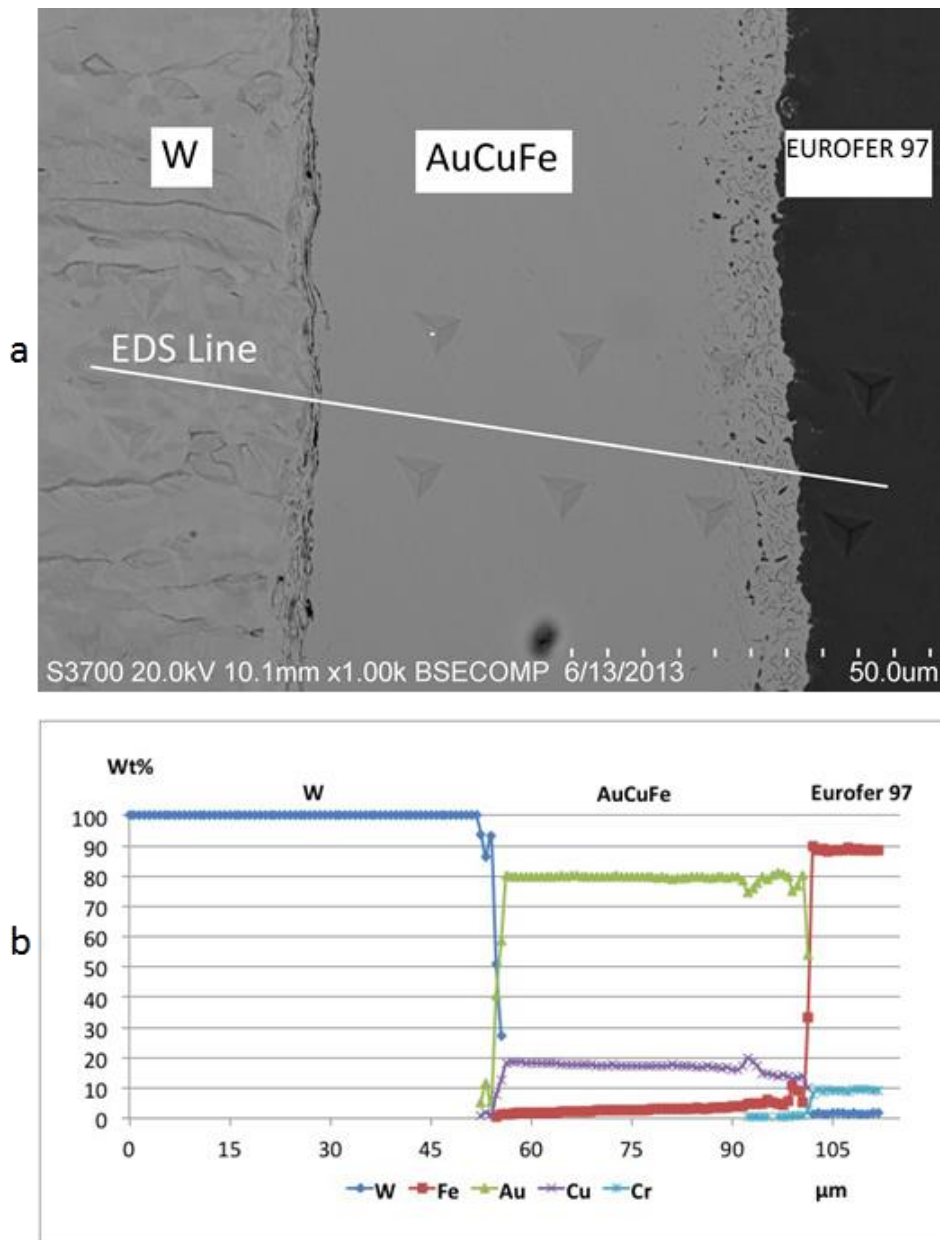
Figure 3- 15: (a) Backscatter SEM image of W/AuCuFe/EUROFER joint

(b) EDS analysis across the joint

An elemental mapping analysis was generated at the interface of the AuCuFe/EUROFER 97 joint in order to understand the diffusion behaviour, and the results are shown in Figure 3-16. Figure 3-16 (a) is an SEM image showing the microstructure of the diffusion region at x5000, (b) shows elemental maps of the primary elements Au, Cu, Fe and Cr. The elemental maps demonstrate the dispersion

behaviour of these elements after brazing. The iron dispersion map showed that the dark microstructures at the diffusion region were majorly formed by diffused iron.
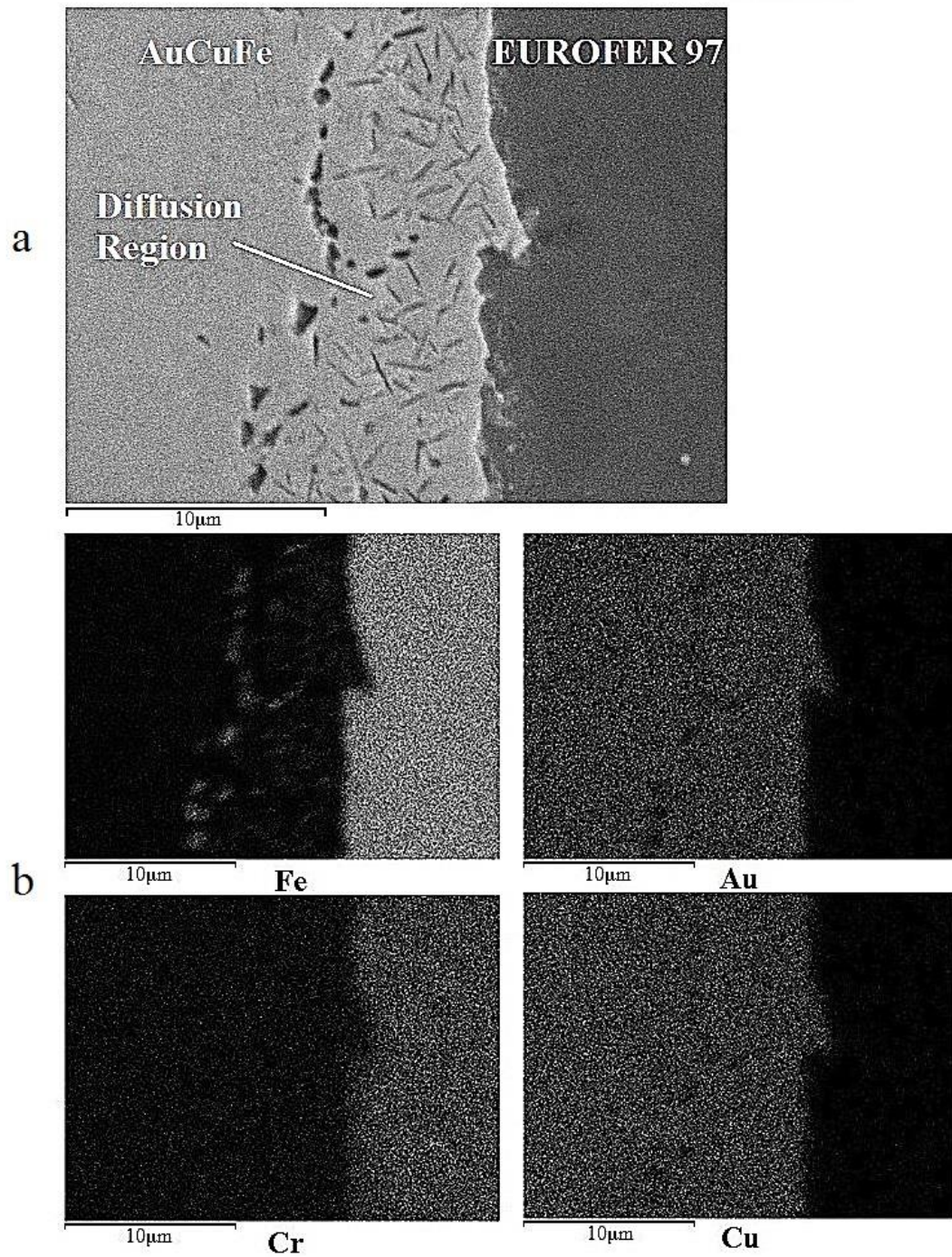
Figure 3- 16: (a) SEM image at interface of AuCuFe/EUROFER 97

(b) Elemental maps of primary elements in the brazed joint

Nanoindentation tests were conducted at the interface of the AuCuFe/EUROFER 97 joint, with a maximum indent depth of 1000nm. The indents were numbered from 1 to 12, as shown in Figure 3-17(a) and correlated to the composition measurements shown in Figure 3-17 (b). Indents 1 to 4 were located in the AuCuFe, 5 to 8 were located in the diffusion region, and 9 to 12 were located at the edge of the EUROFER 97.
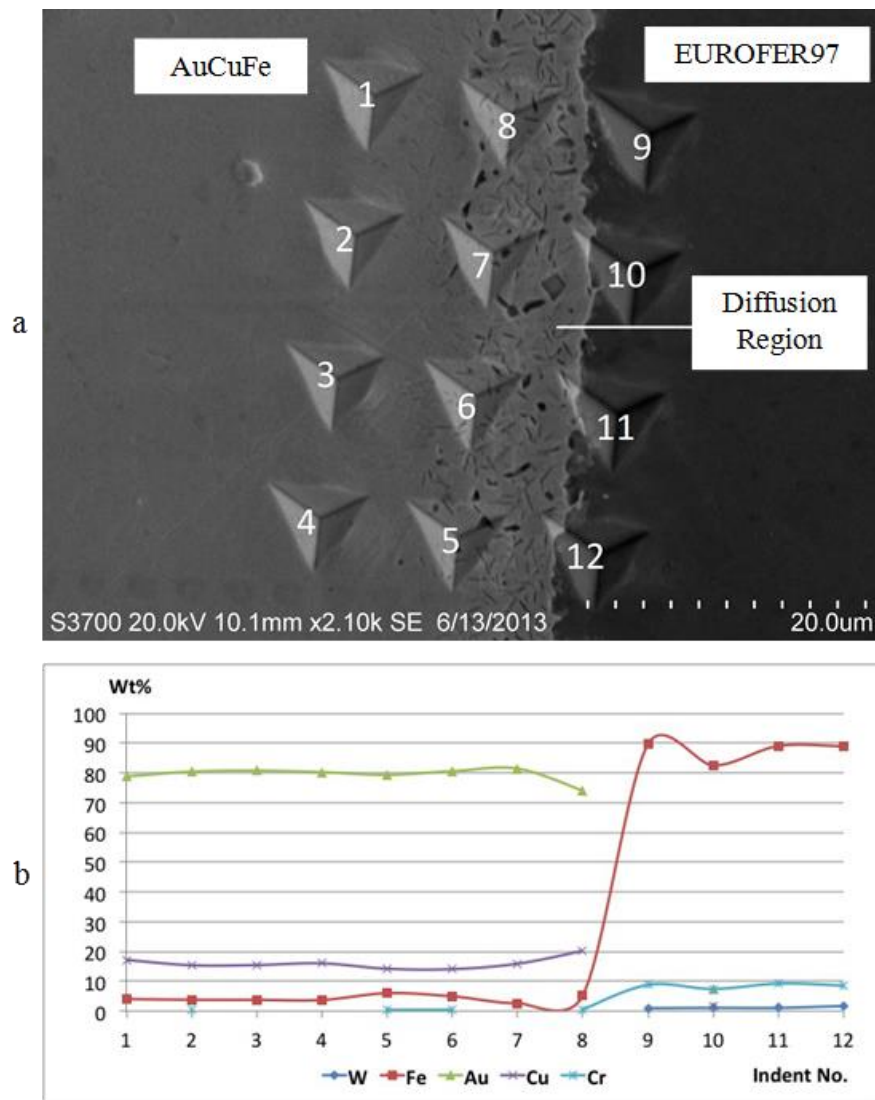
Figure 3- 17: (a) SEM image shows indentation locations

(b) Element compositions of indentations

The results of elastic modulus and hardness are shown in Figure 3-18. The values of modulus and hardness were calculated from 100 - 400nm as the filler and Eurofer 97

are un-etched, and the surface texture is smooth. For the indents 1-4 at filler region, E = 136.98 ± 6.81 GPa, and H = 4.54 ± 0.28 GPa. For the indents 5-8 at diffusion region, E = 140.71 ± 8.78 GPa, and H = 4.11 ± 0.26 GPa. For the indents 5-12 at EUROFER region, E = 235.22 ± 15.11 GPa and H = 3.2 ± 0.77 GPa. The results measured at the diffusion region have similar mechanical properties to those at the AuCuFe filler. This is indicating that no embrittlement effects happened due to the diffusion and interface alloying.
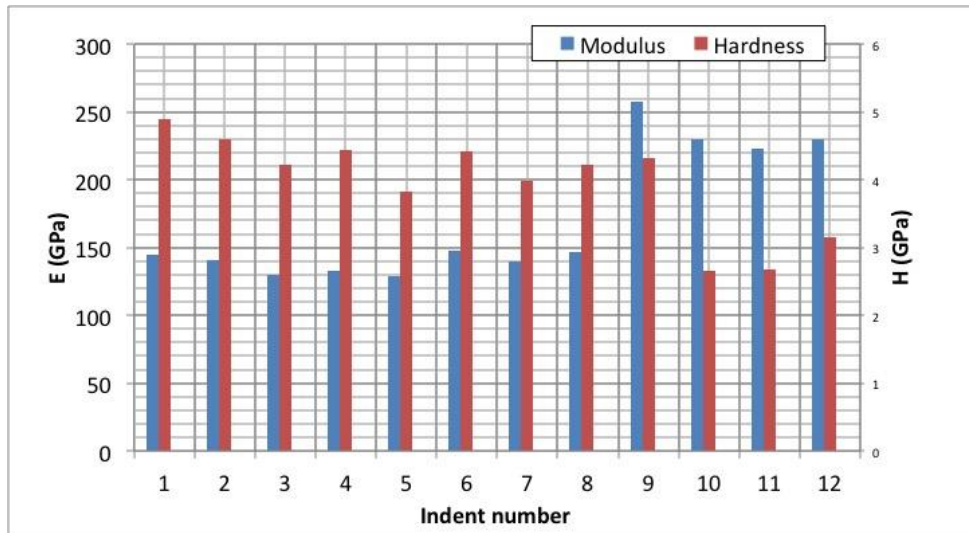
Figure 3- 18: Elastic modulus and Hardness measured from nanoindentation

3.4 W- Cu joint

The brazed joint between W and Cu/Cu alloys are preferred in the water-cooled divertor concept. However, the formation of brittle intermetallic compounds should be avoided in the W-Cu joint, and W solid solution should be minimised. A backscatter SEM image of the joint in Figure 3-19 (a) shows a very smooth diffusion region at the interface between the AuCuFe and Cu. The EDS line analysis location shown in Figure 3-19 (a) used 150 points over 200µm across the brazed layer. In Figure 3-19 (b), the results clearly show that in the brazed joint, the composition of Cu was increased from 19% to about 30% as a result of diffusion. Diffused Au created a smooth transition region around 40 microns thick, and Cu was observed at the interface

between the braze filler and the Cu. Results at the W interface were as reported earlier in the W-W joint.
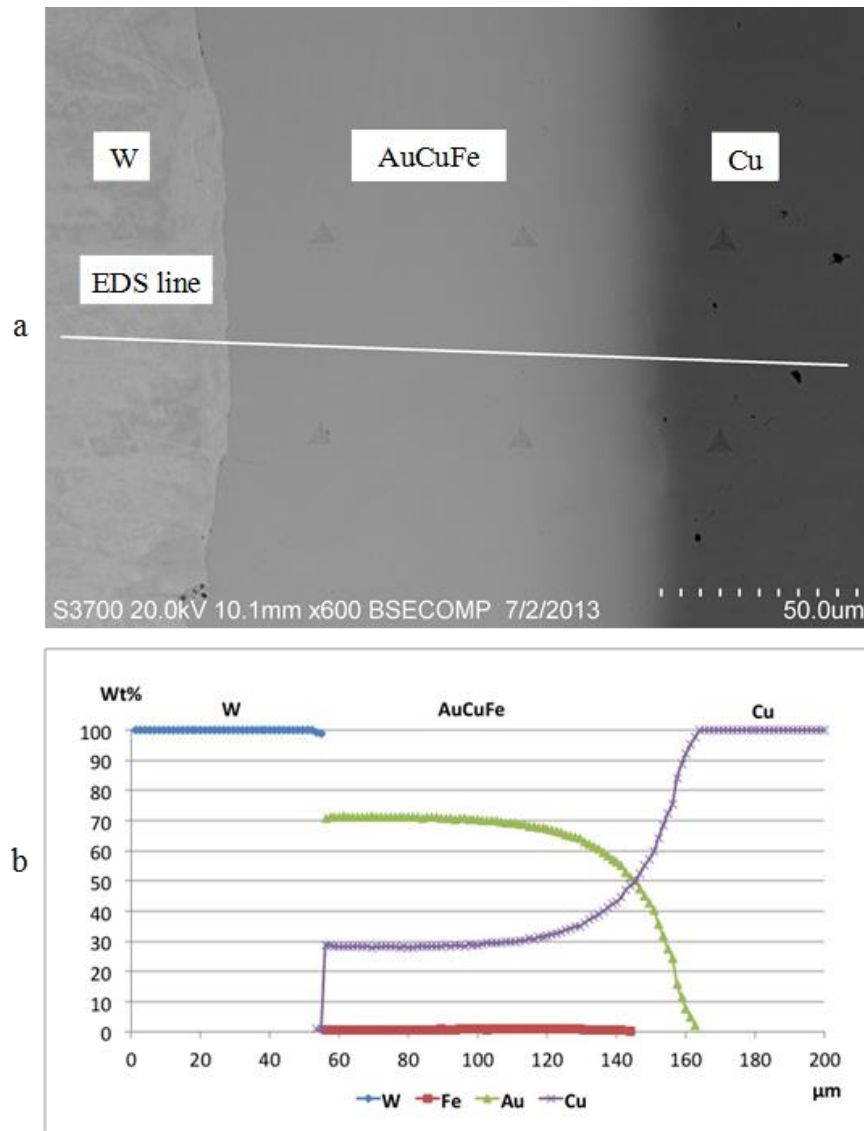
Figure 3- 19: (a) Backscatter SEM image of W-Cu brazed joint

(b) EDS analysis across the joint

Nanoindentation was performed at the interface between the AuCuFe and the Cu, with a maximum indent depth of 800nm. The indents were numbered from 1 to 12, as shown in Figure 3-20 (a) and elemental composition is shown in Figure 3-20 (b). The results for elastic modulus and hardness were also shown in Figure 3-21. Values of E and H measured at filler region were E = 135.04 ± 4.22 GPa and H = 2.39 ± 0.23 GPa. At diffusion region, E = 149.76 ± 4.92 GPa, and H = 1.94 ± 0.27 GPa. At the Cu

region, E = 145.57 ± 1.1 GPa and H = 1.57 ± 0.27 GPa. Compared with other brazed joints, the hardness values measured at the filler region in this joint were distinctly smaller. This is due to the diffusion of Cu from the parent material. The values measured at the diffusion region were similar to those measured in the brazed interlayer (AuCuFe). This shows that the homogeneous conditions produced in this region have resulted in uniform properties across the interface of the brazed joint on the pure copper side whereas, considering the EDS results showed in Figure 3-19 (b), a more heterogeneous and nonuniform property distribution was identified on the pure W side of the brazed joint.
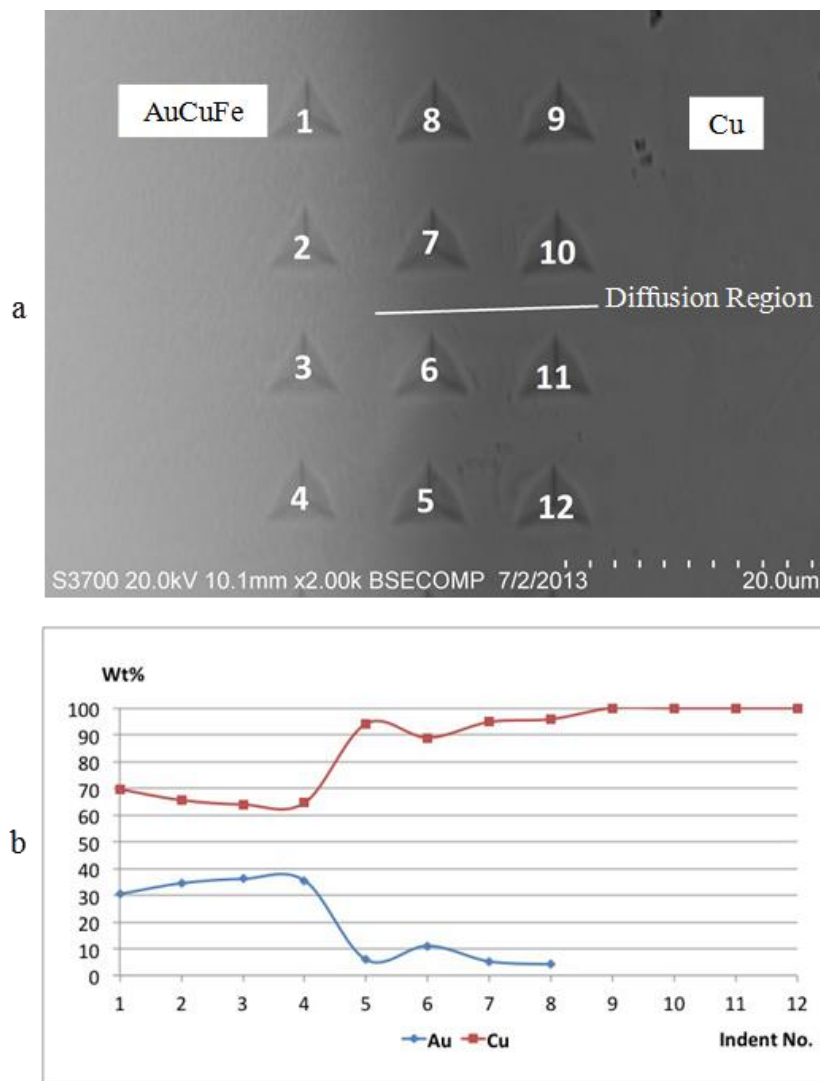
Figure 3- 20: (a) SEM image shows indentation locations

(b) Element compositions of indentations
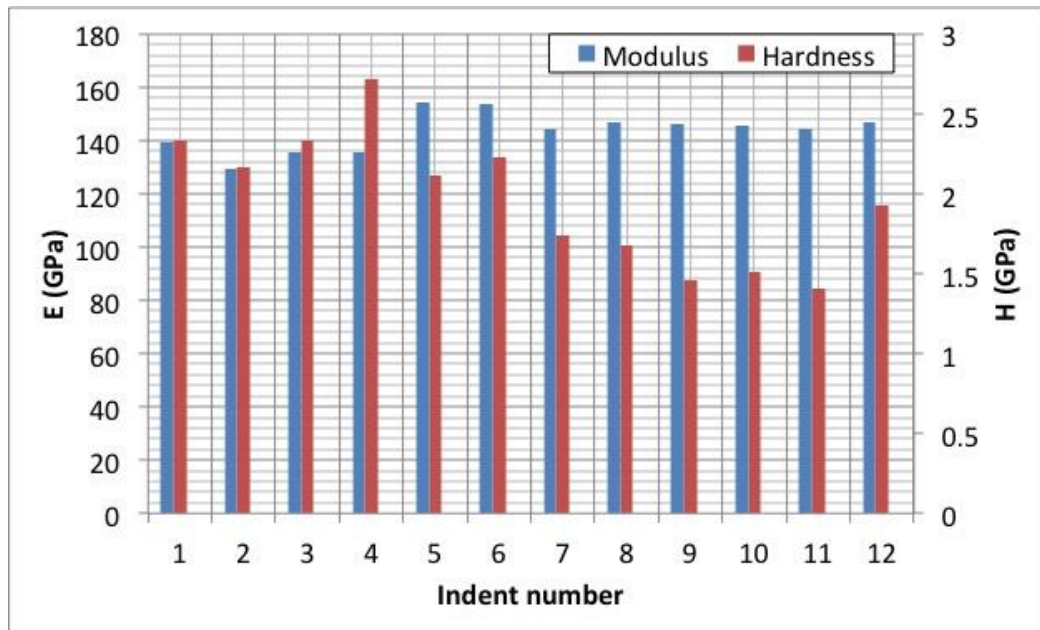
Figure 3- 21: Elastic modulus and Hardness measured from nanoindentation

3.5 W- SS316L joint

SS316L is an additional option for Eurofer steel. SS316L has been selected as the primary structural materials for ITER and a candidate for divertor and blanket design. A backscatter SEM image of the W-SS316L joint is shown in Figure 3-22 (a), and an EDS line analysis was performed across the joint from the W to the SS316L. The analysis took 150 measurements within 125 µm distance across the brazed joint, and elemental transition results were shown in Figure 3-22 (b). Both Fe and Cr diffuse across the filler region, and a region with diffused Fe, Cr and Ni are apparent in the AuCuFe adjacent to the SS316L. Nanoindentation tests were also performed at the interface of the AuCuFe/SS316L with a maximum load of 10 µN and maximum indent depth of 1000nm. The indents were numbered from 1 to 12, as shown in Figure 3-23 (a) and correlated to the composition measurements shown in Figure 3-23 (b). Indents 1 to 4 were located in the AuCuFe, 5 to 8 were located in the diffusion region, and 9 to 12 were located in the SS316L. The results of elastic modulus and hardness were shown in Figure 3-24. Values measured at filler region were E = 135.27 ± 1.34 GPa and H = 4.12 ± 0.06 GPa. At diffusion region, E = 141.58 ± 2.82 GPa, and H = 3.75

± 0.0.09 GPa. At SS316L region, E = 207.7 ± 1.93 GPa and H = 3.45 ± 0.27 GPa. No embrittlement effects relating to high hardness due to diffusion were detected at the interface. The measurements at the diffusion region show similar mechanical properties to those in the AuCuFe filler.
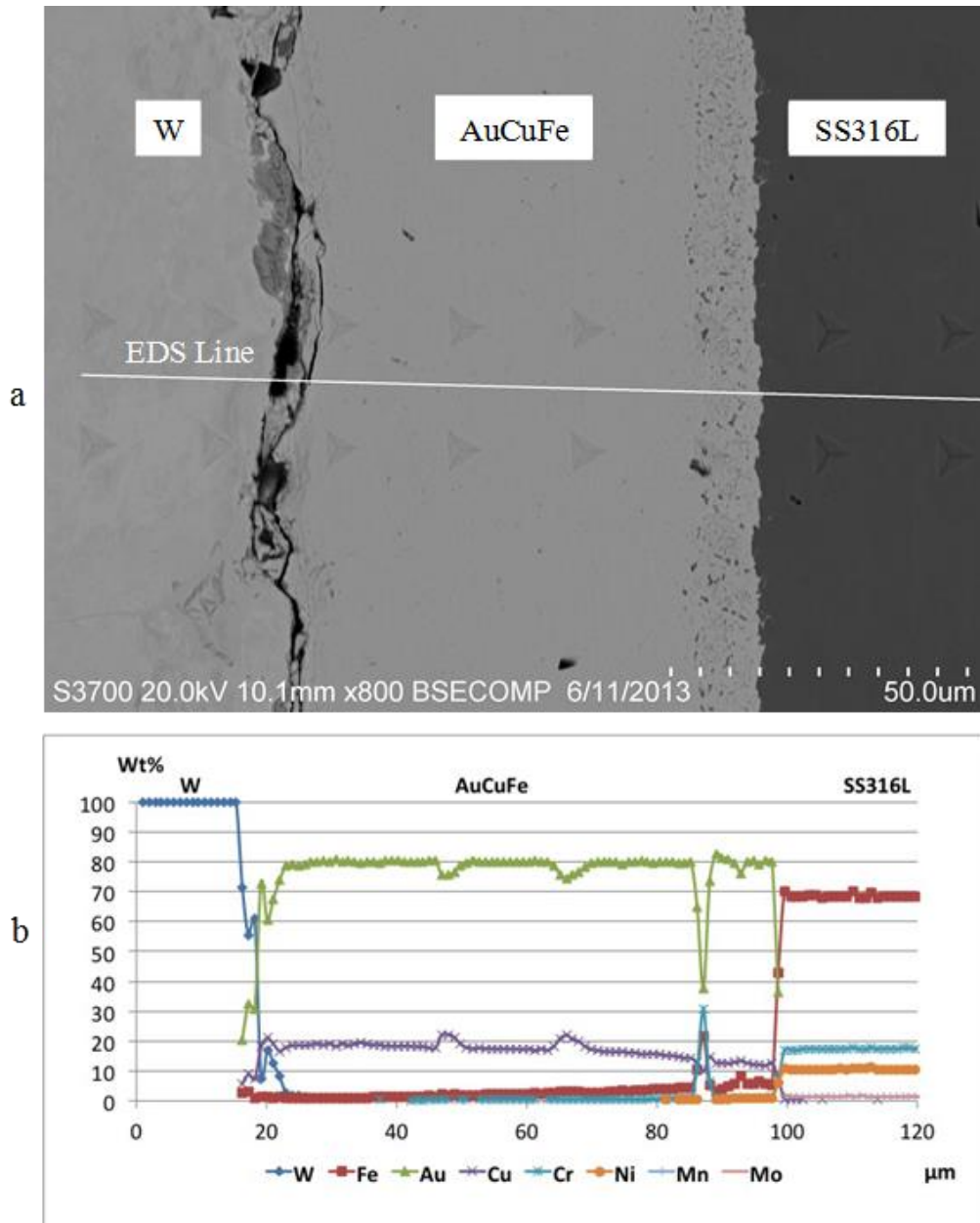
Figure 3- 22: (a) Backscatter SEM image of W-Cu brazed joint

(b) EDS analysis across the joint
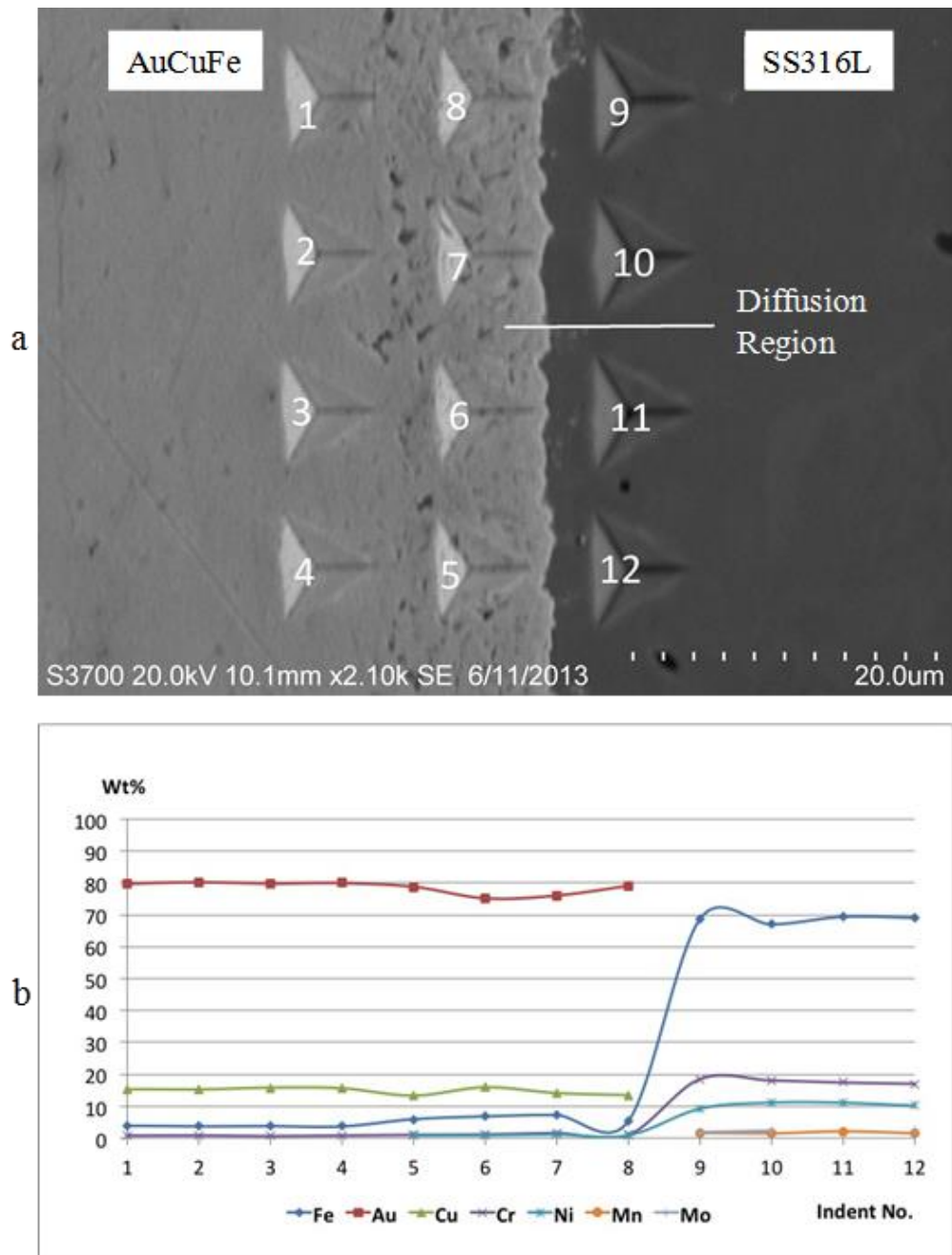
Figure 3- 23: (a) SEM image shows indentation locations

(b) Element compositions of indentations
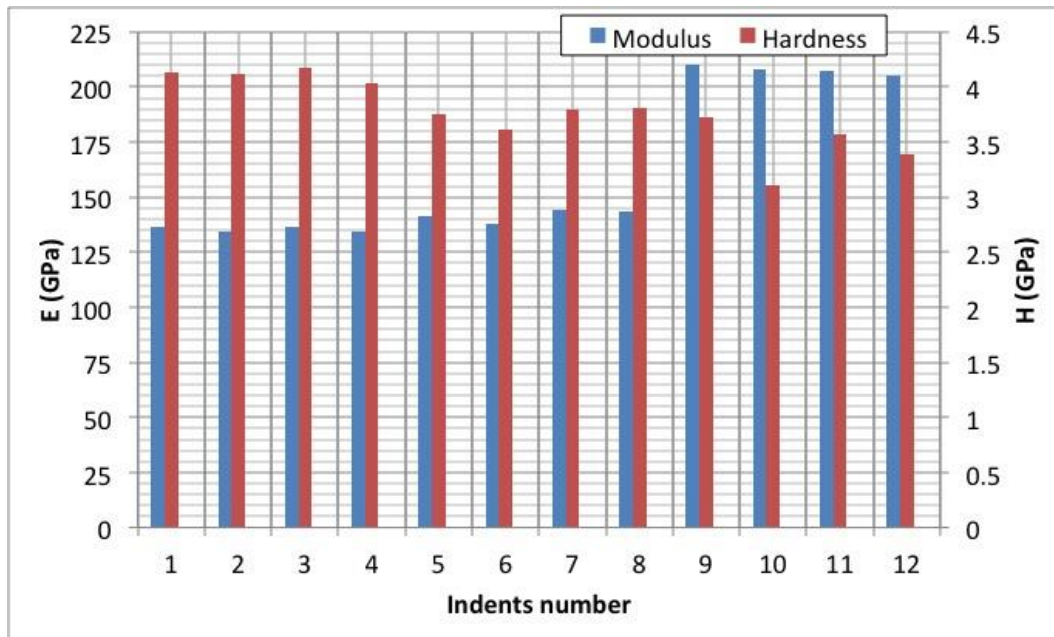
Figure 3- 24: Elastic modulus and Hardness values measured from nanoindentation

3.6 Key findings of the metallurgy and mechanical properties in the brazed joints created with Au80Cu19Fe1

This thesis section is part of a project aimed at designing and fabricating reliable brazed joints between W and other dissimilar materials. The samples were furnace brazed in butt joint form under vacuum with Au80Cu19Fe1 filler. EDS analysis and nanoindentation were performed at the joint to understand interfacial metallurgy and generate elastic modulus and nano-hardness values. The results of this study can be concluded as follows:

3.6.1 W-W

The microstructures and hardness of W did not change due to brazing. AuCuFe filler creates a uniform joint between W butts. The EDS analysis did not detect elemental transition at the brazed interface between the W and AuCuFe filler. However, melted filler material penetrating the W was observed by optical microscopy. This is likely to be due to grain boundary diffusion or micro cracks on the W surface that have been

filled with brazing material. A further analysis detected no filler material penetration and elemental transitions beyond 1 µm from the interface.

Nanoindentations were performed at the interface between the AuCuFe and W. The elastic modulus and hardness values measured in the AuCuFe were constant, while the modulus and hardness measured in the W side adjacent to the braze show larger variations because of surface conditions.

3.6.2 W-EUROFER 97

The presence of carbide precipitated phases leading to a large increase of micro-hardness was detected in the post brazing specimen. This increase in hardness also indicates an increase in yield and tensile stress but a decrease in ductility and toughness.

An EDS line analysis performed across the brazed layer showed no elemental transitions either from W to AuCuFe or AuCuFe to W. A transition region with complex microstructures were observed at the interface between the AuCuFe filler and the EUROFER 97 after brazing. Elemental mapping analysis confirmed that the transition region consisted of diffused Fe microstructures. Nanoindentations were performed at the adjacent region between the AuCuFe and the EUROFER 97, and the transition region showed similar mechanical properties to the AuCuFe filler. No embrittlement effects due to diffusion were detected at the interface of AuCuFe and EUROFER 97.

3.6.3 W-Cu

Significant grain growth, leading to a large micro-hardness reduction, was detected in the post brazing Cu. No elemental transitions were detected at the W and AuCuFe interface. A very smooth elemental transition was detected at the adjacent region between the AuCuFe and Cu. The smooth transition of elements indicated that the material properties are changing smoothly. The mechanical properties of the diffusion region were similar to the braze layer. The homogenous conditions

produced in this region resulted in uniform properties across the brazed joint interface on the pure copper side.

3.6.4 W-SS316L

Recrystallised grains were detected in the post brazing specimen, and the micro-hardness of SS316L decreases. The EDS line analysis performed across the brazed layer found no elemental transitions at the W and AuCuFe interface. A transition region created at the adjacent region between the AuCuFe and SS316L was detected. No embrittlement effects due to diffusion were detected at the interface.

3. 7 Summary of Au80Cu19Fe1 filler

• AuCuFe filler can be used to fabricate brazed joint between W and the dissimilar materials considered, EUROFER 97, Cu and SS316L, and create a uniform brazed layer.

• The finial formation of brazed layers has maintained the joint clearance and showed no reduction in thicknesses.

• The parent materials showed no evidence of erosion under these brazing conditions.

• No elemental transitions were detected between the W and the AuCuFe filler in either direction.

• No W solid solutions or intermetallic compounds were found in the joint.

• No evidence of oxidations was detected.

• Transition regions between the AuCuFe filler to EUROFER97/316L showed similar elastic modulus and hardness to the braze filler.

• A very smooth elemental transition was detected between the AuCuFe filler and Cu. This would indicate that the material properties were changing smoothly from filler to Cu.

- Due to the abrupt change of chemical compositions and material properties at the interface between W and AuCuFe, different degrees of diffusion exist at the interfaces between AuCuFe and Eurofer 97/SS316l/Cu, the W/AuCuFe interface is likely to be the most critical area in all the brazed joints created here. The maximum stress concentration under mechanical or thermal loadings should be at the free edge along with the W/AuCuFe interface.

4 Metallurgical study of Au80Cu20 brazed joints using vacuum brazing and induction brazing

4.1 Introduction

Chapter 2 presented the first stage of brazing work for the joining of short butt specimens with the gold-based Au80Cu19Fe filler and the interfacial study of the brazed layers. Various defects were reported, including bonding imperfections, recessed brazed fillets, cavities, pores, and gap filling imperfections. Moreover, the total coverage of the brazed layer was around 70% of the joint interface, which is not acceptable according to the nuclear codes.

As discussed in section 1.5.2, the defects within the brazed layers can strongly influence the strength of the brazed joints. The local geometries at the free edges of the brazed layers, e.g. recessed brazed fillet, can result in local stress concentrations (LSC) and stress singularities. Furthermore, considering the function of plasma-facing components, these defects will also reduce the heat removal capacity of the brazed layers. This thesis is a part of a project aiming to design and fabricate reliable brazed joints between W and other fusion candidate materials for characterisation. Consequently, to obtain qualified brazed specimens, an important aspect of brazing assessment quality, this chapter presents the development of optimised furnace brazing procedures based on the experiences obtained from the earlier work. In this case, an induction brazing process is developed for fabricating brazed specimens with consistent quality.

4.2 Considerations of developing dissimilar brazed specimens

The characterisation and interfacial studies in the previous chapter has shown that the gold-based filler Au80Cu19Fe1 is generally capable of creating uniform brazed layers between W and the dissimilar materials considered for DEMO divertor components EUROFER 97, OHFC Cu and SS316L. The brazed layers are free from detrimental W solid solutions and intermetallic compounds, which shows that Au80Cu19Fe1 is a very promising filler. Nevertheless, as discussed in section 3.3.3, various defects have been detected in these brazed joints, and these defects will lead

to uncertainty in mechanical testing. Therefore, the following development based on the experiences gained from Au80Cu19Fe1 filler should optimise furnace brazing procedures in order to obtain defects free brazed specimens.

Besides considerations relating to defects within the brazed layers, mechanical testing also raises specific requirements for the quality of brazed joints. BS EN 12797:2000 [90] and AWS C3.2M/C3.2: 2008 [91] have provided guidance for standard mechanical testing of brazed joints, including specimen designs and preparation, brazing and post brazing procedures. BS 7910:2013 [92] has provided some guidelines for assessing the acceptability of flaws in relation and shape imperfection relating to the fatigue performance in welded structures. Considering the similar nature of welding and brazing, these guidelines can be adopted for reference. BS 7910 recommends that besides the butt-welded joint's flaws, the shape imperfections, e.g., misalignment, undercut and local thinned areas caused by corrosion/erosion, should be assessed in fatigue testing. Therefore, the design objective of the induction brazing procedure in this work is to minimise the misalignment of butt brazed joints. Figure 4-1 shows the basic types of misalignment in butt brazed joints: axial and angular.
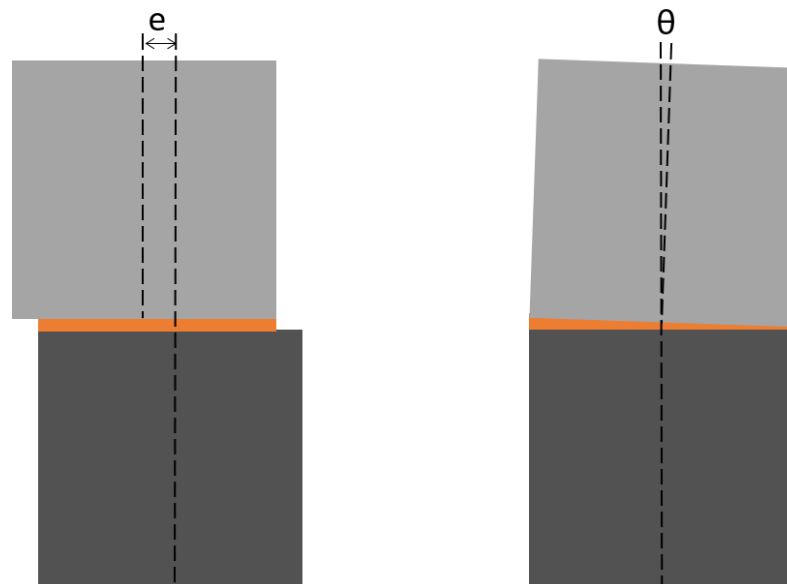
Figure 4- 1: Schematic of two basic forms of misalignment in butt brazed specimens: Axial (left) and Angular (right)

4.3   Optimised furnace brazing procedures and results

It should be emphasised that the brazing filler metal has been changed from 'Orobraze 910' Au80Cu19Fe1 to the new 'Orobraze 890' Au80Cu20, both are supplied from Johnson Matthey. In Johnson Matthey's and their previous publication [47], the iron was added to the Au80Cu20 metal to control/block the order-disorder transformation which occurs in this alloy during the mechanically cold working and results in cracking issues during manufacturing. The new Au80Cu20 filler metal has replaced the obsolete Au80Cu19Fe1 filler following the upgrade of manufacturing techniques. Both filler metals are equivalent and have the same brazing characteristics, properties and mechanical performance. The major difference between these two fillers is the working temperature: Au80Cu19Fe1 has a working temperature of 908-910 °C while Au80Cu20 has a fixed melting temperature of 890 °C. The Au80Cu20 filler used in this chapter was also supplied as a foil with a thickness of 0.0508 mm (0.002 inches). The specimens of W, OFHC copper and SS316L are Φ12.7 x 10 mm cylinders, and the Eurofer 97 are Φ10 x 10 mm cylinders. The parent materials used for vacuum furnace brazing were the same as those used in Chapter 3 and CNC lathed. The W used for induction brazing development was produced by EDM wire cutting.

The brazing procedures are optimised based on the experiences obtained from the study reported in Chapter 2 in order to increase the quality of brazed joints and create defects free specimens. According to Chapter 2, the brazed layers created by Au80Cu19Fe1 filler are uniform across the jointed region, but they all contain defects that are not acceptable according to the nuclear design codes. At the current stage of work, only short butt parent materials are brazed. Development of brazing full-sized dissimilar specimens is discussed in the future work section.

In the previous brazing development work, the as supplied filler metal foil was punched into Φ10 mm disks which were smaller than the joint interface areas of parent material samples. The microstructural observations and elemental analysis of the brazed layers developed in Chapter 3 demonstrated that the brazed layers' final

formations maintained the set joint clearances, which is the thickness of the filler foils. This led to a suspicion that the unbonded and unfilled regions in the brazed layers are likely to be due to insufficient filler metal. Therefore, this chapter's experiments used Au80Cu20 foils punched into disks of the same diameters as the parent materials.

Instead of using an experimental set up with add-on weights in Chapter 2, new set up jigs, shown in Figure 4-2, were used to align the pre-brazed specimens. The materials were thoroughly cleaned by an ultrasonic alcohol bath and then a final cleaning with acetone. The specimens were then carefully aligned and heavily clamped by tightening the bolts. All specimens are set in the vacuum muffle furnace and brazed at a vacuum level of 1×10^{-4} to 1×10^{-5} millibar. The furnace heating cycle of brazing was set to heat up by a rate of 10 °C/min to T_{braze} 950°C, which is 60°C higher than the melting point of Au80Cu20 filler. The furnace dwelled at T_{braze} for 5 minutes and then slowly cooled down over several hours to avoid thermal shock.
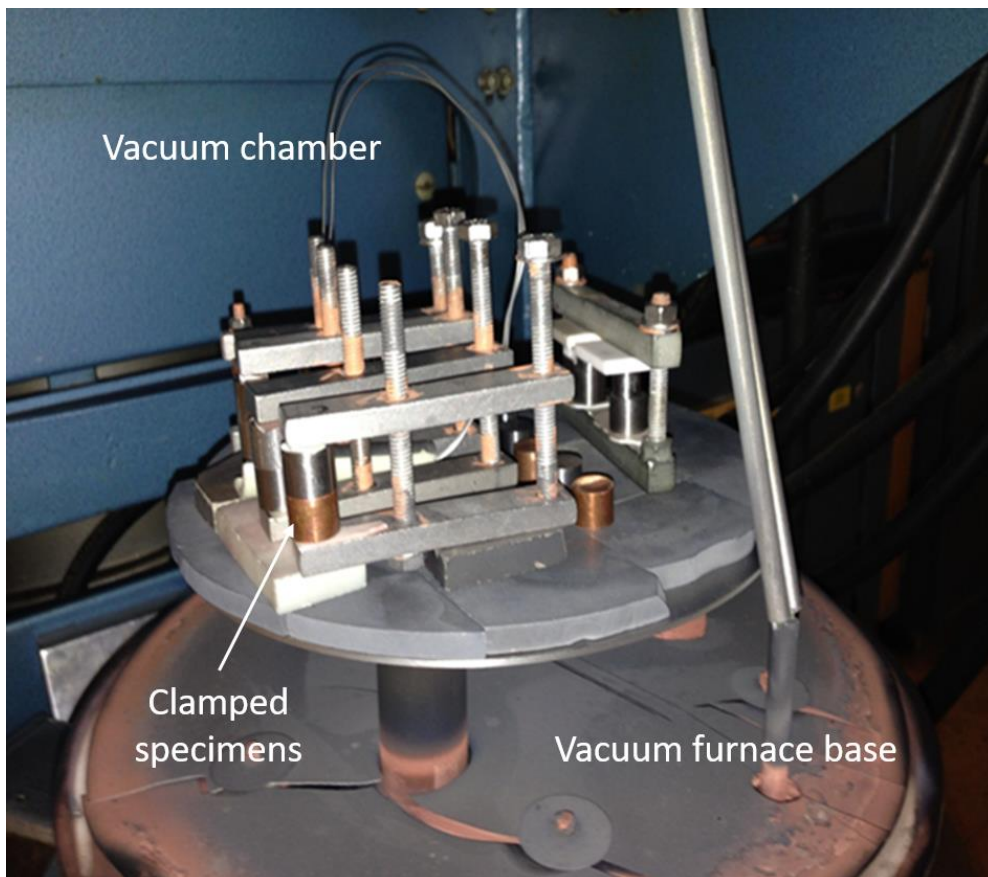
Figure 4- 2: Vacuum furnace brazing set up
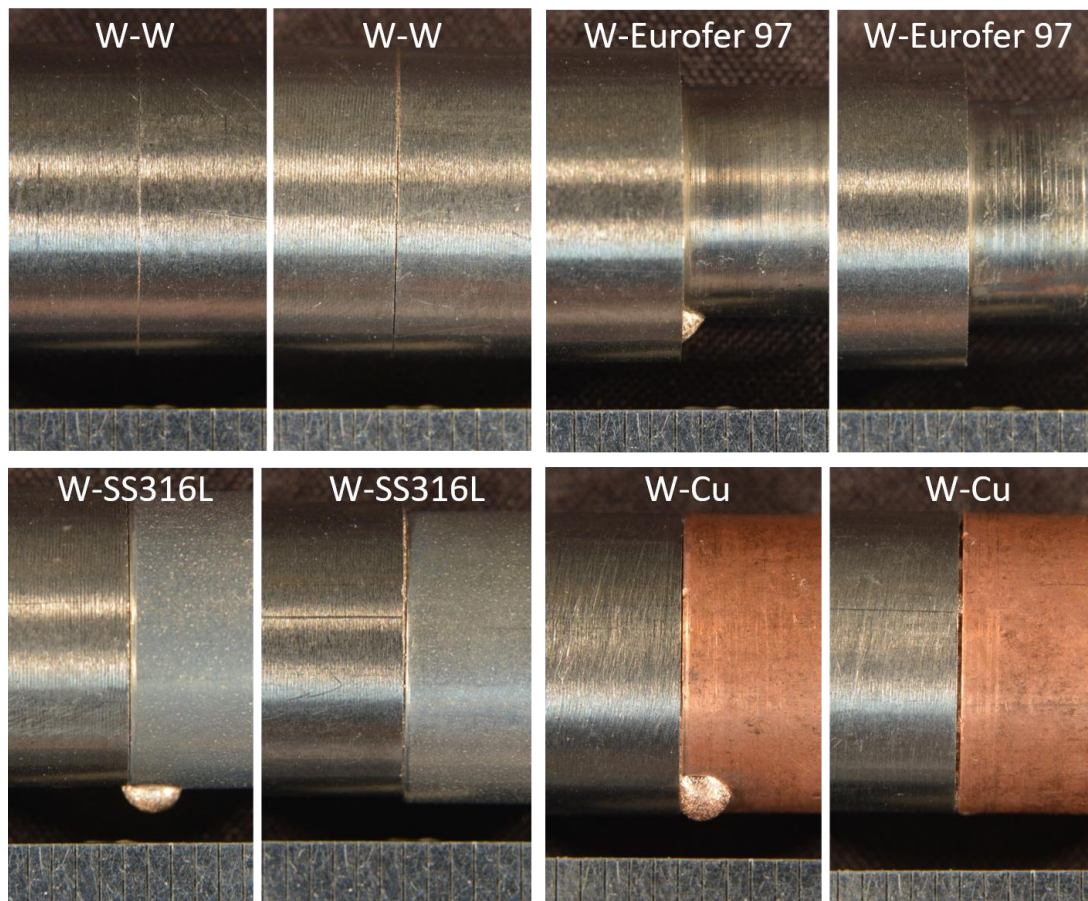
Figure 4- 3: The brazed joints viewed at 6× magnification

For each material combination, two short butt specimens were brazed for inspection. Figure 4-3 are photos of all the dissimilar brazed joints taken by a bench-mounted camera with a 6x magnification lens, and visual inspection are performed to comply with the guidance of British standard BS EN 12799:2000 [93]. The observations can be summarised as follows:

- All the brazed layers are uniform and continuous
- Recessed fillets can be detected in all specimens, but it isn't easy to estimate the depth of the recess
- Excess filler metal is detected in the W-Eurofer 97, W-SS316L and W-Cu specimens
- The W-W and W-Cu specimens are well aligned, while axial misalignments can be detected in the W-SS316L specimens.

4.4 Development of induction brazing

4.4.1 Background of induction heating

Induction heating is one of the typical heat sources for brazing along with other sources like furnace, torch, infrared, etc. During the induction heating process, the heat is generated within the workpiece by electro-magnetic induction, which is a non-contact and uniform process. As illustrated in Figure 4-4, the inductor is similar to a primary electrical transformer, and the workpiece is equivalent to the secondary transformer [94]. The fundamental part of an induction heating machine is a high-frequency generator that generates high-frequency alternating currents [95]. An inductive coil connected to the generator produces a high-frequency electro-magnetic field which will induce electrical currents, so-called the eddy currents, in the electrically-conductive workpiece positioned within or near the coil [95], [96]. Then, the electrical resistance of the workpiece and the induced eddy current will generate heating power and heat the workpiece [34], [96].
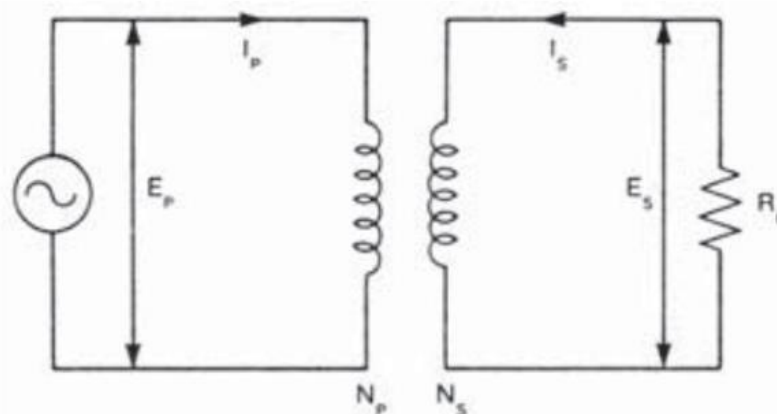
E_p = primary voltage (V); I_p = primary current (A); N_p = number of primary turns; I_s = secondary current (A); N_s = number of secondary turns; E_s = secondary voltage (V); R_l = load resistance(Ω)

Figure 4- 4: Electrical circuit illustrating the induction heating and the transformer, reproduced from [94]

Induction heating can also be applied to non-conductive materials by adding a conductive material as the heat conductor, e.g. graphite. The joint clearance for brazing is recommended to be 0.038 to 0.050 mm [34].

Compared to the vacuum furnace brazing process used in this work, induction heating has the following benefits [34], [95]:

- The heating cycle of induction brazing is very fast compared with furnace heating
- The induction heating region can be controlled and targeted to the workpiece
- The non-contact heating process minimised material contamination
- Induction brazing can produce consistent and repeatable results because the key brazing parameters such as input currents, heating-up and holding time, and working temperature can be well controlled.
- The heating process is uniform and easy to control

The disadvantages of induction brazing are the geometric limitations of the induction coil and the requirement of preproduction development work for brazing processes. Therefore, the principal objective of developing induction brazing in this work is to design appropriate induction heating processes to create consistent brazing specimens rapidly.

4.4.2 The induction heater, induction coils and vacuum vessel

A water-cooled induction heater, Yuelon Model HF-25kW, was specially selected to perform the brazing and casting work, and the specification of the unit is shown in Table 4-1. This machine can convert a 3 phase 380 V power supply to 25 kW output power with the frequencies range 30 - 80 kHz and the currents range 200 – 1000 Amps. The 25kW output power makes the machine capable of melting a maximum 4 kg of metal. The frequency is adjusted by the heater depending on the geometry and material properties of the workpiece. An infrared sensor, Optris Model CT 2MH, equipped with a digital temperature programmer, is installed on the heater for precisely controlling the heat cycles. The sensor has a temperature measurement

range of 200 to 1500°C, and the system accuracy is 2 °C + 0.3% of reading. The heater can be operated either manually with a remote foot pedal or automatically by pre-setting the programmer.

Table 4- 1: Specifications of Yuelon Model HF-25kW induction heater

Output Voltage	Output power	Output frequency	Heating current	Retaining current	Cooling water pressure
380 V± 10%	25 kW	30-80 kHz	200-1000 A	200-1000 A	0.05-0.2 MPa

The critical nature of induction heating is that the induced eddy currents are generated on the surface of a workpiece and diminish toward the interior, and this is called the skin effect [34], [96]. The depth of the skin effect depends on the output frequency of alternating currents, material properties of the workpiece, and the output current in the coil [34]. The higher the output frequency of alternating currents, the faster heating with the swallower heating penetration depth. Practically, heating smaller samples with induction require higher frequencies (> 50 kHz) and larger samples are more efficiently heated with lower frequencies (>10 kHz) and more heating penetration depth [97]. Therefore, the selected induction heater has the 30-80 kHz frequencies range, which can cover both the lower and higher frequencies, and the heater can adjust the operation frequencies depending on the volume and properties of the workpiece. With correct selections of induction coils, it can heat various types of workpiece up to the brazing temperature efficiently.

The induction coils are usually made from high conductivity annealed copper tube with water passing through as the coolant [95]. The coils can vary in shape and size depending on the characteristics of the workpiece. 2 different copper coils, as shown in Figure 4-5, were designed by the author and manufactured by the supplier. Both coils are multiturn round type, both insulated with glass fibre clothes.

The smaller coil is 50 mm in diameter and 50 mm in height and was tightly wound 6 turns to generate a relatively intense magnetic field in the centre and achieve high heating efficiency for quickly heating small target regions or melting. With the infrared sensor and programmer, this coil can also be used for performing thermal testing. This coil was used for air casting/brazing, which will be discussed in Chapter 5.

The larger coil is 90 mm in diameter and 150 mm in height and loosely wound 6 turns with greater gaps (approx. 30 mm) between each coil turn. This will result in a reduced eddy current flux and a lower heating efficiency compared with the smaller coil. This coil was designed to comply with the requirements of using a vacuum vessel set for performing vacuum or controlled atmosphere brazing.

Figure 4- 5: Two different induction coils containing the same graphite crucible.
Left: Φ50 x 50 mm, 6 turns; Right: Φ90 x 150 mm, 6 turns.

Figure 4- 6: Assembly of the vacuum vessel

A setup of a vacuum vessel was selected to carry the vacuum induction brazing work. The vacuum vessel included an 80 mm OD quartz tube, a high purity graphite crucible (50 mm OD × 35.9 mm ID × 77.5 mm H), a set of Al_2O_3 holder and lid for holding the graphite crucible, and a vacuum flange with a mechanical pressure gauge and two valves for inert gas/vacuum release. The parts and assembly of the vacuum vessel are shown in Figure 4-6.

One of the critical features of induction heating is that the electro-magnetic energy flux is most concentrated close to the coil turns, and decreases farther from the coil. Therefore the geometric centre of the coil is a weak flux path [94]. Consequently, to get maximum energy transfer, the coil should be coupled to the workpiece as closely as possible. Whereas a workpiece placed off centre in a round coil will lead to a non-

uniform heating pattern, as shown in Figure 4-7 [94]. Thus, the workpiece should be positioned in the geometric centre of the coil to achieve a uniform heating pattern that is very important for brazing. A commonly used method to solve this issue is to introduce a susceptor made of graphite.

Because the volumes of brazing specimens (Φ12.7 × 10 mm) are relatively small compared with the coil (Φ90 × 150 mm), it cannot absorb enough electro-magnetic flux for conversion into heat. Therefore, in this setup, the graphite crucible is used as a susceptor to increase the heating efficiency and to contain the workpiece. The graphite crucible can be heated up efficiently and uniformly by the coil with a smaller coupling distance to the coil, and the pre-brazing setup specimens in the graphite crucible can be heated by the means of thermal radiation and conduction.
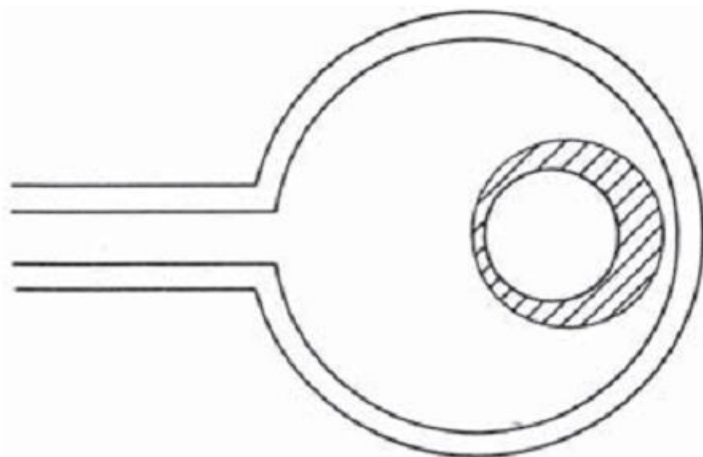
Figure 4- 7: Induction heating pattern proceeded in a round bar placed off centre in a round induction coil [94]

The ceramic holder can closely accommodate the crucible inside, as shown in Figure 4-6. The holder is made of Al_2O_3, which has a very low coefficient of thermal conductivity. Thus, it is acting as insulation to protect the quartz tube from the heated workpiece and also improving the heating efficiency.

Quartz is commonly used in induction heating applications as it is not affected by electro-magnetic fields, can work under high pressures and temperatures, and is also suitable for use with the infrared sensor. The quartz tube is sealed at the top by the vacuum flange with a combination of rubber sealing rings. Before brazing, the ceramic holder holding the crucible and workpiece can be arranged to be positioned in the centre of the quartz tube, as shown in Figure 4-6. The assembled vacuum vessel is connected to a vacuum pump and an inert gas inlet and is operated by two valves.

Figure 4-8 shows the final setup of the induction heater with the vacuum vessel positioned in the larger coil. A metal stand was used to grip the vessel, and an infrared sensor targeting directly to the crucible. A disadvantage of performing brazing with this system is the vacuum vessel must be re-assembled after each experiment, but the efficiency improves with the increase of the operator's proficiency.
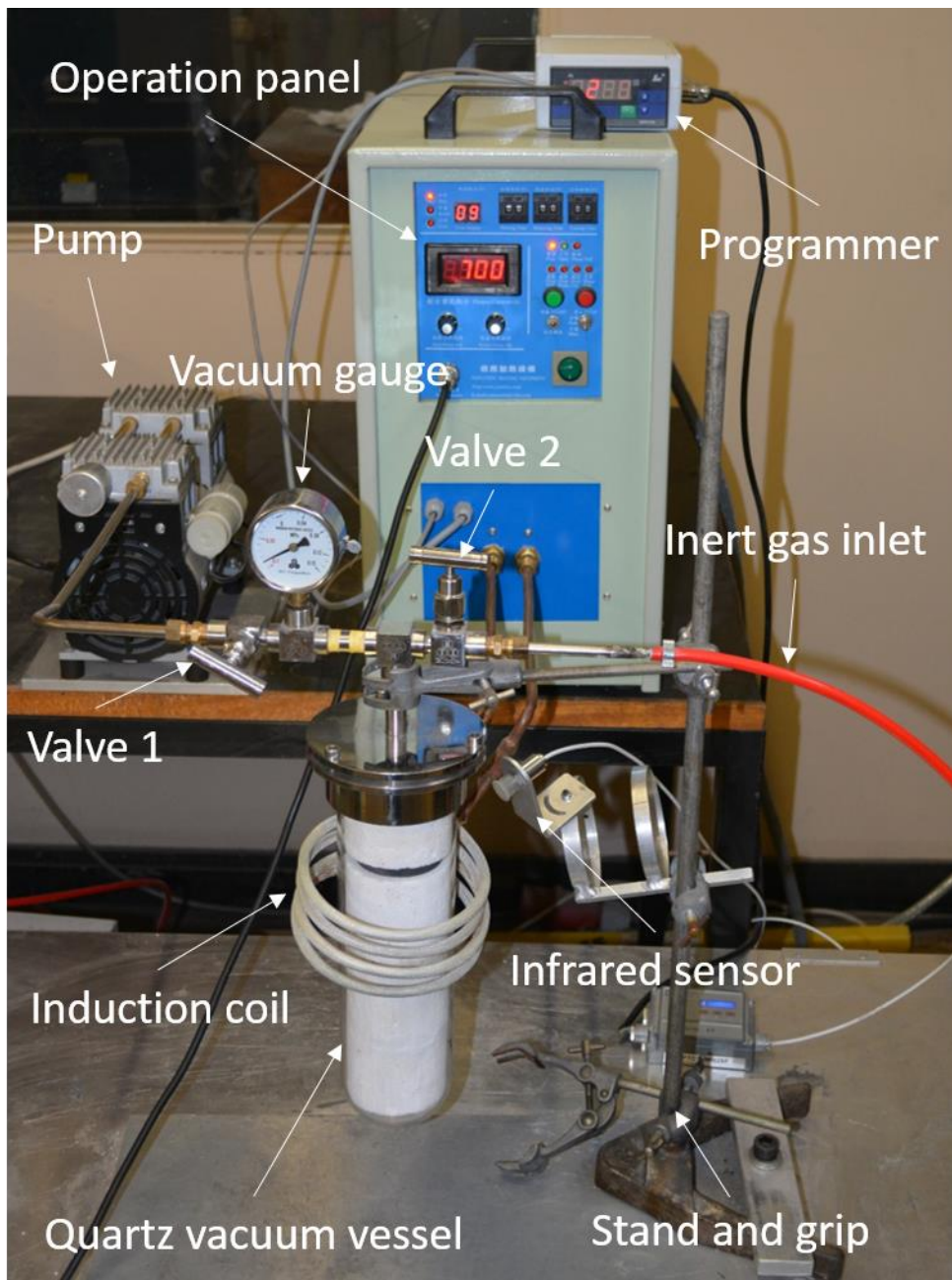
Figure 4- 8: Experiment setup of the induction heater and vacuum vessel

4.4.3 Design of the gripping device for induction brazing

As discussed in Section 4.2, geometry misalignment (angular and axial) should be minimised in the butt brazed specimens. Therefore, a gripping device needs to be designed to precisely align the pre-brazing workpiece in the graphite crucible.

Considering the specific needs for butt brazing and experiences gains based on previously unpublished work, the design should meet the following technical requirements:

- Allow effective alignment of the pre-brazing workpiece.
- Securely hold the workpiece within the vacuum vessel.
- Should be functional at the working temperature.
- Be able to cope with the thermal expansion of the workpiece in both axial and radial direction.
- Should not prevent the workpiece from the heating source.
- Should avoid contacting the braze region to prevent unwanted capillary action.
- Should be capable of applying sufficient axial loading to prevent the surface tension of the liquidus filler metal pushing the parent materials apart.
- Should avoid applying excess axial loading that can squeeze the liquidus filler metal out from the interface.
- Should be relatively easy to manufacture.

Various designs have been considered, and a concept as shown in Figure 4-9 was chosen. This concept consists of two platforms connected by three vertical supports, and the workpiece is gripped at the centre between the top and bottom. As shown in Figure 4-9, the top platform can be either with a centre-locating pin or a flat platform to provide two different gripping mechanisms. The pin can precisely grip specimens with locating marks at the top, e.g., a small indentation. The flat-top can be used as a universal grip. The device uses three vertical studs to connect the platforms to provide stabilised gripping force, and the studs connect the platforms using clearance holes and nuts. This design is capable of aligning and gripping the pre-brazing samples securely without interfering with the brazing regions. Technical drawings of the parts of the device are attached in Appendix 1-3.

All the parts of the device were made from 316L stainless steel and dimensions were designed based on the size of the crucible and the thermal expansion of the device.
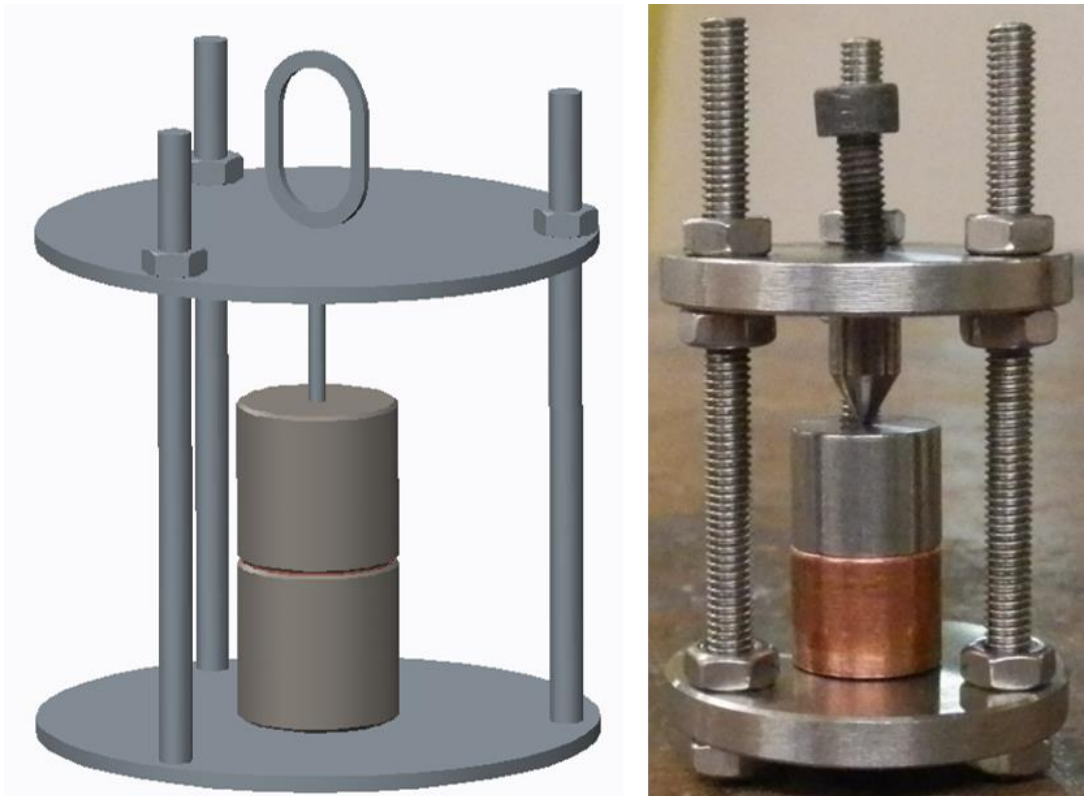
Figure 4- 9: Gripping device concept and assemblies two different ways of grips

4.4.3 Induction brazing experiment procedures and results

Preproduction experiments with various brazing parameters were performed to confirm the best procedures for harvesting qualified brazed specimens. The parameters considered are listed in Table 4-2.

Table 4- 2: Parameters considered for induction brazing experiments

Temperature (°C)	Holding time (Min)	Gripping type	Gripping level
900, 950, 1050	1, 1.5, 2, 5	Pin, Flat	Moderate, Severe

The output heating current used for brazing work was firstly verified by manual operation. The output current should efficiently heat the workpiece to working temperature whilst not resulting in non-uniform heating or overheating. Based on the results of practices, the output current was set as 700 amps throughout the work.

It took 110 seconds for the machine to heat the graphite crucible in the vacuum vessel from room temperature to 950 °C, which is the recommended brazing temperature for Au80Cu filler.

The ceramic crucible holder can absorb moistures in the air over time and released moistures during heating in the vacuum vessel. The moistures will react with the brazing workpiece and cause corrosions which result in the failure of brazing. Therefore, the vacuum vessel must be preheated before carrying out brazing work. The vacuum vessel can be heated with a lower output current, i.e. 300-500 amps to 250 °C and held for 20 minutes. Moistures can be drawn out of the vessel by the vacuum pump during the preheating process.

Two different gripping levels were applied to assemble the specimens by thread tightening. The moderate level gripped aligned specimens firmly enough, so they did not move during the brazing. The severe level gripped the specimens with great force by excessively tightening the nuts.

The vacuum vessel and specimens must be reassembled for each experiment. The vessel was drawn to a vacuum level of 1×10^2 millibars and held steadily for 1 minute. Then the vessel was slowly filled with argon and held for 1 minute. And after that, the vessel was drawn vacuum again. This process was repeated three times for each individual experiment in order to achieve a stable brazing environment.

Verification experiments were carried out with W-W joints and then proceeded to W-Cu joints. The various brazing parameters showed in Table 4-2 were examined by experiments. With 700 amps output current, the induction machine heated the vessel to 950 °C in 110s. Then the temperature was held at 950 °C for 2 minutes, and then the vessel was left to cool down with retained vacuum. The crucible cooling took around 100 minutes to below 200°C.
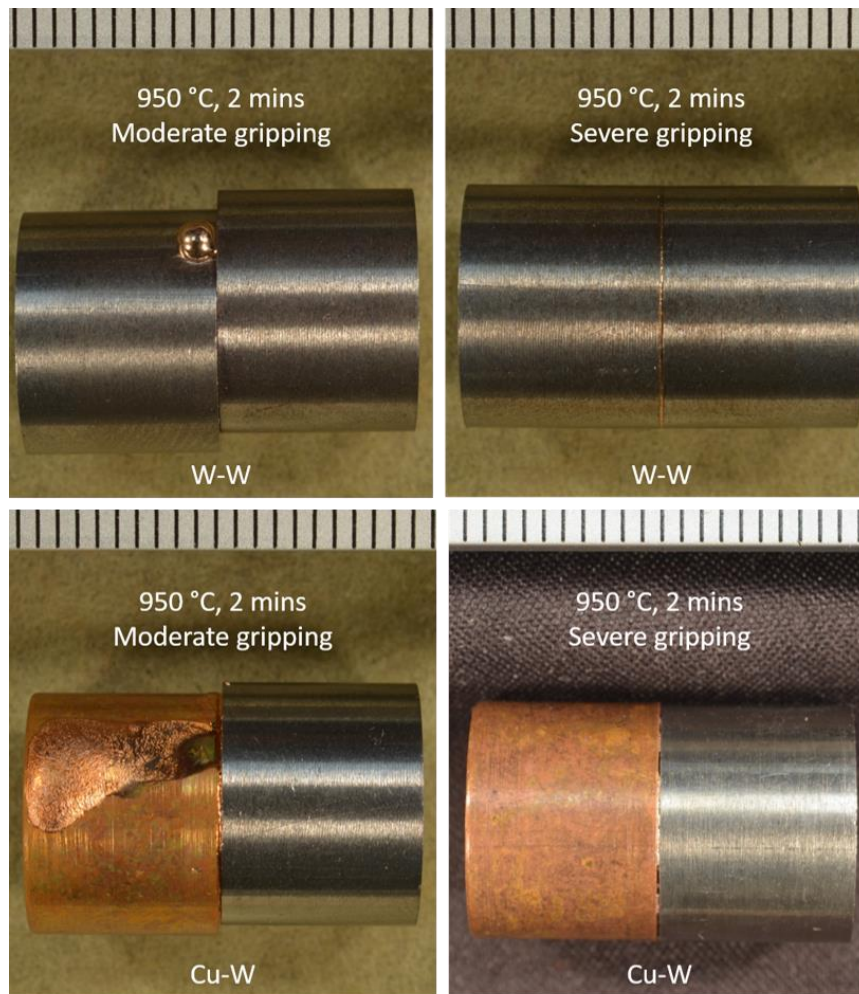
Figure 4- 10: W-W and Cu-W brazed specimens with different gripping levels

The processes of these experiments and their results can be summarised as follows:

- All the specimens gripped by the centre-locating pin top platform failed to be brazed, while the flat top platform and 2 minutes holding time provided satisfying results.

- 900 °C working temperature brazing trials of W-W joints failed as the filler foil was not melted.

- W-W can be brazed at 1050 °C, but the molten filler pooled at the edge of brazed layers and the joint was broken during sectioning.

- Among all the verifications, the best specimens were obtained from severely flat gripped workpieces brazed at 950 °C and held for 2 minutes.

- It was found that the final formations of the brazed specimens were susceptible to the gripping level. As shown in Figure 4-10, the W-W and Cu-W specimens brazed at 950 °C with moderate gripping had distinct axial misalignments. In these specimens, the filler was drawn to the edges and pooled on the surfaces of the parent materials. In the Cu-W specimen, the pooled filler even caused erosion on the Cu surface. These defects could act as stress concentrators and degrade fatigue life.

- As shown in Figure 4-10, W-W and Cu-W specimens brazed with severe gripping were well aligned. Based on visual observations of the brazed specimens, the final formations of brazed layers were uniform, and no fillers were drawn out of the joint regions.

4.5 Metallurgical study and mechanical properties of W-Cu joints

The new Au80Cu20 filler metal has replaced the obsolete Au80Cu19Fe1 filler, which was used for initial brazing designs and characterisation works following the upgrade of manufacturing techniques. Both filler metals are equivalent and should have the same brazing characteristics, properties and mechanical performance. Nevertheless, there is still a suspicion that new filler can lead to different microstructure and result in different mechanical properties. Therefore, successfully brazed W-Cu samples with the new Au80Cu20 filler harvested from both furnace brazing and induction brazing processes are prepared for metallurgical analysis and nanoindentation tests.

The samples were sectioned by silicon carbide disks on a Struers Accutom precision cut off machine, as explained in Chapter 2. The sectioned samples were mounted with conductive carbon resin and then went through standard metallographic preparations processes including grinding, polishing and etching. The quality of joints was examined and assessed by an optical microscope. An SEM with EDS functions was used to perform metallurgical analysis. The regional mechanical properties of the joints were tested by nanoindentation.

4.5.1 Vacuum Furnace brazed W-Cu joint

Figure 4-11 (a) show the microstructure of the W-Cu brazed joint with Au80Cu19Fe1 filler obtained from previous work discussed in Chapter 3, named batch 1. Table 4-3 shows the differences in brazing parameters of the two batches. Figure 4-11 (b) show microstructures of the same area within the W-Cu brazed joint with the new Au80Cu20 under different magnification, named batch 2.
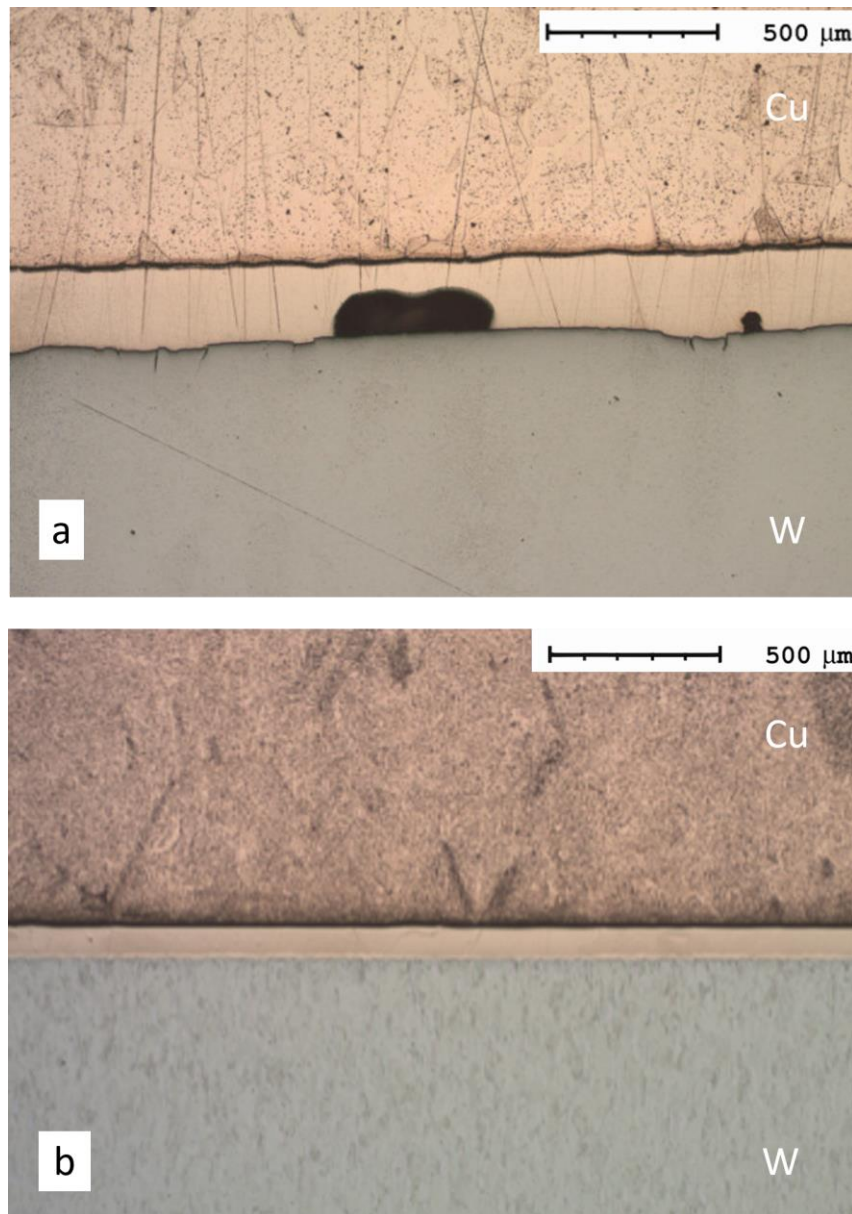
Figure 4- 11: (a) W-Cu brazed joint with old Au80Cu19Fe1 x50

(b) W-Cu brazed joint with new Au80Cu20 x50

Table 4- 3: Brazing parameters of W-Cu brazed joints

Batch No.	Filler material	Foil size	Gripping level
1	Au80Cu19Fe1	0.05 mm × ϕ10 mm	Moderate
2	Au80Cu20	0.05 mm × ϕ12.7 mm	Severe

The joints were accessed for flaws and imperfections complying with the International Standard EN ISO 18279:2003. The quality of batch 2 brazed joints had been improved remarkably comparing to batch 1 with Au80Cu19Fe1 filler. The batch No.2 W-Cu joints with Au80Cu20 filler solidified uniformly without noticeable flaws and cracks under the optical microscope. The entire joint was wetted by filler without filling or banding imperfections.

Although Au80Cu19Fe1 and Au80Cu20 are designed to be the equivalent products, the newer Oro890 no longer has a 1%wt Fe in its compositions. Fe is one of the active elements used to assist W sintering processes [98] as Fe can increase the wettability of tungsten particles [99]. The Fe free Oro890 filler has no advantages in improving the wettability or solubility of tungsten. Therefore, the optimised brazing procedure, which implied a bigger coverage of filler materials and greater clamping force improved the joint quality. In this case, the joint quality of batch No. 2 met the requirements stated by both EN ISO 18279:2003 and ASME 2004 Section IX.

Figure 4-12 shows the results of an SEM analysis at the interface of the Cu-W joint from batch No. 2. The white line in Figure 4-12 (a) shows the EDS line analysis of the brazed joint. This analysis took 200 measurements over about 170 microns across the braze layer, and the result is shown in Figure 4-12 (b). It can be observed that the composition of Cu within the brazed layer was increased from 20% to more than 30% due to diffusion. Same as the specimen tested in batch No. 1, a smooth transition region was formed between Au and AuCu, but an abrupt change of elements was found between W and AuCu.
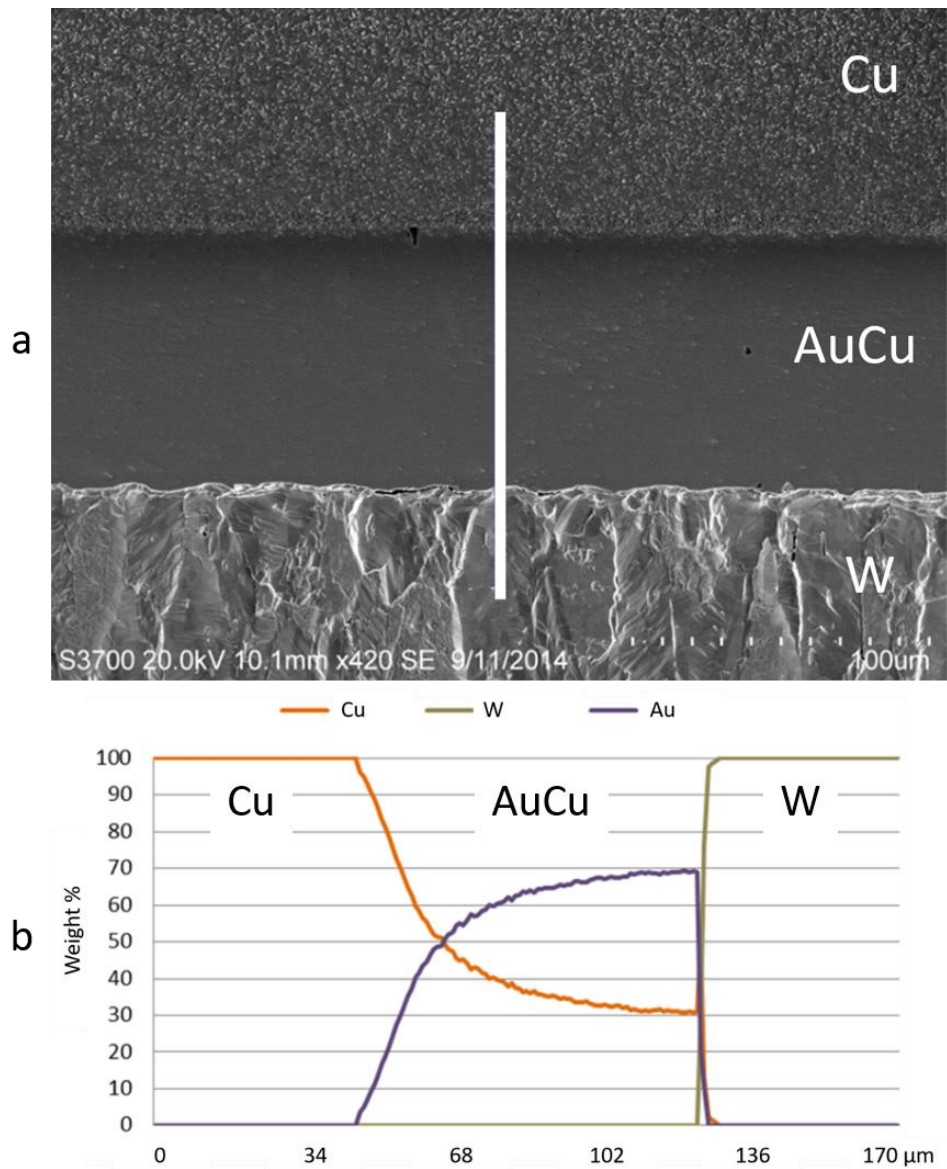
Figure 4- 12: (a) Backscatter SEM image of W/AuCu/Cu joint

(b) EDS analysis across the joint

4.5.2 Induction brazed W-Cu joint

The principal objective of induction brazing development in this work was to develop a quick turnaround and low-cost method to harvest brazed joints with consistent quality for mechanical testing. Another purpose was to determine the optimal surface roughness of parent materials and the selection of material grade to achieve the best joint quality. This was a collaborative effort between the author and co-researchers and was subsequently reported in the published literature [100].

Figure 4-13 (a) shows the W-Cu specimen induction brazed at 950°C with 2 minutes holding time. It can be observed that some braze filler materials solidified on the outside of Cu due to capillary action during the brazing process. This should be taken into consideration when fabricating fatigue testing samples as the filler material on edge is acting as a stress concentrator and could degrade the fatigue life.
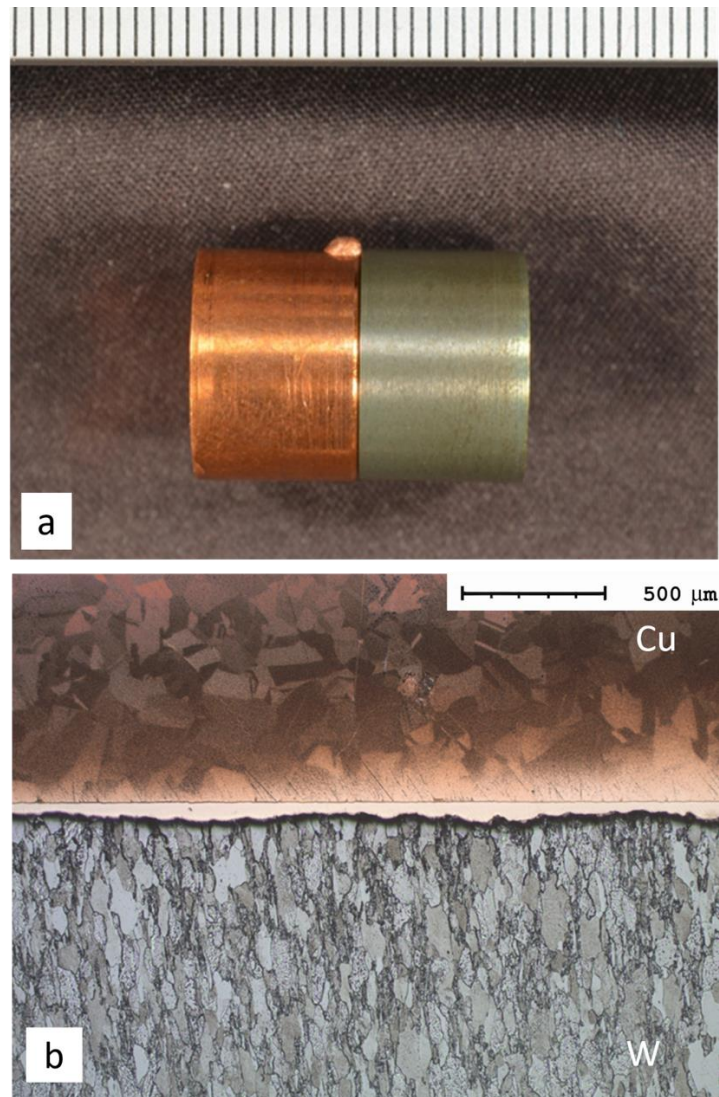
Figure 4- 13: (a) Post braze W-Cu joint specimen

(b) Brazed layer x50

Figure 4-13 (b) is an optical microscope image of the brazed layer with Cu etched. There are no visible voids or defects throughout the brazed layer. The sound quality of the brazed layer suggests the induction brazing under vacuum could be used for

fabricating mechanical testing specimens. Beyond that, it can be observed that the brazed layer is nonuniform in thickness across the joint. This is due to the EDM wire cutting process, which left burning marks and leads to high surface roughness on the W parent material. The effect on the strength of the brazed joint is worth to be researched in future works.

4.6 Nano indentation testing of W-Cu joints

The properties of the brazed joints created by vacuum and induction furnace are suspected of showing diversity due to their different heating and cooling profiles, as shown in Table 4-4.

Table 4- 4: Heating and cooling cycles of vacuum furnace and induction

	Heating rate	Brazing temperature	Brazing time	Cooling time
Furnace	10 °C/min	950°C	5 minutes	Several hours to room temperature
Induction	500 °C/min	950°C	2 minutes	100 minutes to 200°C

The specimens brazed in the vacuum muffle furnace followed the same brazing procedure reported in Chapter 2. The furnace was set for heating up to 950°C in 95 minutes at a rate of 10 °C/min and the temperature dwelled at 950°C for 5 minutes before the heat source was switched off. Then the specimens were left in the furnace at the same vacuum level and slowly cooled down to room temperature over several hours to avoid thermal shock. In contrast, the induction heater provided a much faster heating process. The crucible containing specimen was heated in the vessel to 950 °C in 110 seconds which converted to a heating rate of 500°C/min. Then the temperature was held at 950 °C for 2 minutes, and then the vessel was left to cool down with retained vacuum. The cooling of the vacuum vessel took around 100 minutes to below 200°C.

A similar methodology utilising nanoindentation, which developed in Chapter 3, had been applied at the brazed joint to further assess the mechanical properties of W-Cu joints created by both vacuum furnace and induction heater.

Figure 4-14 is an image of the tested furnace and induction brazed joints shown by overlapping the images at the interfaces between the brazed layer and W. Although the boundaries are blurred, it can be observed the brazed layer derived by the vacuum furnace is thicker than induction heater. The much longer heating and cooling cycle during furnace brazing did result in a more significant elemental transition process than induction brazing and could lead to different mechanical properties.

Nanoindentation tests took 45 measures for every 15 μm across both brazed joints as the indents shown in Figure 4-14. In order to generate more measurements at brazed layers, the tests were performed at an angle of 45° to the interface. Modulus and hardness values were calculated by CSM.
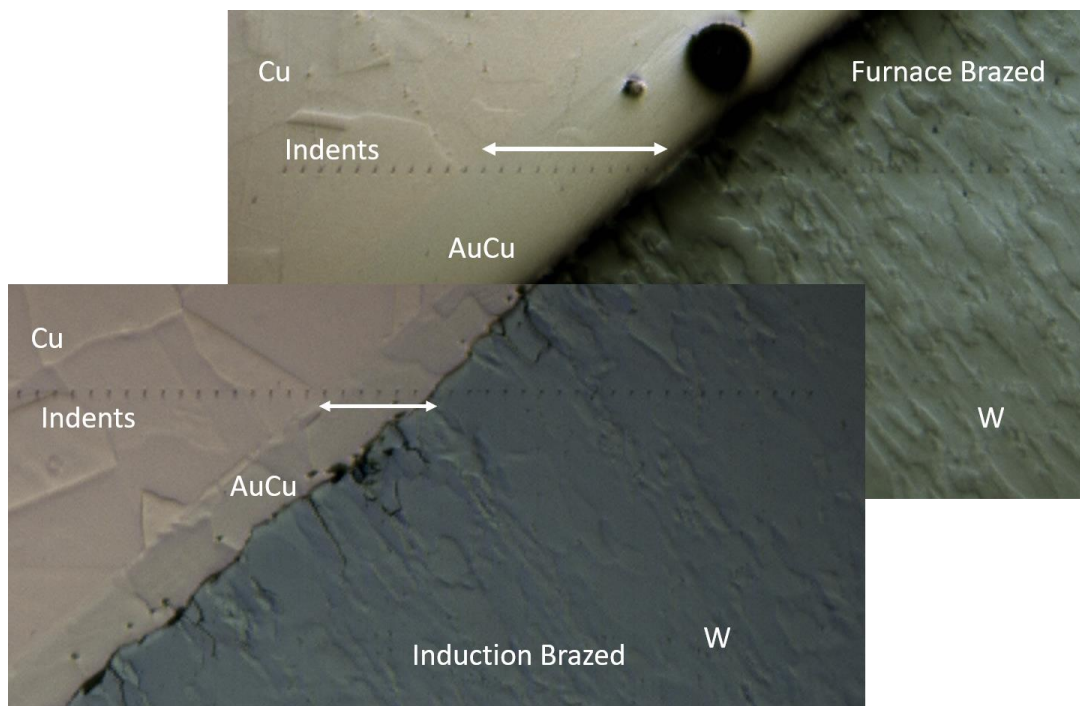
Figure 4- 14: Furnace and induction brazed joints with nanoindentation marks

Figure 4-15 shows the modulus at each indent. For both furnace and induction brazed joints, modulus values changed abruptly, which indicated the location of the interface between the brazed layer and W. While for both types of brazed joints, the modulus values from Cu to the brazed layer/W interface were continuous, the interface between Cu and brazed layers cannot be identified.
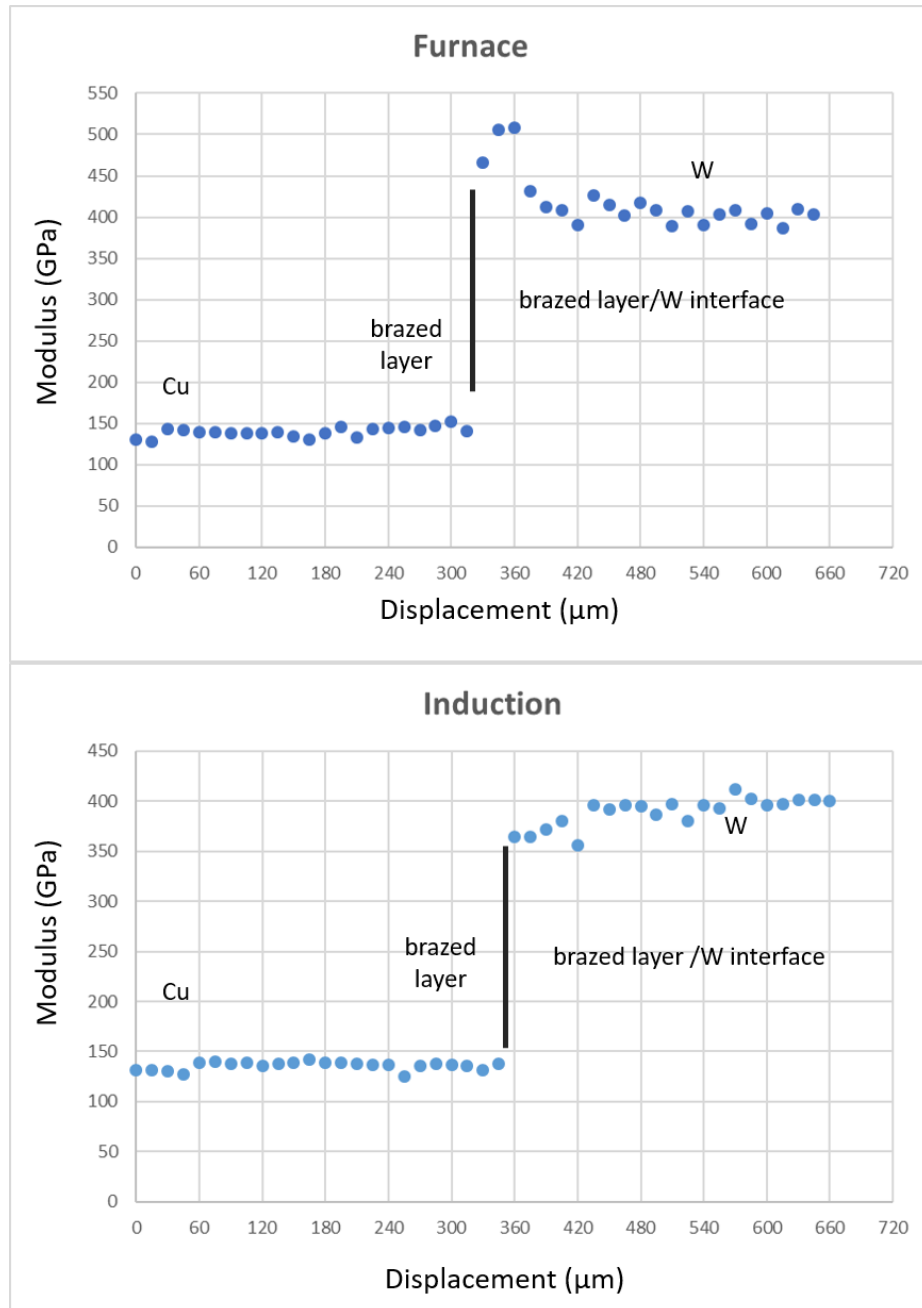
Figure 4- 15: Modulus measured at the brazed joints
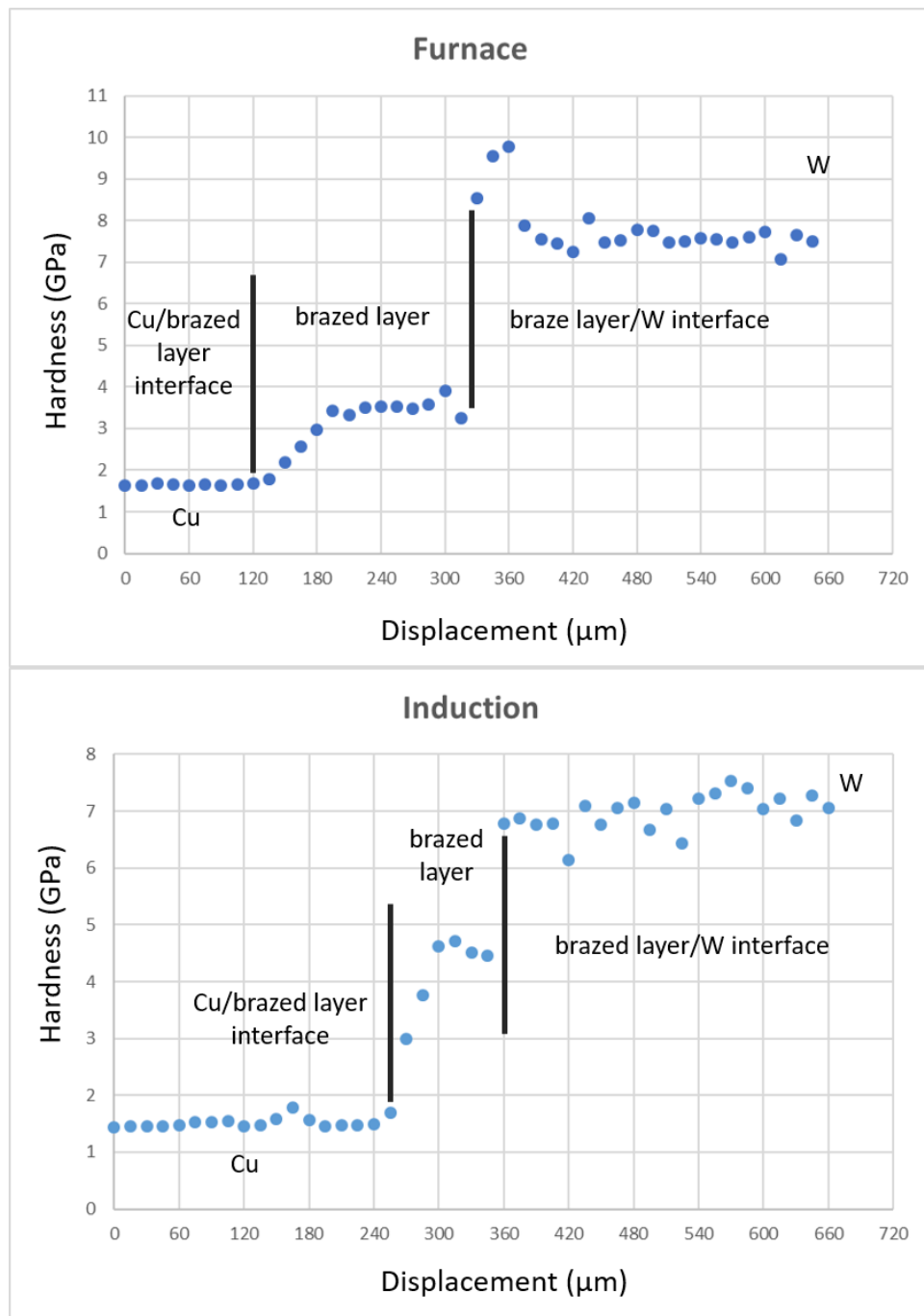
Figure 4- 16: Hardness measured at the brazed joints

Figure 4-16 shows the results of hardness testing at both brazed joints. For both brazed joints, the hardness values had similar abrupt changes at the interface between the brazed layer and W. Both brazed layers consist of a section of filler material with stable hardness values and a section of diffusion region with gradual changes of hardness. Furthermore, the interface between the brazed layer, diffusion

region and their interface to Cu can be identified by tracing changes in hardness. Hence, the thickness of the furnace brazed layers can be estimated to be approx. 127 μm and the thickness of the induction brazed layer to be approx. 64 μm.

Based on the observations, the modulus and hardness measurements in brazed joints can be summarised as follows:

- In the furnace brazed joint.
    - At W region, E= 417.48 ± 32.91 GPa, H= 7.81 ± 0.66 GPa.
    - At filler material region, E= 141.38 ± 5.97 GPa, H= 3.5 ± 0.18 GPa
    - At Cu region, E= 137.42 ± 4.51GPa, H = 1.65 ± 0.02GPa
- In the induction brazed joint.
    - At W region, E= 389.3 ± 14.23 GPa, H= 6.97 ± 0.32 GPa
    - At filler region, E= 135.35 ± 2.60 GPa, H = 4.58 ± 0.10 GPa
    - At Cu region, E = 136.5235 GPa, H= 1.51 ± 0.08 GPa

It can be found that the mechanical properties of W and Cu parent materials were not affected by different brazing methods. The solidified filler material in the induction brazed joint has a higher hardness than the filler in the furnace brazed joint, 4.58 GPa to 3.5 GPa. This is due to the increased Cu composition in the furnace brazed joint with the longer heating time in the process. Referring to Figure 4-12, the composition of Cu in the solidified furnace brazed layer was increased from 20% of Au80Cu20 filler to more than 30% due to diffusion from the Cu parent material.

Moreover, comparing with the results reported in section 3.5, in the W-AuCuFe-W joint where no diffusion between the brazed layer and W, H was measured at the solidified AuCuFe region as 4.54 ± 0.28 GPa, which is equivalated to the induction brazed joint 4.58 ± 0.10 GPa. This demonstrates that with a much shorter heating cycle, the element transition of Cu into AuCu filler during the induction brazing process was restricted in the diffusion region and did not go through the whole brazed layer.

4.7   Summary

This chapter discussed the considerations of developing dissimilar brazed for mechanical testing to guide the design of the brazing process. The design of an optimised vacuum brazing procedure based on the experience from the brazing development in Chapter 3 was reported in section 4.3. The optimised brazing procedure had successfully improved the quality of butt-type brazed joints created with Au80Cu20 filler and the alignment performance.

An induction brazing procedure, including the equipment, was successfully developed within the university facility to produce good quality brazing specimens in low volume for characterisation testing. The metallurgical study showed that the different heating and cooling process of the furnace and induction brazing had resulted in different diffusion behaviours and thickness of the diffusion layers between Cu and Au80Cu20. Due to the much longer heating and cooling cycle, the furnace brazing did result in a greater elemental transition process than induction brazing. It was observed that the brazed layer derived by the vacuum furnace is thicker than the brazed layer derived by the induction heater.

Nanoindentation performed in this chapter confirmed that the mechanical properties of the W and Cu parent materials were not affected by different brazing methods. For both furnace and induction brazed joints, modulus values changed abruptly at the interface between AuCu and W. For both types of brazed joints, the modulus values from Cu to the brazed layer/W interface were continuous.

The hardness of the induction brazed layer was higher than the furnace brazed layer due to the much shorter heating cycle of the induction brazing process restricted the element transition of Cu into AuCu filler. By tracing the change in hardness value, the interfaces between AuCu, diffusion region and Cu were be identified. Hence, the thickness of the brazed layer could be correctly measured, which was essential for FEA modelling this type of brazed joint.

5 Development of casting specimens toward generating mechanical properties of a brazed layer

5.1 Introduction and objectives

Following the brazing development and assessment work reported in Chapter 3 and 4, good quality brazed joints of tungsten using gold-based filler metal have been fabricated.

The development of designing and manufacturing mechanical testing specimens is beyond the scope of this thesis. Considering the nanoindentation testing performed in Chapter 3 and 4 was undertaken to predict the mechanical properties of Au based brazed joint, this chapter aims to prove the prediction is accurate to build up the level of confidence on the properties generated by nanoindentation to be feed into design work. A casting procedure is developed to generate sub-sized test specimens in the 'as cast' condition that can be tested with standard tensile testing to achieve this objective. The mechanical properties generated by macro tensile testing can then be compared and correlated with the properties of the brazed layer generated by nanoindentation. This is aiming to develop a methodology to address the challenges described in section 1.5:

- Due to differences in thermal expansion coefficient and Young's modulus, highly significant residual stresses can develop in dissimilar material joints and result in failure of the joint during manufacture or under cyclic thermal loadings. Hence residual stresses due to brazing must be considered in any FEA or failure assessment for dissimilar brazed joints.
- To create an accurate FE model and assess the integrity of a brazed joint, the mechanical properties of a brazed layer need to be characterised. However, the properties of brazed layers are very difficult to be directly tested and appropriately characterised.

Due to the high cost of Orobraze 890 materials, this approach has to accept the compromise of using a commercially available non-fusion relevant filler material. A

Cu based binary Cu60Zn40 material was chosen in this work as the raw material for fabricating casting samples and also as the filler material for joining SS316L and OFHC. However, the SS316L-OFHC combination with the Cu based filler alloy bears relevance to the water-cooled divertor concept. The melting range of the Cu60Zn40 alloy is between 875-895°C which is also close to the fixed melting temperature of Orobraze 890 at 890°C.

In this chapter, microstructural properties of filler materials derived from both brazing and casting are investigated, and the mechanical properties of the brazed layer and casting samples are generated and analysed. As cast specimens were tested by micro/nanoindentation and macro mechanical testing to predict material properties of a brazed layer, mechanical properties generated from nano/micro indentation testing, sub-sized samples are compared and discussed.

5.2   Overview of Cu60Zn40 filler material used for brazing and casting

The brazing filler material Cu60Zn40 used in this investigation is a standard commercial grade brass EN 1044: CU 302, also known as Muntz metal [101]. It was made up of 60 wt% copper, 39.4 wt% zinc with 0.3 wt% tin and silicon and supplied as Φ3 × 800 mm rods. Figure 5-1 shows the Cu-Zn phase diagram with Cu60Zn40 marked, and Table 5-1 shows compositions of different phases in the Cu-Zn system. As found in the phase diagram, 2 main phases constituted the compositions of Cu60Zn40 structures: alpha (α) phase and beta (β) phase. The α phase is stable for concentrations up to approximately 35%wt Zn [102]. This phase has a face-centred cubic (fcc) crystal structure and is relatively soft, ductile and easily cold worked. Brass alloys having a higher Zn content contain both α and β phases at room temperature. The β phase has an ordered body-centred cubic (bcc) crystal structure and is harder and stronger than the α phase; consequently, α+ β alloys are generally hot worked [102].

Referring to Figure 5-1 and Table 5-1, during the process of solidification, the maximum solid solution of α phase occurred at 454°C with 38.95% Zn. From this point, the β phase would precipitate out of the solution into the α matrix upon cooling to

ambient conditions. Zinc acts as single substitution impurities through the copper lattice at lower compositions. In the β phase, zinc levels can be up to 56.5%. For Cu60Zn40, from 903°C to about 450°C, the alloy is in the alpha plus beta (α+ β) phase with the copper and zinc randomly locating in the lattice. The Cu-Zn alloys on cooling below about 450°C forms an ordered structure called a superlattice. This structure is identified as alpha plus beta prime (α+ β'), which consists of Zn from about 38% to about 48% [103]. The single-phase α brasses maintain the cold workability from copper and have good strength with good ductility in the material. The higher alloying content in β acted to increase the strength and hardness of the brass but also decrease the ductility. Furthermore, CuZn brass can develop a martensitic phase during quenching.
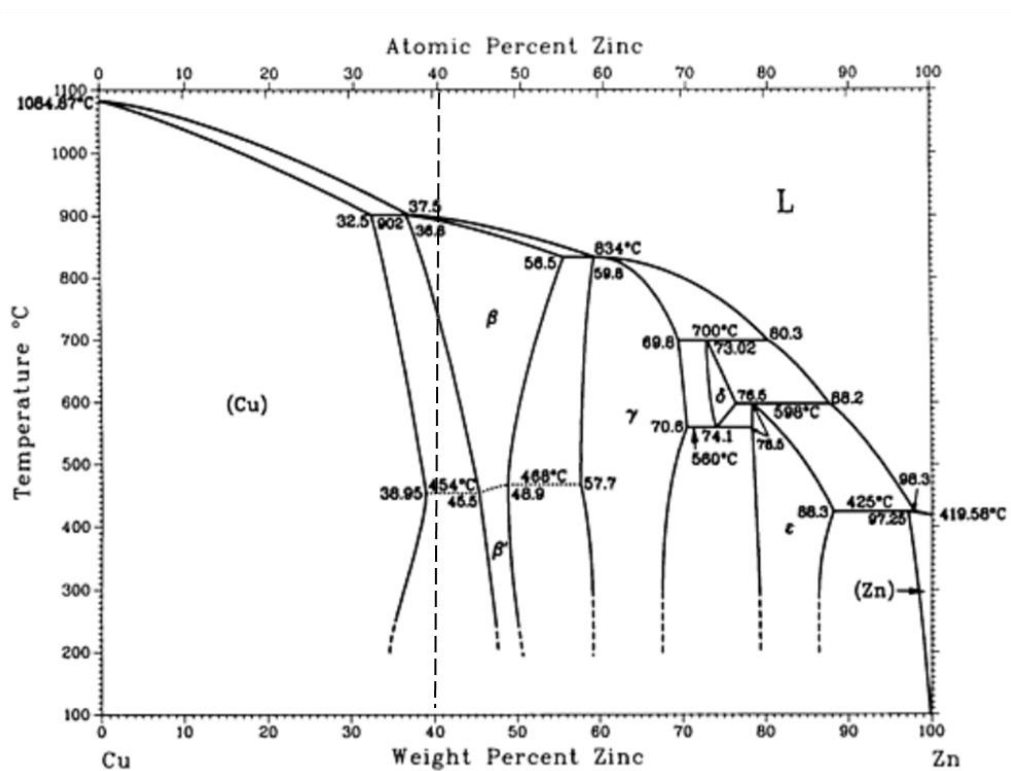
Figure 5- 1: Cu-Zn phase diagram with Cu60Zn40 marked [44]

Table 5- 1: Cu-Zn system phases composition data [44]

Phase	α or (Cu)	β	β′	γ	δ	ε	η or (Zn)
Composition, wt% Zn	0 to 38.95	36.8 to 56.5	45.5 to 50.7	57.7 to 70.6	73.02 to 76.5	78.5 to 88.3	97.25 to 100

The melting range of the Cu60Zn40 alloy is between 875-895°C, and the tin and silicon additives act as stabilisation elements. Copper can wet and dissolve iron adequately in solution, but the addition of zinc and silicon significantly improves the wettability to ferrous materials, nickel and aluminium. The small tin content can enhance the wettability of stainless steels and act to help the flow of the filler materials on the surfaces of the parent metals. The increased flow property is also an advantage for casting. However, the high content of zinc is a disadvantage. Zinc may be volatile at high temperatures and has a vaporized temperature of 907°C, close to the melting temperature range of 875-895°C. Furthermore, in an air atmosphere, zinc is very reactive to oxygen. In brazing applications, Cu60Zn40 alloy would require a flux to prevent oxygen contacting with zinc, but in casting, which involves longer melting time and pouring, excess oxidation of zinc could be a severe problem.
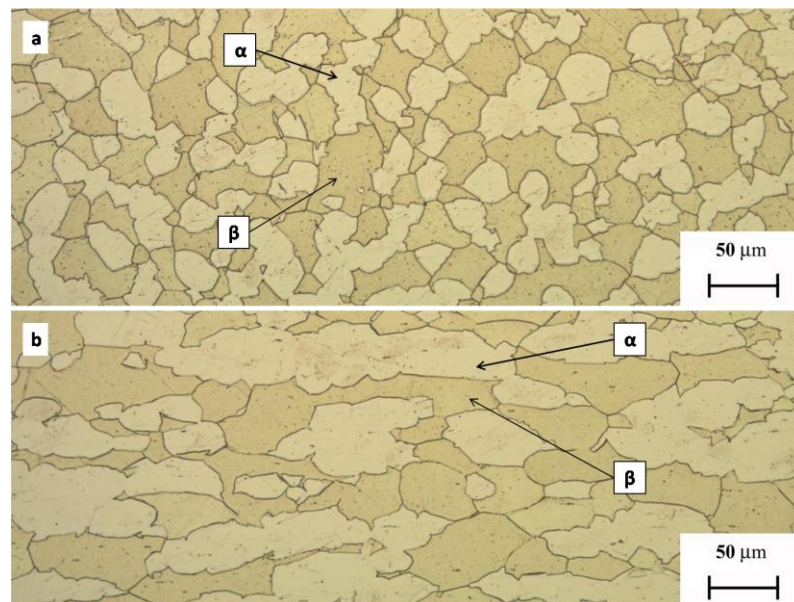
Figure 5- 2: Microstructure of Cu60Zn40 as supplied condition

(a) Cross section (b) Longitudinal section

The microstructure of as supplied Cu60Zn40 rods is shown in Figure 5-2 (a) cross-sectioned and (b) longitudinal sectioned, which is observed by optical microscopy. α + β brass Figure 5-2 (a) and (b) show microstructures consist α, and β phases appeared in equal sizes, instead of forming Widmanstätten structure as expected for high Zn content brass after casting. Furthermore, elongated grains can be observed in the longitudinal direction. This indicates that the as supplied material is fabricated wrought followed by stress-relieving.

5.3   Brazing procedures with Cu60Zn40 filler

To understand the magnitude of the challenge, an investigation into the microstructure and composition of the brazed layer and adjacent material was carried out. The parent materials of SS316L-OFHC joints were the same batch of materials used in chapter 3 and 4 and CNC machine lathed into cylindrical butt form with dimensions of Φ12.7 mm × 10 mm. SS316L- SS316L joints were created with another batch of CNC lathed SS316L specimens with dimensions of Φ10 mm × 10 mm. The filler was cold-pressed into Φ10 mm × 0.5 mm disks from the as supplied Cu60Zn40 rods. The pre-brazing parent and filler materials were cleaned by acetone and then gripped with the device developed in Section 4.4, as shown in Figure 5-3.

The temperature control of the muffle furnace relied on an internal thermocouple set on the back wall of the chamber, so a number of furnace brazing trials were performed until successful joints were obtained. The furnace was heated to 1080°C and retained the temperature for 20 minutes before brazing to achieve a uniform temperature distribution in the furnace chamber. In order to retain a more stable temperature for the brazing workpiece, a ceramic crucible was pre-set in the centre of the furnace chamber and preheated along with the furnace. The gripped workpiece was then put inside the crucible and held for 6 minutes. The specimens were then taken out and cooled to room temperature in the air.

Induction brazing was performed by the same induction heating system with a vacuum vessel as described in Chapter 4. An infrared sensor was used to detect temperature. The aligned samples were set in the vessel with an argon atmosphere.

A Φ150 mm induction coil was used and the input current of the induction heater was set as 900 Amp. The sample was brazed at 950°C and held for 1 minute. After brazing, the brazed samples were taken out of the vessel with the crucible and then cooled in the air. The temperature profile during the cooling process was monitored by the infrared sensor, and the cooling profile is shown in Figure 5-4. The cooling from 1000°C down to 200°C took less than 9 minutes.
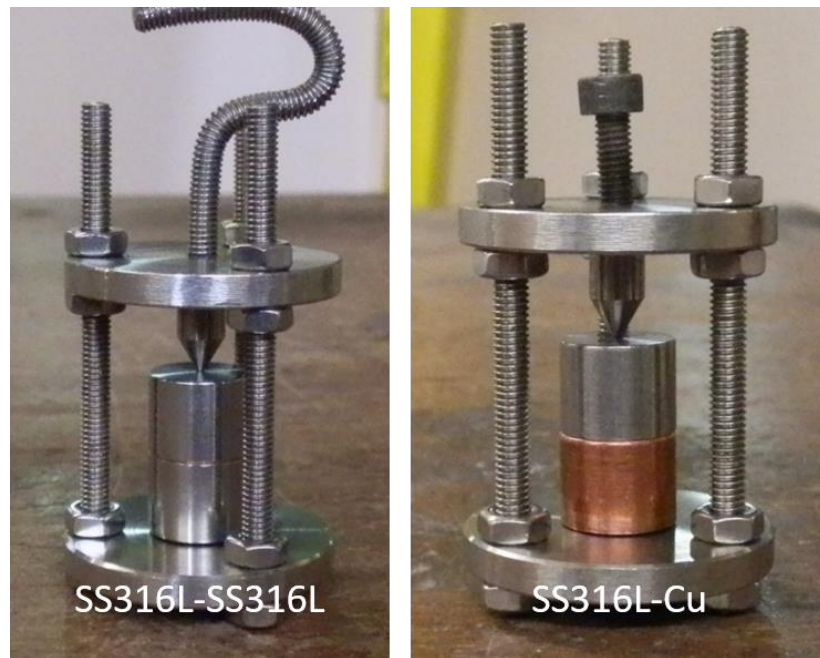
Figure 5- 3: SS316L-SS316L and SS316L-Cu joints setup in the gripping device before brazing
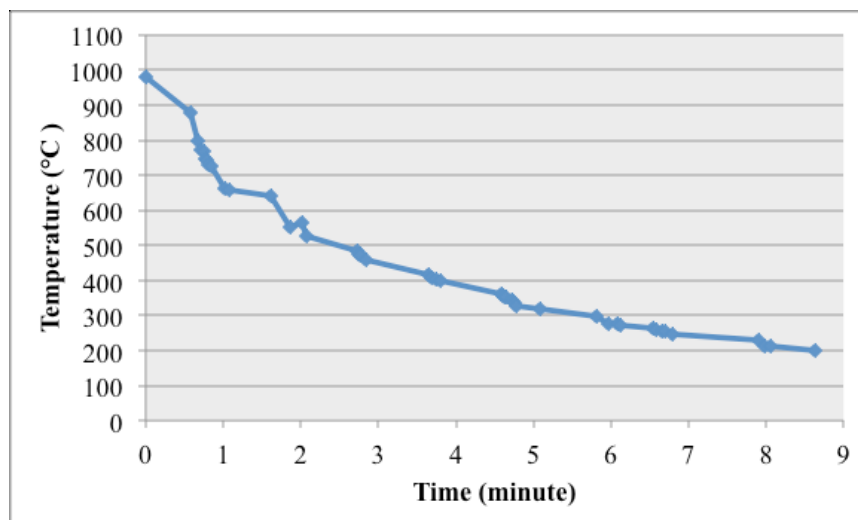
Figure 5- 4: Cooling profile of induction brazed SS316L-SS316L joint

5.4   Mould design and casting procedures

In this work, plaster of Paris ($CaSO_4 \cdot 0.5H_2O$) was used to create casting moulds as the specimens required were generally small in size. Plaster is a desirable material for casting brass. It can obtain good surface finishes, maintain dimensional accuracy and provide the slowest cooling rate compared with other types of mould due to low heat capacity [104]. The slow cooling rate can improve pouring molten metal and reduce the voiding and shrinkage effect during solidification. Nevertheless, slow cooling needs a longer production time and can lower the strength of the casting workpiece [104].

To make the plaster mould, the plaster of Paris should firstly be mixed with water to form a slurry. The weight ratio of plaster and water was strictly controlled to be 45:100. The slurry was stirred for 2-4 minutes until air bubbles were eliminated in order to avoid air pores or cavities formed in the mould. As shown in Figure 5-5, the wet plaster was poured into a Φ36 mm x 80 mm acetal tube and left for 5-8 minutes to semi-solidified. A Φ15 mm x 200 mm aluminium pattern was inserted into the plaster through the bottom of the mould, and then the mould was taken out from the plastic tube. The inner surface of the plastic tube and the entire surface of the pattern was coated with a silicon-content mould release agent in order to prevent the semi-solid plaster from sticking to the plastic tube and aid the removal of the pattern from the mould. The pattern stayed in the mould for a further 8 minutes so the plaster could sufficiently harden. Thereafter, the pattern was carefully taken out of the plaster. Based on the experience gained in practice casting trials, a cone shape was formed into the plaster to create the mould with the tapered top, as shown in Figure 5-5. This was to improve the feeding of molten brass into the mould and prevent overspill. Finally, the mould was put into a muffle furnace set at 200 °C and heated for 4 hours to dry out the plaster thoroughly.

The casting procedures were developed with the use of the same muffle furnace to carry out the brazing work. The as supplied Cu60Zn40 rods were cut into 50 mm

length before casting, and a graphite crucible was used for melting. The same moulds, crucible and filler rod sizes were used throughout the work.

Figure 5- 5: Configuration of mould making, plaster mould and successful cast specimen

The muffle furnace was preheated to 1100 °C and held for 20 minutes to achieve uniform temperature distribution in the chamber and prevent the formation of excess oxidation during melting. The melting time was between 5 – 7 minutes, depending on the volume of filler. The plaster mould heated to 200 °C for 2 hours and took out right before the pouring process. This was to dry out the moisture absorbed in the plaster moulds after they were made. The preheated process could also reduce the temperature difference between the mould and molten metal and avoid moulds cracking during pouring due to the thermal shock. The mould was seated upon a graphite sleeve to prevent the spillage from the bottom of the mould. A mould could be used for two casting processes before cracking and failure.

A successful as-cast specimen with a smooth surface finish is shown in Figure 5-5, where a degree of shrinkage can be observed. The as-cast specimens were machined into required mechanical and thermal testing specimens. The oxidation and defects on the outer surface were removed by the machining process.

5.5 Microstructural analysis of the Cu60Zn40 filler in the brazed joint and as cast specimens

Figure 5-6 shows the different microstructures of the Cu60Zn40 brass obtained from casting (a), (b) and brazing (c). As the Cu60Zn40 filler is a two phases alloy, it can be observed that the grains were formed by α+ β dendrites. It was noted that the α phase has is relatively soft, ductile and easily cold worked microstructure. Brass alloys having a higher Zn content contain both α and β phases at room temperature. The β phase tends to be harder and stronger than the α phase.
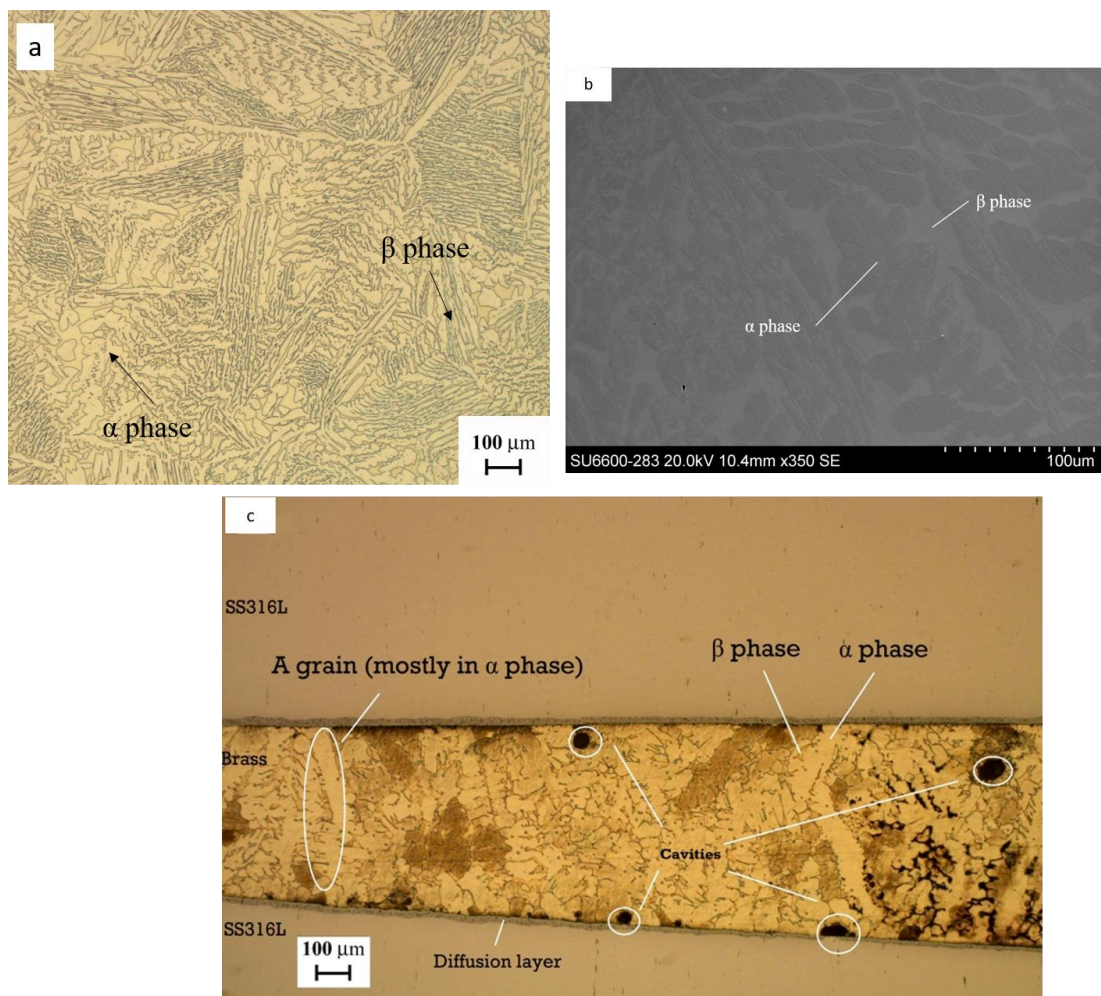
Figure 5- 6: Microstructures at x50 magnification: (a) Cast Cu60Zn40 (b) SEM image within a α+ β grain (c) SS316L brazed with Cu60Zn40

Figure 5-6 shows the differences between the two samples. The casting sample (Figure 5-6 a) has a larger mass of material and experienced a slower cooling rate

than the brazed sample. The resultant cast sample has a dendritic structure formed by both α and β phases dendrites. The random dendritic direction shows the heat conduction is uniform in different directions. The brazed sample (Figure 5-6 b) has a brazed layer that is approx. 500 μm thick, and there are some cavities found in the brazed layer. Due to the faster cooling rate. Most of the alloy formed into α phase but less β phase. Because the heat was conducting from the brazed layer to stainless steel, the grains were elongated vertically. Considering these microstructural differences, the mechanical properties will also be different with the smaller grains resulting in higher hardness and strength.

Figure 5-7 is an SEM image taken at the interface between the SS316L and brazed layer with the elemental maps created for primary elements. To demonstrate the interface microstructures, coloured individual phases derived from an EDS composition map was superimposed onto the SEM image (brass in orange, stainless steel in green). The figure shows that a diffusion layer, approx. 30 μm, occurred at the interface of the two materials. A new phase that diffused into the brass can clearly be observed. An EDS elemental mapping analysis, shown in Figure 5-7, was performed to understand how the elemental diffusion occurred in the brazed joint. It can be observed that the Fe and Cr from the 316L diffused into the brass and created the new phase in the brazed layer. The elemental maps show how each element distributes on the phase map. Comparing with the coloured SEM image, it can be confirmed that the new phases (shown in green colouration) in the brass are Fe-Cr rich due to diffusion. Cu and Zn only diffused a small distance from the interface and formed the diffusion layer within 316L.
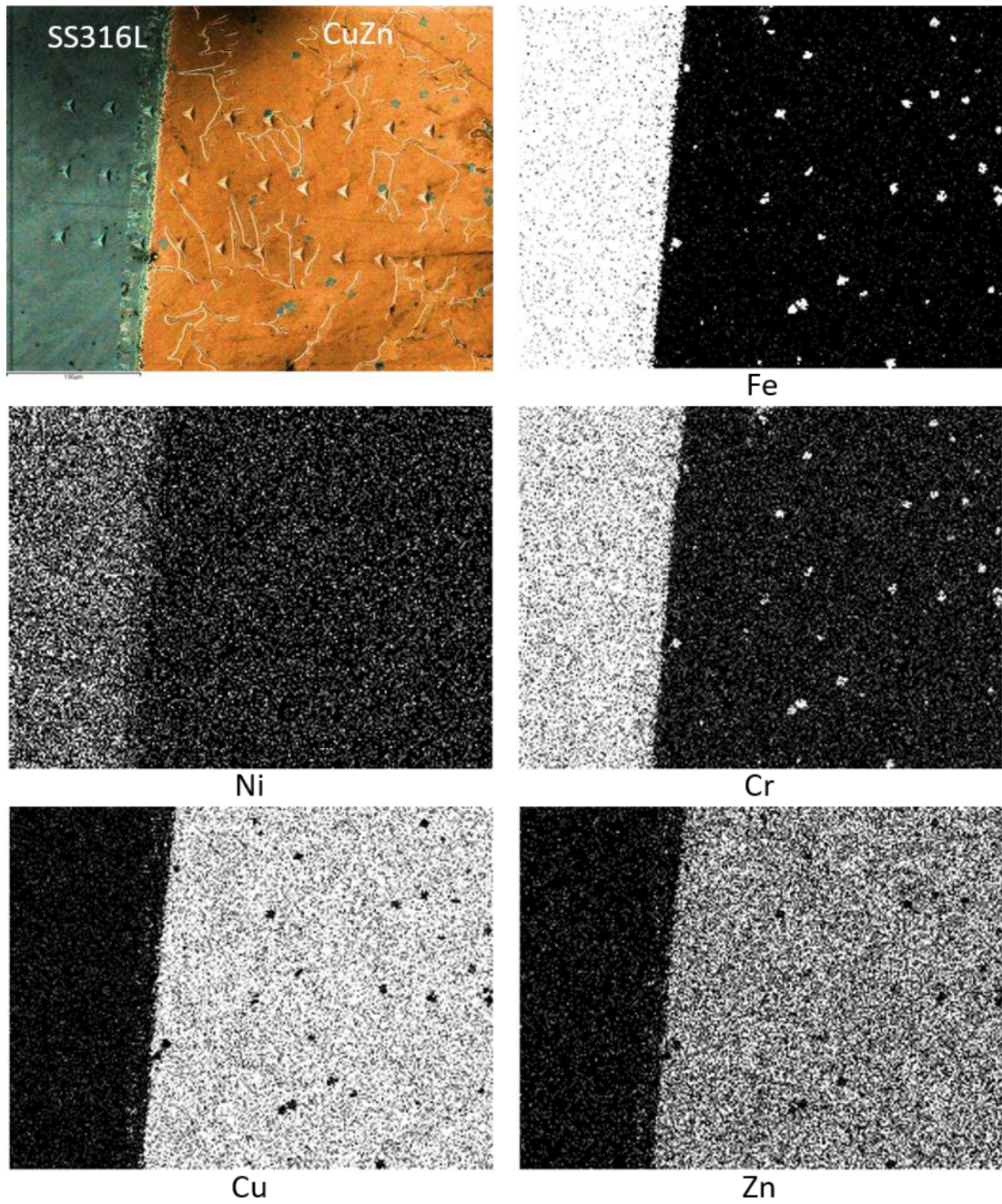
Figure 5- 7: EDS cameo image superimposing compositions SEM image and elemental maps for primary elements
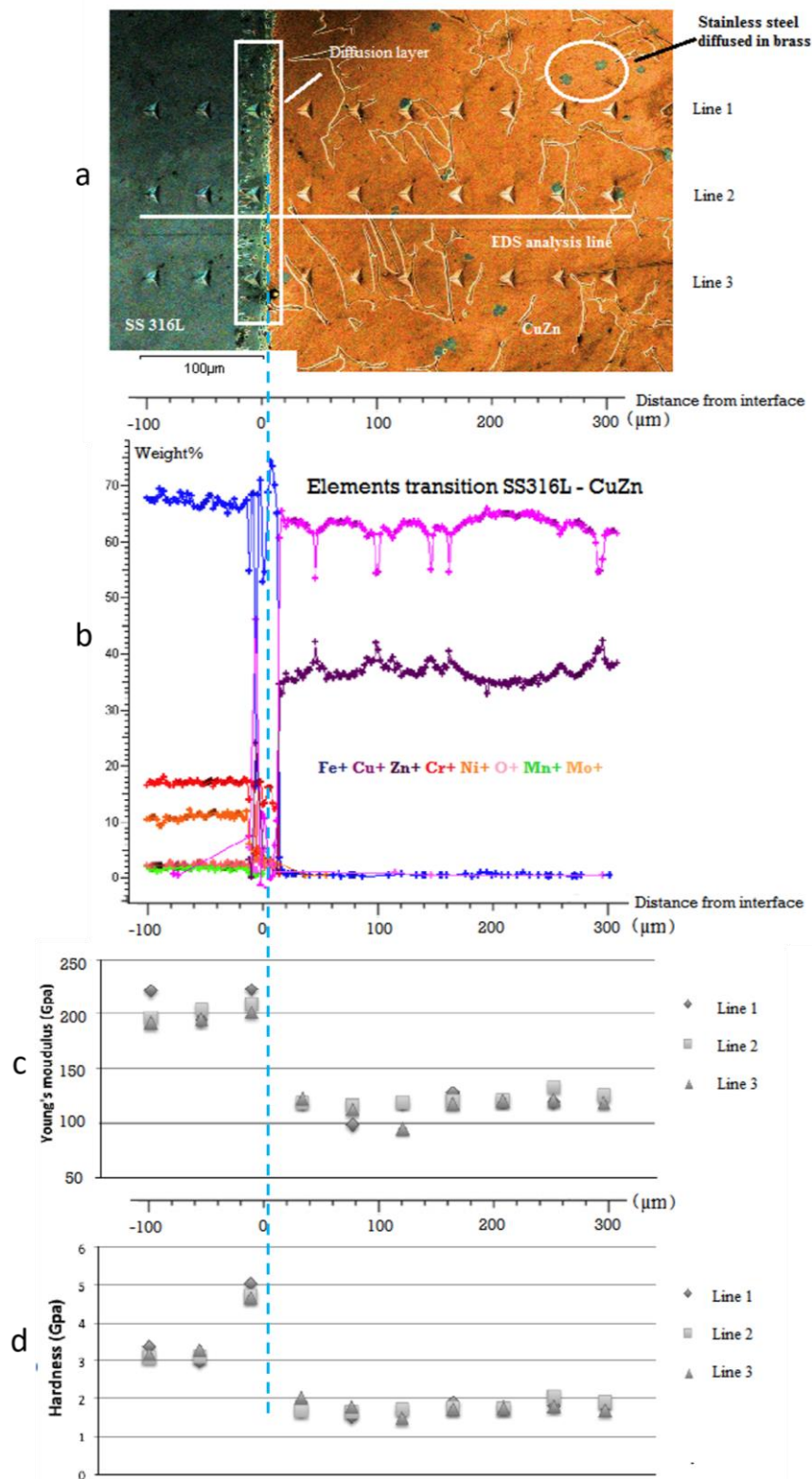
Figure 5- 8:(a) coloured image superimposing EDS composition map onto brazed layer SEM image with nano indents (b) Elemental transition across the brazed layer, analysed by EDS (c) Young's modulus and (d) Hardness measured by nanoindentation.

An EDS line analysis was performed, as shown in Figure 5-8(a). The scan was along with the same orientation as the nanoindentation tests. Figure 5-8(b) shows that elemental transfer from 316L to brass and from brass to 316L occurred within the diffusion layer. Fe and Cr were found to diffuse freely into the brass, whereas Cu and Zn could only be found in the diffusion layer on the 316L region.

In Figure 5-8 (a), three lines of nano indents can be observed. The nanoindentation tests take three measurements every 40 μm away from the diffusion layer at the interface between 316L and brass，each measurement has a vertical 60 μm spacing. CSM was used for the measurement, and the results were calculated from the testing over the depth range between 200nm-500nm. Figure 5-8 (c) and (d) show the values of Young's modulus and hardness measured by nanoindentation with the distance from the braze interface. At the SS316L region, E= 200.47 ± 8.23 GPa, H = 3.17 ± 0.13 GPa. At the diffusion region, E= 210.96 ± 8.49 GPa, H = 4.81 ± 0.17 GPa. At the Cu60Zn40 region, E= 118.59 ± 8.23 GPa, H= 1.76 ± 0.14 GPa.

According to the results, the diffusion layer has a slightly higher Young's modulus than the parent material SS316L. In contrast, the hardness of the diffusion layer is significantly higher than both the SS316L and Cu60Zn40. There is also a complex microstructure and several alloy phases within this small diffusion zone, so a range of properties would be expected.

5.6 Mechanical tests of cast Cu60Zn40 specimens

Two types of cast Cu60Zn40 specimens, naturally cooled and annealed, were created by the casting method developed in section 5.4 to represent different cooling rate in heat treatment or brazing processes. The naturally cooled cast specimens were allowed to cool down to room temperature in the plaster moulds slowly. While the annealed specimens were allowed to cool and solidify for 3 minutes and then placed in a furnace to anneal for 90 minutes at 600 °C, and then cooled to 400 °C, 200 °C and room temperature at regular intervals of 20 minutes.

The naturally cooled specimens had the microstructure, as shown in Figure 5-6 (a). In the solidified specimens, α+β phase grains were formed with alpha grains grown into large elongated dendrites covering a large area of the beta matrix. The alpha grains grew along preferential routes at the grain boundaries and crystallographic dislocations.

In the annealed specimens, the microstructure still showed α+β phase grains, while the α phase dendrites were thinner and longer than those in naturally cooled specimens, as shown in Figure 5-9. This is due to the gradual cooling processes that allowed α phase grains to elongate and grow across the entire beta matrix.

Referring to the phase diagram shown in Figure 5-1, at the annealing temperature, α grains would recrystallize, and this allowed the long continuous alpha needles to grow over the length of larger beta phases. The elongated needles of α filling the β matrix would soften the entire material and promote more ductile properties.
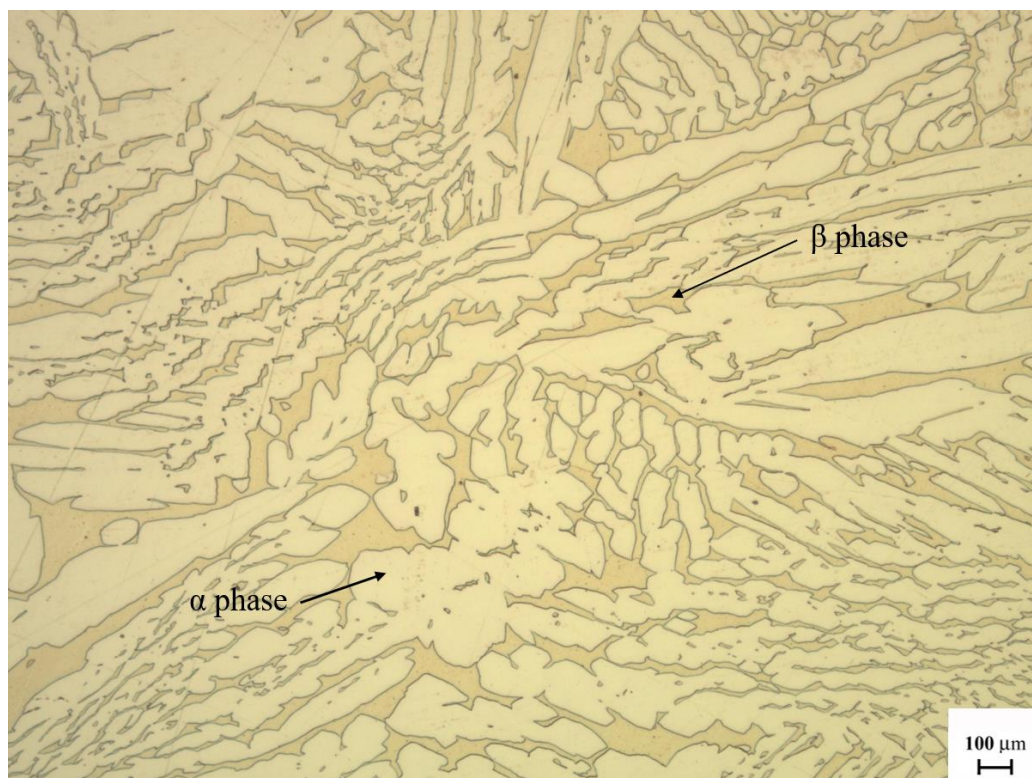
Figure 5- 9: Microstructure of annealed cast specimen x200

Microindentation tests were taken for the cast specimens. A diamond tip was used to perform the test, and 10 indentations were taken across the metal. The naturally cooled specimen had a mean hardness value of 117.1 ± 2.91 HV, and the annealed specimen had a mean hardness value of 109.9 ± 4.44 HV. The typical hardness was provided from the Cu60Zn40 filler supplier as 130HV [105].
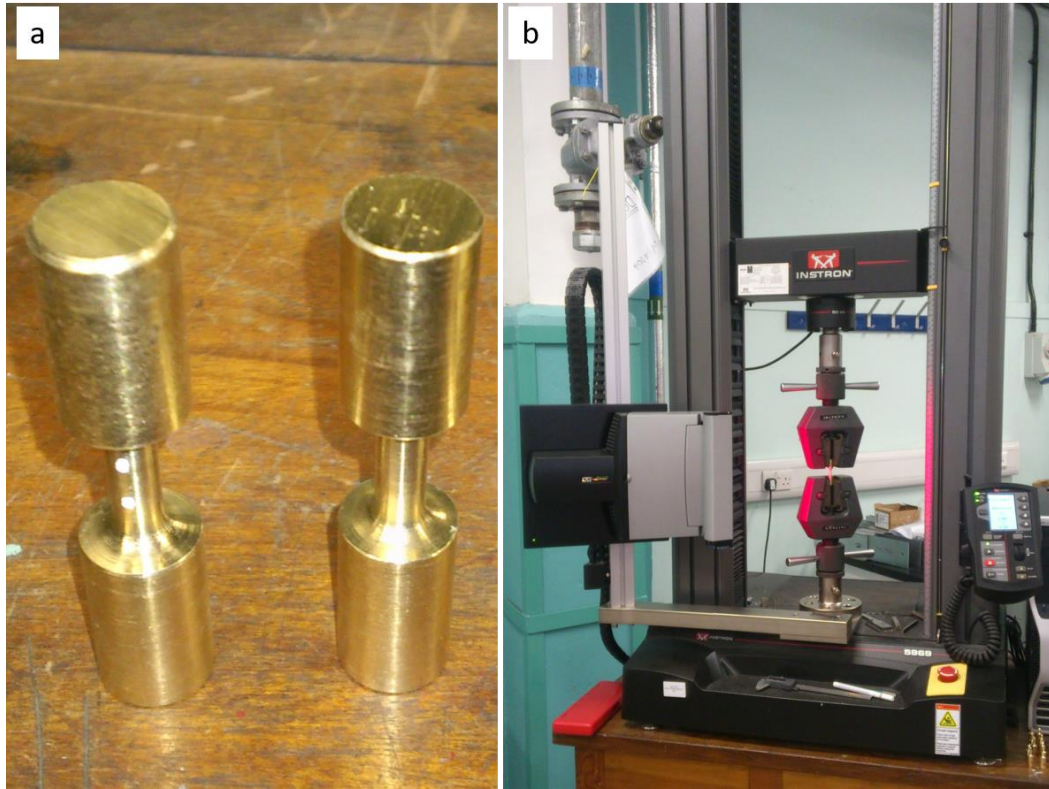
Figure 5- 10: (a) Tensile specimens (b) Axial tensile testing setup with a visual extensometer

Figure 5-10 showed two of the cast and machined micro tensile specimens and tensile testing setup. The specimen was adapted from ASTM standard [106], and the drawing was shown in Appendix 4. The gauge length was reduced by marking areas for the extensometer to take reference points for the strain extension, and each sample was given a gauge length along the reduced section of 5.50mm. The strain rate applied to each specimen was 1mm/min. For both naturally cooled and annealed conditions, five specimens were tensile tested, and the stress-strain curves show below were drawn from the average stress-strain results.
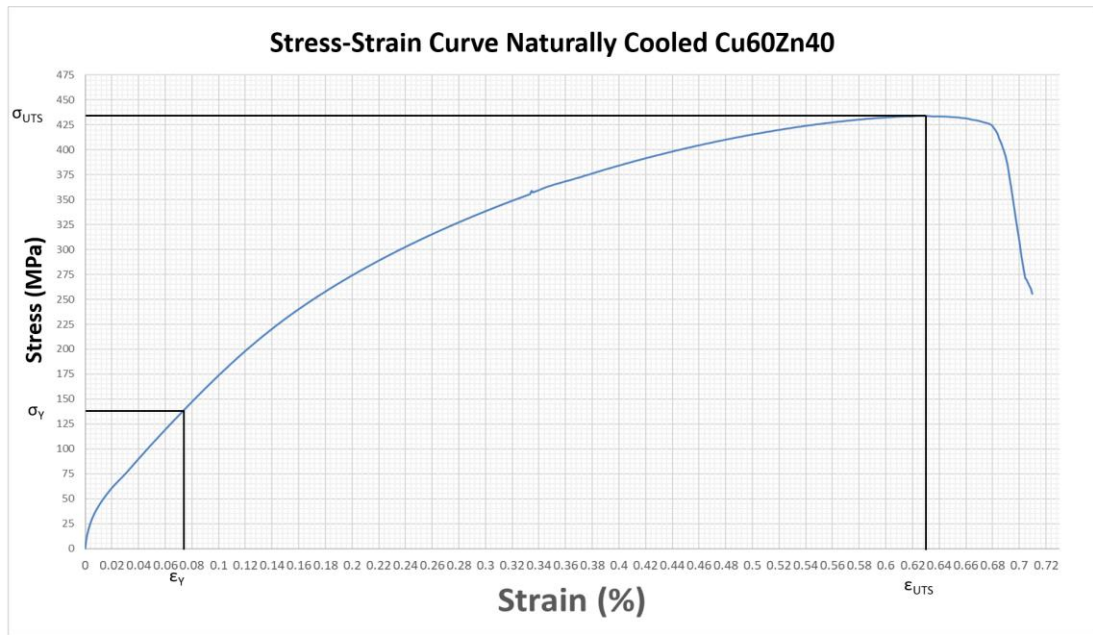
Figure 5- 11: Stress strain curve of naturally cooled Cu60Zn40
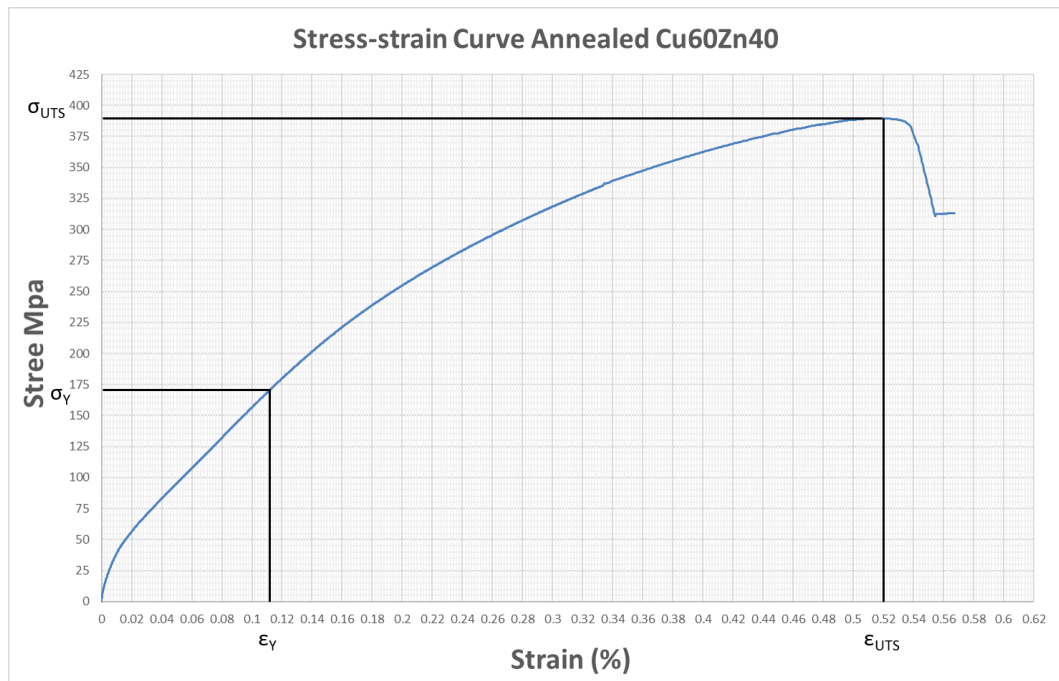
Figure 5- 12: Stress strain curve of annealed Cu60Zn40

Figure 5-11 and 5-12 showed the engineering stress-strain curves drawn from the tensile tests of both naturally cooled and annealed cast specimens. In each case, it is observed that no evidence of elastic behaviour is recorded. This is a typical

characteristic of visual extensometers where plastic deformation is accounted for in the absence of elastic behaviour.

The yield strength σ_Y, ultimate tensile strength σ_{UTS} and the young's modulus E can be derived from the curves. To the confidence level of 95%, 1.96 times standard deviations away from the mean value was applied. The results were shown in table 5-2. Figure 5-13 shows the failure profiles of the tensile specimens. It can be observed that both the naturally cooled specimen and the annealed specimen had a relatively ductile failure with small necking and elongation before fracture.

Table 5- 2: Tensile test results

Specimen	σ_Y (MPa)	ε_Y (%)	σ_{UTS} (MPa)	ε_{UTS} (%)	E (GPa)
Naturally cooled	137 ± 35.97	0.073 ± 0.003	434 ± 10.88	0.631 ± 0.001	137.97
Annealed	170 ± 52.54	0.110 ± 0.003	389.64 ± 59.33	0.518 ± 0.216	126.99
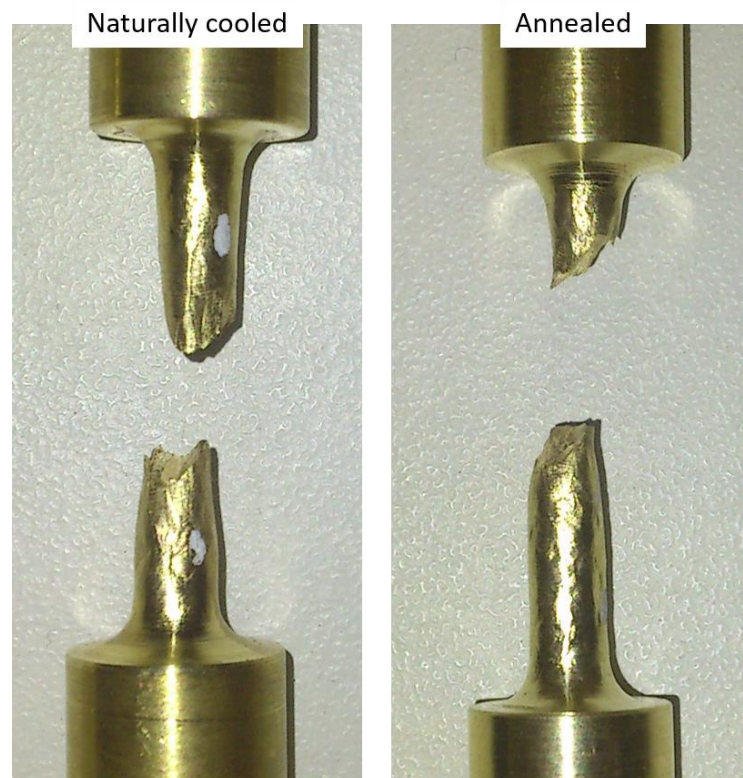
Figure 5- 13: Failure profiles of tensile specimens

According to Figure 5-11 and 5-12, it can be observed that the annealed specimens had a greater σ_y and ε_y than naturally cooled specimens. The annealing heat treatment allowed more α phase to grow and resulted in a softer material with a longer elastic process compare with the naturally cooled specimen [102]. Therefore, the annealed specimens yielded at 0.11% extension compare with the naturally cooled specimens yielding at 0.073%. On the contrary, this resulted in σ_{UTS} of the annealed specimens being lower than σ_{UTS} of the naturally cooled cast specimens. Moreover, naturally cooled specimens had a bigger elastic modulus value.

5.7 Comparison of mechanical properties generated by different testing methods

At this point, elastic modulus and hardness had been generated by nanoindentation, microindentation and macro tensile tests, and the comparison of these results are shown in Table 5-3 and 5-4.

Table 5- 3: Elastic modulus from different testing methods

Cu60Zn40	E nanoindentation (GPa)	E tensile testing (GPa)	Difference from nanoindentation
Brazed layer	118.59		
Naturally cooled cast		137.97	16.3%
Annealed cast		126.99	7.1%

Table 5- 4: Hardness from different testing methods

Cu60Zn40	H nanoindentation (GPa)	H microhardness (GPa)	Difference from nanoindentation
Brazed layer	1.76		
Naturally cooled cast		1.15	-34.7%
Annealed cast		1.08	-38.6%

The elastic modulus derived from macro casting specimens is generally higher than the modulus of the brazed layer, however this is maybe due to experimental accuracy. The modulus of the naturally cooled cast Cu60Zn40 is 16.3% higher than the brazed layer, while the annealed cast Cu60Zn40 is 7.1% higher than the brazed layer. This indicts with a heat treatment to let α phase grain grow further within the cast specimen, the modulus of cast piece could approach the modulus of the brazed layer.

The hardness measured from nanoindentation and microindentation show more significant differences. It appeared that Cu60Zn40 formed in the brazed layer was much harder than which in the casting specimens. Figure 5-6 showed that the brazed layer did have smaller grain sizes comparing with casting specimens. Furthermore, research has been done on this phenomenon by Qian et al. [107]. It was found that the nanoindentation hardness is about 10-30% in magnitude larger than the microhardness. The nanoindentation hardness of copper, stainless steel and nickel titanium-alloy all showed an obvious indentation size effect, which the hardness decreases with the increase of depth. Furthermore, should sink-in or piles up occurred during nanoindentation, the larger difference would occur between nano hardness and micro-hardness.

According to Qian et al. [107], the smaller indentation depth would derive a bigger hardness value. In this test approach, nano modulus and hardness were generated from the 200-500 nm range. The nano hardness can be significantly affected by the size effect and surface effect. Hence, nanoindentation hardness can be approximately used to imply the material's ability against deformation.

5.8   Summary of findings and discussions

The brazed SS316L-SS316L brazed joint with the Cu60Zn40 filler was assessed. A casting procedure was developed to create Cu60Zn40 raw materials with different cooling profiles for mechanical and thermal testing. Microstructural properties of filler materials derived from both brazing and casting were investigated and compared. The mechanical and thermal properties of the brazed layer and casting samples were generated and analysed.

Section 5.5 discussed the differences between the casting and brazing microstructures. The resultant cast sample had coarser grains and both α and β phases form dendrites. The random dendritic direction shows the heat conduction is uniform in different directions. The brazed sample had a different grain structure due to the faster cooling rate; most of the alloy formed into α phase but less β phase. As the heat was conducting from the brazed layer to stainless steel, the grains were elongated vertically. It could be observed that the Fe and Cr from the 316L diffused through the brazed layer and travelled into the Cu60Zn40 layer with a distance. However, the effect of this new phase on the material properties of the brazed layer could not be assessed. An EDS scan showed that elemental transfer from 316L to brass and from brass to 316L occurred within the diffusion layer. Fe and Cr were found to diffuse freely into the brass, whereas Cu and Zn could only be found in the diffusion layer on the 316L region. According to nanoindentation tests performed at the interface, the diffusion layer had a slightly higher elastic modulus than the parent material SS316L, while the hardness of the diffusion layer was significantly higher than both the SS316L and Cu60Zn40. There was also a complex microstructure and several alloy phases within this small diffusion zone, so a range of properties would be expected.

Referring to section 5.7, the elastic modulus derived from macro casting specimens are both higher than the modulus of the brazed layer. But the annealed cast Cu60Zn40 had a smaller difference comparing with the naturally cooled Cu60Zn40. This indicates that with a more extended heat treatment to let α phase grain grow further within the cast specimen, the modulus of the cast piece could approach the modulus of the brazed layer. This also agrees with the microstructure of the brazed layer, in which most of the alloy forms into the α phase with less β phase comparing with the casting sample. Therefore, the elastic modulus of the brazed layer outside of the diffusion zone can be predicted by macro mechanical testing with casting specimen.

In contrast, the hardness of the brazed layer measured from nanoindentation is over 30% higher than the hardness of both casting specimen measured by microindentation. As discussed in section 5.7, as the smaller indentation depth would derive a bigger hardness value, the nano hardness can be greatly affected by size effect and surface effect. Hence, nanoindentation hardness can be approximately used to imply the material's ability against deformation. This should be taken into consideration when using the data.

6   Conclusions and future work

Engineering designers in nuclear fusion communities are facing many challenges in the design and failure assessment of structures involving brazed joints because of the lack of universal acceptable assessment criteria/methodology. Common criteria cannot accurately predict the failure of brazed joints. It is different to identify the stress-strain of brazed joints, hence the yield and plasticity properties of the filler metal, which are the key properties relating to the development of residual stresses in dissimilar brazed joints.

The thin brazed layer with complex microstructures and unknown material properties in a brazed joint brings many challenges in the numerical studies of brazed joints. Material properties of the brazed layer are the heart of any procedures to assess the failure of brazed joints. The major objectives of this work are fabricating and assessing the dissimilar brazed joints with DEMO divertor candidate materials and generating material properties of the brazed layers in these joints.

As described in Chapter 1, the use of W using gold-based alloys for joining DEMO divertor components is a new approach. Chapter 2 discussed the design of brazing work and experimental methodology for characterising the brazed joints.

In order to generate the basic knowledge of these dissimilar brazed joints, this work aimed to develop acceptable brazing procedures in order to create sound and defects free brazed joints for testing. Metallurgical studies and nanoindentation tests were performed to understand the nature of these brazed joints. The brazed joints created with these alloys with different brazing techniques and assessment of these joints were reported in Chapter 3 and 4.

In order to build up the level of confidence of the properties generated by nanoindentation, Chapter 5 developed a casting procedure towards generating sub-sized test specimens in the 'as cast' condition to compare with the mechanical properties generated by nanoindentation in Chapter 3 and 4.

6.1   Summary and discussion of key findings

6.1.1   Au80Cu19Fe1 filler

Referring to Chapter 3, the AuCuFe filler was successfully used to fabricate brazed joint between W and the dissimilar materials considered for fusion application, EUROFER 97, Cu and SS316L, and create a uniform brazed layer. The interfacial metallurgy studies of four different material combinations can be summarised as follows:

•   The final formation of brazed layers has maintained the joint clearance and showed no reduction in thicknesses.

•   Parent materials showed no evidence of erosion under these brazing conditions.

•   No elemental transitions were detected between the W and the AuCuFe filler in either direction.

•   No W solid solutions or intermetallic compounds were found in the joint.

•   No evidence of oxidations was detected.

•   Transition regions between the AuCuFe filler to EUROFER97/316L showed similar elastic modulus and hardness to the braze filler.

•   A very smooth elemental transition was detected between the AuCuFe filler and Cu. This would indicate that the material properties were gradually changing from filler to Cu.

•   Due to the abrupt change of chemical compositions and material properties at the interface between the W and the AuCuFe, there are different degrees of diffusion existing at the interfaces between AuCuFe and Eurofer 97/SS316l/Cu, the W/AuCuFe interface is likely to be the most critical area in all the brazed joints created here. The maximum stress concentration under mechanical or thermal loadings should be at the free edge along with the W/AuCuFe interface.

6.1.2 Optimised vacuum furnace brazing and induction brazing development with Au80Fe20 filler

In order to accurately assess the performance of dissimilar joints, the misalignment of brazed joints must be considered. Therefore, the design objective of the induction brazing procedure in this work was to minimise the misalignment of butt brazed joints.

The optimised vacuum brazing procedure reported in section 4.3 had improved the quality of butt-type brazed joints created with updated Au80Cu20 filler as well as the alignment performance. By successfully developing an induction brazing procedure in section 4.4, good quality and well-aligned brazing specimens could be produced in low volume for characterisation testing.

It was be found in section 4.5 that the mechanical properties of W and Cu parent materials were not affected by different brazing methods. Whereas solidified filler material in induction brazed joint has a higher hardness than the filler. This was due to the increased Cu composition in the furnace brazed joint with the longer heating time in the process. The composition of Cu in the solidified furnace brazed layer was increased from 20% of Au80Cu20 filler to more than 30% due to diffusion from Cu parent material. Moreover, comparing with the results reported in section 3.5, in the W-AuCuFe-W joint where no diffusion between brazed layer and W, nanoindentation hardness measured at the solidified AuCuFe region was equivalated to the nanoindentation hardness of AuCu region in the induction brazed W-AuCu-Cu joint. This demonstrates that with a much shorter heating cycle, the element transition of Cu into AuCu filler during the induction brazing process was restricted in the diffusion region and did not go through the whole brazed layer.

In section 4.6, the different heating and cooling of the furnace and induction brazing resulted in different diffusion behaviours and thickness of the diffusion layers between Cu and Au80Cu20. The interfacial microstructural research utilizing the nanoindentation hardness measured in the W/Au80Cu20/Cu brazed joint identified

the interface between Au80Cu20 and Cu. Therefore, the thickness of the brazed layer could be identified, which was essential for FEA modelling this type of brazed joint.

6.1.3 Casting development towards generating mechanical properties of a brazed layer

The casting procedure reported in section 5.4 was developed to create Cu60Zn40 raw materials with different cooling profiles to be machined into specimens for mechanical and thermal testing. The experimental work focused on fabricating dissimilar brazed samples and casting samples with a relative economic binary brazing alloy Cu60Zn40. Induction brazed SS316L-SS316L brazed joint with the Cu60Zn40 filler was obtained for analysis. A detailed microstructural analysis of the Cu60Zn40 filler in the brazed joint and cast condition was reported in section 5.5.

In section 5.6, sub-sized tensile specimens machined from cast pieces were tested and analysed. The elastic modulus derived from macro casting specimens is higher than the modulus of the brazed layer. The elastic modulus of naturally cooled cast Cu60Zn40 was 16.3% higher than the brazed layer while the modulus annealed cast Cu60Zn40 is 7.1% higher than the brazed layer. This indicates that extended heat treatment would allow the α phase to grow further within the cast specimen, the modulus of the cast piece could approach the modulus of the brazed layer. This also agrees with the microstructure of the brazed layer, in which most of the alloy forms into the α phase with less β phase comparing with the casting sample. Therefore, the elastic modulus of the brazed layer outside of the diffusion zone can be predicted by macro mechanical testing with casting specimen.

In contrast, the hardness of the brazed layer measured from nanoindentation is over 30% higher than the hardness of both casting specimen measured by microindentation. As discussed in section 5.6, as the smaller indentation depth would derive a higher hardness value, the nano hardness can be greatly affected by size effect and surface effect. Hence, nanoindentation hardness can be

approximately used to imply the material's ability against deformation. This should be taken into consideration when using the data.

6.2   Future work

Although brazed joints had been successfully created with gold-based filler materials by both furnace and induction brazing process, the joint clearance has not been considered. The joint clearance has a strong influence on the capillary action, the joint strength and residual stresses in dissimilar brazed joints. The design of joint clearance considered at brazing temperature is worth to be approached to achieve better brazing quality. Further brazing practice needs to be done in order to develop the procedure to keep the consistency of microstructural properties of brazed joints.

In this work, the metallurgy study to assess the joint quality were performed on sectioned brazed joints. This method will result in a lack of information for the whole brazed joint. Non-destructive testing (NDT) is worth being a future lead in assessing the quality of an integrated brazed layer. At the time of this work, a trial was performed with a scanning acoustical microscope (SAM) to assess joint quality. This approach of NDT was still at a very early stage and having difficulties in getting reliable results.

With the setup of induction brazing procedure and apparatus designed in Chapter 4, full-sized brazed specimens for tensile, shear strength and fatigue testing can be fabricated in house. Further metrology method needs to be practised in order to better assess the misalignment of the brazed specimen.

The tensile tests require a further design for W-Cu brazed specimen. Figure 6-1 shows an early tensile testing trial of the WL10 rod. The specimen broke in the grip soon after the test started. During the tensile test, the grip applied increased gripping force along with axial loading and fractured the brittle WL10 alloy. Considering performing a tensile test on standard cylindrical W-Cu brazed specimen, even W doesn't break in the grip, the soft Cu would be pressed and deformed by the grip. This will very likely lead to an extra angular loading along with the axial loading and make the test invalid.

One possible solution is to design protecting sleeves for W and Cu in the test. The sleeve should be ductile to protect W from breaking by gripping force. The sleeve for Cu could be designed to be able to compensate for the deformation of Cu and eliminate angular loading. However, how to attached the sleeves with the parent materials is still a problem.

Figure 6- 1: WL10 rod broke in the grip at the initial stage

Referring to the brazed joint in Chapter 3 and 4, there are always some surface imperfections on the edge of brazed layers, such as recessed fillet and pooled filler material which creates stress concentrations and needs to be removed before mechanical testing. Some approaches have been made with slow grinding to remove

the imperfections by the author's colleague [11], and the results are shown in Figure 6-2.
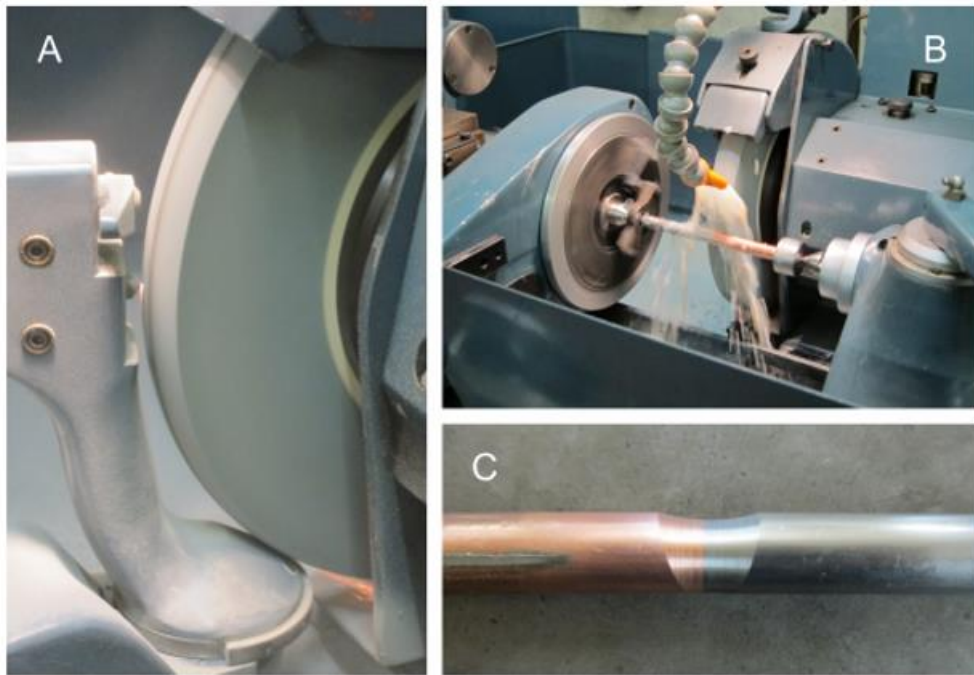
Figure 6- 2: A: Grinding wheel, B: Specimen during grinding, C: Final result, remade from [11]

The grinding wheel had a continuous 25.4mm radius curvature. The final results showed varying depth around the circumference due to the misalignment of the brazed specimen. Further experimental work needs to be developed to provide a solution to remove defects, imperfections and potential surface cracks of a brazed specimen by machining.

The work presented in this thesis has been focused on characterising the brazed layer at multi-scales. There is an opportunity to develop miniature mechanical testing specimens representing the brazed layer for material characterisation. The metallurgical knowledge and properties generate in this thesis can be used to further expand to other in situ testing such as micro cantilever testing.

Appendix

Appendix 1 – Top Platform Technical Drawing
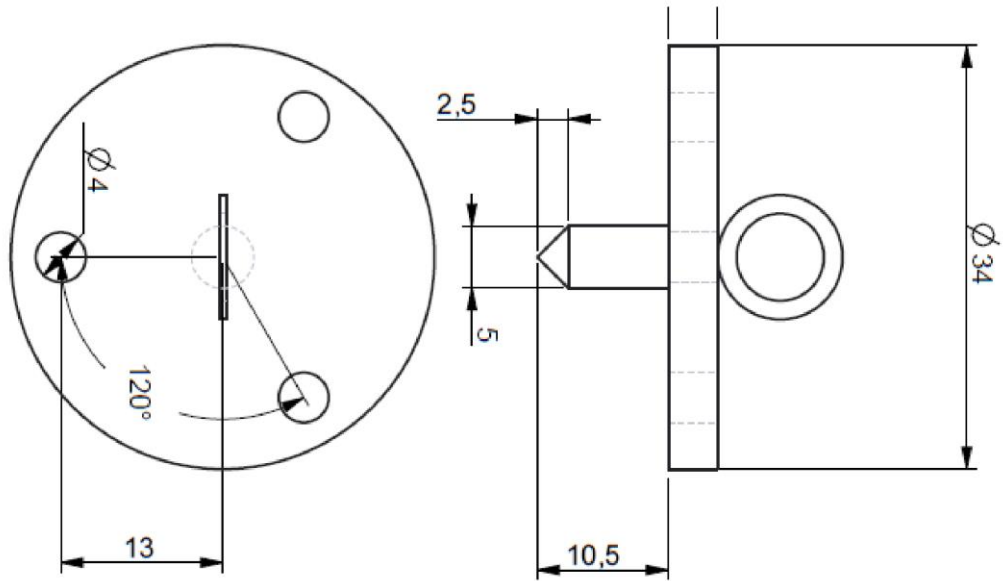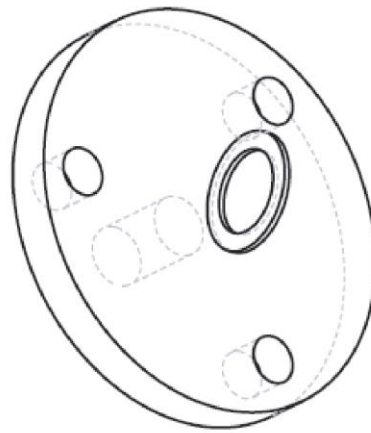
SCALE 2,000

Appendix 2 – Base Platform Technical Drawing
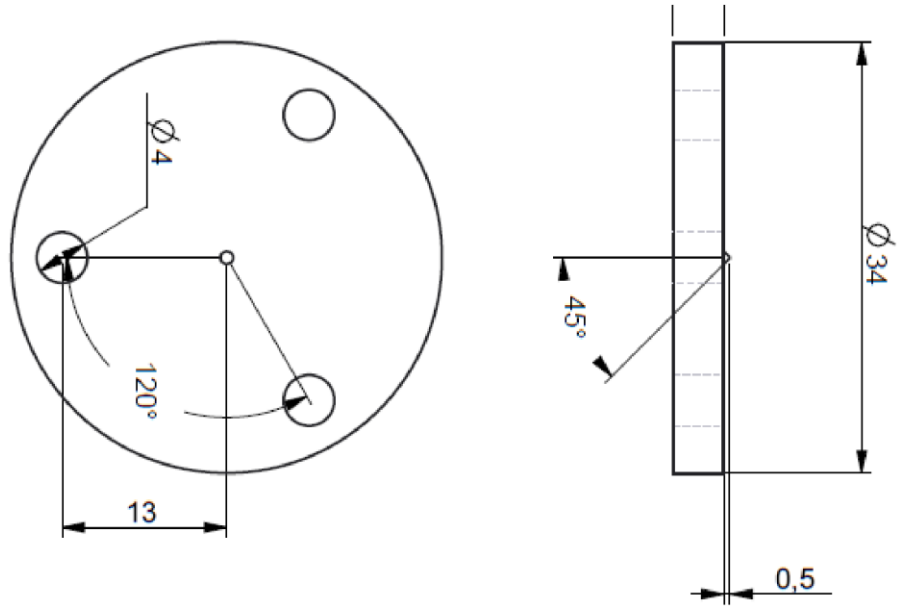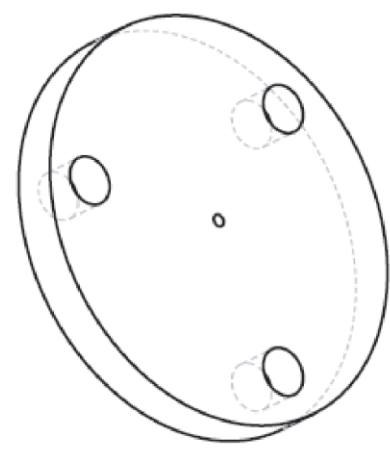
SCALE 2,000

Appendix 3 – Studding Technical Drawing
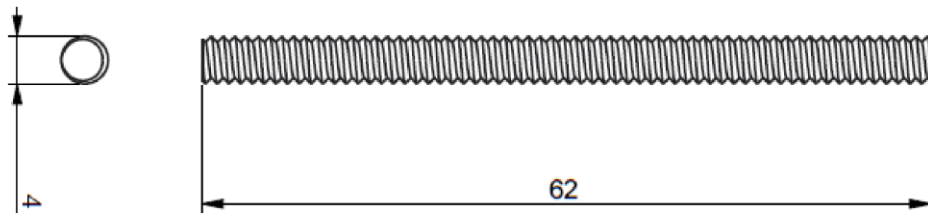
SCALE 2,000

Appendix 4 – Micro Tensile Bar Technical Drawing
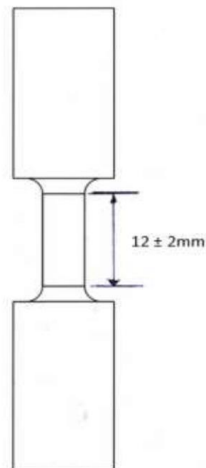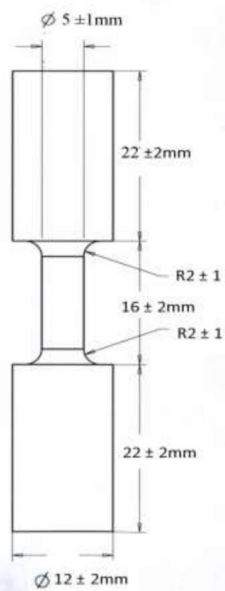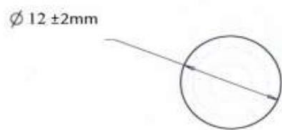
TITLE		
Round Tensile Bar Specimen		
SIZE	DRAWING NUMBER	REF
C	DRW_001	-
SCALE: 4:1		

References

[1]   L. R. Grisham, "Nuclear Fusion," in *Future Energy*, Elsevier, 2014, pp. 199–211.

[2]   R. L. Murray and K. E. Holbert, *Nuclear Energy*. Elsevier, 2015.

[3]   "ITER Website." www.iter.org.

[4]   C. Bachmann *et al.*, "Overview over DEMO design integration challenges and their impact on component design concepts," *Fusion Eng. Des.*, vol. 136, pp. 87–95, 2018, doi: https://doi.org/10.1016/j.fusengdes.2017.12.040.

[5]   M. Merola, F. Escourbiac, A. R. Raffray, P. Chappuis, T. Hirai, and S. Gicquel, "Engineering challenges and development of the ITER Blanket System and Divertor," *Fusion Eng. Des.*, vol. 96–97, pp. 34–41, 2015, doi: https://doi.org/10.1016/j.fusengdes.2015.06.045.

[6]   P. Norajitra *et al.*, "Divertor conceptual designs for a fusion power plant," *Fusion Eng. Des.*, vol. 83, no. 7–9, pp. 893–902, Dec. 2008, doi: 10.1016/j.fusengdes.2008.05.022.

[7]   M. Rieth *et al.*, "Recent progress in research on tungsten materials for nuclear fusion applications in Europe," *J. Nucl. Mater.*, vol. 432, no. 1–3, pp. 482–500, Jan. 2013, doi: 10.1016/j.jnucmat.2012.08.018.

[8]   D. Hancock, D. Homfray, M. Porton, I. Todd, and B. Wynne, "Refractory metals as structural materials for fusion high heat flux components," *J. Nucl. Mater.*, vol. 512, pp. 169–183, 2018, doi: https://doi.org/10.1016/j.jnucmat.2018.09.052.

[9]   D. Stork *et al.*, "Materials R&D for a timely DEMO: Key findings and recommendations of the EU Roadmap Materials Assessment Group," *Fusion Eng. Des.*, vol. 89, no. 7–8, pp. 1586–1594, Oct. 2014, doi: 10.1016/j.fusengdes.2013.11.007.

[10]   G. Federici *et al.*, "Overview of EU DEMO design and R&D activities," *Fusion*

Eng. Des., vol. 89, no. 7–8, pp. 882–889, Oct. 2014, doi: 10.1016/j.fusengdes.2014.01.070.

[11]   M. B. O. Robbie, "A Study of Joints between Dissimilar Materials with a View to Fatigue Performance in Fusion Reactor Applications," University of Strathclyde, 2016.

[12]   N. R. Hamilton, "Thesis - The development of residual stresses in, and thermal autofrettage of, dissimilar material brazed joints," University of Strathclyde - Department of Mechanical and Aerospace Engineering, 2013.

[13]   G. Kalinin *et al.*, "ITER R&D: Vacuum Vessel and In-vessel Components: Materials Development and Test," *Fusion Eng. Des.*, vol. 55, no. 2–3, pp. 231–246, Jul. 2001, doi: 10.1016/S0920-3796(01)00213-7.

[14]   T. Hirai *et al.*, "ITER tungsten divertor design development and qualification program," *Fusion Eng. Des.*, vol. 88, no. 9–10, pp. 1798–1801, Oct. 2013, doi: 10.1016/j.fusengdes.2013.05.010.

[15]   V. Barabash *et al.*, "Materials challenges for ITER – Current status and future activities," *J. Nucl. Mater.*, vol. 367–370, pp. 21–32, Aug. 2007, doi: 10.1016/j.jnucmat.2007.03.017.

[16]   M. Merola, W. Dänner, and M. Pick, "EU R&D on divertor components," *Fusion Eng. Des.*, vol. 75–79, pp. 325–331, Nov. 2005, doi: 10.1016/j.fusengdes.2005.06.139.

[17]   J. Reiser and M. Rieth, "Optimization and limitations of known DEMO divertor concepts," *Fusion Eng. Des.*, vol. 87, no. 5–6, pp. 718–721, Aug. 2012, doi: 10.1016/j.fusengdes.2012.02.010.

[18]   M. Rieth *et al.*, "Review on the EFDA programme on tungsten materials technology and science," *J. Nucl. Mater.*, vol. 417, no. 1–3, pp. 463–467, Oct. 2011, doi: 10.1016/j.jnucmat.2011.01.075.

[19]   M. Rieth *et al.*, "A brief summary of the progress on the EFDA tungsten materials program," *J. Nucl. Mater.*, vol. 442, no. 1–3, pp. S173–S180, Nov. 2013, doi: 10.1016/j.jnucmat.2013.03.062.

[20]   A. Li-Puma, M. Richou, P. Magaud, M. Missirlian, E. Visca, and V. P. Ridolfini, "Potential and limits of water cooled divertor concepts based on monoblock design as possible candidates for a DEMO reactor," *Fusion Eng. Des.*, vol. 88, no. 9–10, pp. 1836–1843, 2013, doi: 10.1016/j.fusengdes.2013.05.114.

[21]   D. Stork *et al.*, "Developing structural, high-heat flux and plasma facing materials for a near-term DEMO fusion power plant: The EU assessment," *J. Nucl. Mater.*, vol. 455, no. 1–3, pp. 277–291, 2014, doi: 10.1016/j.jnucmat.2014.06.014.

[22]   K. Ehrlich, "Materials research towards a fusion reactor," *Fusion Eng. Des.*, vol. 56–57, pp. 71–82, Oct. 2001, doi: 10.1016/S0920-3796(01)00236-8.

[23]   E. . Bloom, S. . Zinkle, and F. . Wiffen, "Materials to deliver the promise of fusion power – progress and challenges," *J. Nucl. Mater.*, vol. 329–333, no. 2004, pp. 12–19, Aug. 2004, doi: 10.1016/j.jnucmat.2004.04.141.

[24]   M. Merola *et al.*, "ITER plasma-facing components," *Fusion Eng. Des.*, vol. 85, no. 10–12, pp. 2312–2322, Dec. 2010, doi: 10.1016/j.fusengdes.2010.09.013.

[25]   P. Norajitra *et al.*, "Development of a helium-cooled divertor: Material choice and technological studies," *J. Nucl. Mater.*, vol. 367–370, pp. 1416–1421, Aug. 2007, doi: 10.1016/j.jnucmat.2007.04.027.

[26]   V. Widak and P. Norajitra, "Optimization of He-cooled divertor cooling fingers using a CAD-FEM method," *Fusion Eng. Des.*, vol. 84, no. 7–11, pp. 1973–1978, Jun. 2009, doi: 10.1016/j.fusengdes.2009.02.045.

[27]   P. Norajitra *et al.*, "Progress of He-cooled divertor development for DEMO," *Fusion Eng. Des.*, vol. 86, no. 9–11, pp. 1656–1659, Oct. 2011, doi: 10.1016/j.fusengdes.2010.12.005.

[28]   M. M. Schwartz, *Brazing, Second Edition*. 2003.

[29]   D. Jacobson and G. Humpston, *Principles of brazing*. 2005.

[30]   J. Yang, Y. Xu, S. Zhang, and M. Zhang, "Joining of Mn-Cu alloy and 430 stainless steel using Cu-based filler by SIMA-imitated brazing process," *Mater. Lett.*, vol. 253, pp. 401–404, 2019, doi: https://doi.org/10.1016/j.matlet.2019.06.098.

[31]   L. Shi, J. Yan, B. Peng, and Y. Han, "Deformation behavior of semi-solid Zn–Al alloy filler metal during compression," *Mater. Sci. Eng. A*, vol. 528, no. 22, pp. 7084–7092, 2011, doi: https://doi.org/10.1016/j.msea.2011.05.059.

[32]   D. Yapp, "Assessment of joining technology for a Demonstration Fusion Power Plant." EFDA Task Ref: WP11-DAS-MAT, 2012.

[33]   J. H. You *et al.*, "European divertor target concepts for DEMO: Design rationales and high heat flux performance," *Nucl. Mater. Energy*, vol. 16, pp. 1–11, 2018, doi: https://doi.org/10.1016/j.nme.2018.05.012.

[34]   ASM, *Welding brazing and soldering, ASM handbook*, vol. 6. 1993.

[35]   B. . Kalin, V. . Fedotov, O. . Sevrjukov, A. Moeslang, and M. Rohde, "Development of rapidly quenched brazing foils to join tungsten alloys with ferritic steel," *J. Nucl. Mater.*, vol. 329–333, pp. 1544–1548, Aug. 2004, doi: 10.1016/j.jnucmat.2004.04.170.

[36]   B. a. Kalin *et al.*, "Development of brazing foils to join monocrystalline tungsten alloys with ODS-EUROFER steel," *J. Nucl. Mater.*, vol. 367–370, pp. 1218–1222, Aug. 2007, doi: 10.1016/j.jnucmat.2007.03.222.

[37]   P. Norajitra *et al.*, "Current status of He-cooled divertor development for DEMO," *Fusion Eng. Des.*, vol. 84, no. 7–11, pp. 1429–1433, Jun. 2009, doi: 10.1016/j.fusengdes.2008.11.042.

[38]   C. J. Munez, M. A. Garrido, J. Rams, and A. Ureña, "Experimental study of W–Eurofer laser brazing for divertor application," *J. Nucl. Mater.*, vol. 418, no. 1–

3, pp. 239–248, Nov. 2011, doi: 10.1016/j.jnucmat.2011.07.008.

[39] J. de Prado, M. Roldán, M. Sánchez, V. Bonache, J. Rams, and A. Ureña, "Interfacial characterization by TEM and nanoindentation of W-Eurofer brazed joints for the first wall component of the DEMO fusion reactor," *Mater. Charact.*, vol. 142, pp. 162–169, 2018, doi: https://doi.org/10.1016/j.matchar.2018.05.035.

[40] J. de Prado *et al.*, "High heat flux performance of W-Eurofer brazed joints," *J. Nucl. Mater.*, vol. 499, pp. 225–232, 2018, doi: https://doi.org/10.1016/j.jnucmat.2017.10.054.

[41] D. Bachurina *et al.*, "Joining of tungsten with low-activation ferritic–martensitic steel and vanadium alloys for demo reactor," *Nucl. Mater. Energy*, vol. 15, pp. 135–142, 2018, doi: https://doi.org/10.1016/j.nme.2018.03.010.

[42] A. Forrest, RA and Tabasso, A and Danani, C and Jakhar, S and Shaw, "Handbook of activation data calculated using EASY-2007," *UKAEA FUS*, vol. 552, p. 399, 2009.

[43] R. A. Forrest, "The European Activation File: EAF-2007 biological, clearance and transport libraries," *UKAEA FUS*, vol. 538, 2007.

[44] *Alloy Phase Diagrams, ASM handbook Volume 3*. ASM International, 2004.

[45] H. Okamoto, D. J. Chakrabarti, D. E. Laughlin, and T. B. Massalski, "The Au–Cu (Gold-Copper) system," *J. Phase Equilibria*, vol. 8, no. 5, pp. 454–474, Oct. 1987, doi: 10.1007/BF02893155.

[46] T. Anraku, I. Sakaihara, T. Hoshikawa, and M. Taniwaki, "Phase Transitions and Thermal Expansion Behavior in AuCu Alloy," *Mater. Trans.*, vol. 50, no. 3, pp. 683–688, 2009, doi: 10.2320/matertrans.MER2008410.

[47] M. H. Sloboda, "Industrial Gold Brazing Alloys Their present and future usefulness," *Gold Bull.*, vol. 4, no. 1, 1971.

[48]   S. Hausner and B. Wielage, *Advances in Brazing*. 2013.

[49]   N. Eustathopoulos, M. . Nicholas, and B. Drevet, *Wettability at High Temperatures*. Pergamon , New York, 1999.

[50]   B. McGurran and M. . Nicholas, "A study of factors which affect wetting when brazing stainless steels to copper," *Brazing Solder.*, vol. 8, pp. 43–48, 1985.

[51]   O. Dezellus and N. Eustathopoulos, "Fundamental issues of reactive wetting by liquid metals," *J. Mater. Sci.*, vol. 45, no. 16, pp. 4256–4264, 2010.

[52]   N. Eustathopoulos, "Progress in understanding and modeling reactive wetting of metals on ceramics," *Curr. Opin. Solid State Mater. Sci.*, vol. 9, no. 4–5, pp. 152–160, Aug. 2005, doi: 10.1016/j.cossms.2006.04.004.

[53]   O. Kozlova, "Thesis - Brasage réactif Cu/acier inoxydable et Cu/alumina," Polytechnique Institute of Grenoble , France, 2008.

[54]   *Brazing Handbook, Fourth Edition*. American Welding Society, 1991.

[55]   *Brazing Handbook, 5th Edition*. American Welding Society, 2007.

[56]   P. Norajitra, S. Antusch, L. V. Boccaccini, M. Kuzmic, I. Maione, and L. Spatafora, "He-cooled demo divertor: Design verification testing against mechanical impact loads," *Fusion Eng. Des.*, vol. 87, no. 5–6, pp. 932–934, Aug. 2012, doi: 10.1016/j.fusengdes.2012.02.049.

[57]   N. R. Hamilton, J. Wood, A. Galloway, M. B. Olsson Robbie, and Y. Zhang, "The metallurgy, mechanics, modelling and assessment of dissimilar material brazed joints," *J. Nucl. Mater.*, vol. 432, no. 1–3, pp. 42–51, Jan. 2013, doi: 10.1016/j.jnucmat.2012.07.022.

[58]   N. R. Hamilton, J. Wood, D. Easton, M. B. O. Robbie, Y. Zhang, and A. Galloway, "Thermal autofrettage of dissimilar material brazed joints," *Mater. Des.*, vol. 67, pp. 405–412, Feb. 2015, doi: 10.1016/j.matdes.2014.11.019.

[59] Y. Flom, "Failure Assessment Diagram for Brazed 304 Stainless Steel Joints," *NASA/TM-2011-215876*, no. June, 2011.

[60] Y. Flom and L. Wang, "Flaw Tolerance in Lap Shear Brazed Joints, Part 1," *Weld. J.*, vol. 83, no. January, pp. 32–38, 2004.

[61] M. Koster, A. Lis, W. J. Lee, C. Kenel, and C. Leinenbach, "Influence of elastic-plastic base material properties on the fatigue and cyclic deformation behavior of brazed steel joints," *Int. J. Fatigue*, vol. 82, pp. 49–59, Jan. 2016, doi: 10.1016/j.ijfatigue.2015.07.029.

[62] M. E. Kassner, T. C. Kennedy, and K. K. Schrems, "The mechanism of ductile fracture in constrained thin silver films," *Acta Mater.*, vol. 46, no. 18, pp. 6445–6457, Nov. 1998, doi: 10.1016/S1359-6454(98)00299-7.

[63] C. Leinenbach, H.-J. Schindler, T. A. Başer, N. Rüttimann, and K. Wegener, "Quasistatic fracture behaviour and defect assessment of brazed soft martensitic stainless steel joints," *Eng. Fail. Anal.*, vol. 17, no. 3, pp. 672–682, Apr. 2010, doi: 10.1016/j.engfailanal.2009.05.002.

[64] B. Y. Y. Flom, L. E. N. Wang, M. M. Powell, M. a Soffa, and M. L. Rommel, "Evaluating Margins of Safety in Brazed Joints," *Weld. J.*, pp. 31–37, 2009.

[65] P. Dadras, J.-M. Ting, and M. L. Lake, "Brazing residual stresses in Glidcop-Al12Si Be," *J. Nucl. Mater.*, vol. 230, no. 2, pp. 164–172, Jun. 1996, doi: 10.1016/0022-3115(96)00021-9.

[66] A. Levy, A. Tobin, and G. Busch, "Residual stress analysis and microstructural observations of ceramic-to-metal brazed joints," in *Metal-Ceramic Joining*, 1991, pp. 133–151.

[67] A. Levy, "Thermal Residual Stresses in Ceramic-to-Metal Brazed Joints," *J. Am. Ceram. Soc.*, vol. 74, no. 9, pp. 2141–2147, 1991, doi: 10.1111/j.1151-2916.1991.tb08273.x.

[68] T. Chehtov, J. Aktaa, and O. Kraft, "Mechanical characterization and modeling of brazed EUROFER-tungsten-joints," *J. Nucl. Mater.*, vol. 367–370, pp. 1228–1232, Aug. 2007, doi: 10.1016/j.jnucmat.2007.03.224.

[69] N. R. Hamilton, M. O. Robbie, J. Wood, A. Galloway, I. Katramados, and J. Milnes, "The challenges in predicting the fatigue life of dissimilar brazed joints and initial finite element results for a tungsten to EUROFER97 steel brazed joint," *Fusion Eng. Des.*, vol. 86, no. 9–11, pp. 1642–1645, Oct. 2011, doi: 10.1016/j.fusengdes.2011.04.027.

[70] C. D. Hardie, "Thesis - Micro-Mechanics of Irradiated Fe-Cr Alloys for Fusion Reactors," University of Oxford - Department of Materials, 2013.

[71] N. M. Jennett, G. Aldrich-Smith, and A. S. Maxwell, "Validated measurement of Young's modulus, Poisson ratio, and thickness for thin coatings by combining instrumented nanoindentation and acoustical measurements," *J. Mater. Res.*, vol. 19, no. 1, pp. 143–148, Jan. 2004, doi: 10.1557/jmr.2004.19.1.143.

[72] C. Anthony, "The IBIS Handbook of Nanoindentation," Fischer-Cripps Laboratories, 2005.

[73] J. W. Davis and P. D. Smith, "ITER material properties handbook," *J. Nucl. Mater.*, vol. 233–237, no. Pt B, pp. 1593–1596, 1996, doi: 10.1016/S0022-3115(96)00202-4.

[74] Plansee, "Tungsten." https://www.plansee.com/en/materials/tungsten.html.

[75] Durbin Metals, "No Title." https://www.durbinmetals.co.uk/resources/data-sheets/view/Stainless-Steel-14404-316L-Bar-and-Section_39.

[76] Durbin metals, "No Title." https://www.durbinmetals.co.uk/resources/data-sheets/view/Copper-and-Copper-Alloys-CW004A-Sheet-Plate-and-Bar_32.

[77] K. Geels, *Metallographic and materialographic specimen preparation, light*

microscopy, image analysis, and hardness testing. 2007.

[78]   J. R. Vilella, *Metallographic technique for steel*. American Society for Metals, 1938.

[79]   L. E. Samuels, *Metallographic polishing by mechanical methods*. ASM International, 2003.

[80]   W. C. Oliver and G. M. Pharr, "Measurement of hardness and elastic modulus by instrumented indentation: Advances in understanding and refinements to methodology," *J. Mater. Res.*, vol. 19, no. 01, pp. 3–20, 2004.

[81]   A. C. Fischer-Cripps, *The IBIS Handbook of Nanoindentation*. Fischer-Cripps Laboratories Pty Ltd., 2010.

[82]   Bsi, *BS EN ISO 18279:2003 Brazing — Imperfections in brazed joints*, vol. 3. 2003.

[83]   Z. Lu, R. G. Faulkner, N. Riddle, F. D. Martino, and K. Yang, "Effect of heat treatment on microstructure and hardness of Eurofer 97, Eurofer ODS and T92 steels," *J. Nucl. Mater.*, vol. 386–388, pp. 445–448, Apr. 2009, doi: 10.1016/j.jnucmat.2008.12.152.

[84]   P. Fernández, A. . Lancha, J. Lapeña, and M. Hernández-Mayoral, "Metallurgical characterization of the reduced activation ferritic/martensitic steel Eurofer'97 on as-received condition," *Fusion Eng. Des.*, vol. 58–59, pp. 787–792, Nov. 2001, doi: 10.1016/S0920-3796(01)00563-4.

[85]   H. Hadraba, O. Němec, and I. Dlouhy, "Conversion of transgranular to intergranular fracture in NiCr steels," *Eng. Fract. Mech.*, vol. 75, no. 12, pp. 3677–3691, Aug. 2008, doi: 10.1016/j.engfracmech.2007.08.006.

[86]   ASM, *Metallography and Microstructures 2004 ASM*, vol. 9. 2004.

[87]   P. Norajitra *et al.*, "He-cooled divertor development for DEMO," *Fusion Eng. Des.*, vol. 82, no. 15–24, pp. 2740–2744, Oct. 2007, doi:

10.1016/j.fusengdes.2007.05.027.

[88] J. Reiser *et al.*, "Tungsten foil laminate for structural divertor applications – Joining of tungsten foils," *J. Nucl. Mater.*, vol. 436, no. 1–3, pp. 47–55, May 2013, doi: 10.1016/j.jnucmat.2013.01.295.

[89] T. Weber and J. Aktaa, "Numerical assessment of functionally graded tungsten/steel joints for divertor applications," *Fusion Eng. Des.*, vol. 86, no. 2–3, pp. 220–226, Mar. 2011, doi: 10.1016/j.fusengdes.2010.12.084.

[90] "BS EN 12797:2000 Brazing - Destructive tests of brazed joints." 2000.

[91] AWS C3.2M/C3.2:2008, "Standard Method for Evaluating the Strength of Brazed Joints," vol. 4Th. Editi. p. 29, 2008.

[92] B. 7910:2013+A1:2015, "Guide to methods for assessing the acceptability of flaws in metallic structures," no. 1. 2015.

[93] BS EN 12799:2000, "Brazing- Non-destructive examination of brazed joints," vol. 1. 2000, doi: 10.1017/CBO9781107415324.004.

[94] S. L. Semiatin and S. Zinn, "Coil design and fabrication : basic design and modifications," *Heat Treat.*, no. June, pp. 32–41, 1988.

[95] Johnson Matthey Metals Limited, "Induction brazing," *Brazing materials and applications data sheet 1100:143*. .

[96] S.-Y. Shih, S.-C. Nian, and M.-S. Huang, "Comparison between single- and multiple-zone induction heating of largely curved mold surfaces," *Int. Commun. Heat Mass Transf.*, vol. 75, pp. 24–35, Jul. 2016, doi: 10.1016/j.icheatmasstransfer.2016.03.020.

[97] Ambrell Precision Induction Heating, "About Induction Heating," 2008. http://pdfo.ambrell.com/411-0169-10.pdf (accessed May 12, 2016).

[98] E.-S. Yoon, J.-S. Lee, S.-T. Oh, and B.-K. Kim, "Microstructure and sintering

behavior of W–Cu nanocomposite powder produced by thermo-chemical process," *Int. J. Refract. Met. Hard Mater.*, vol. 20, no. 3, pp. 201–206, 2002, doi: https://doi.org/10.1016/S0263-4368(02)00003-3.

[99] K. Zangeneh-Madar, M. Amirjan, and N. Parvin, "Improvement of physical properties of Cu-infiltrated W compacts via electroless nickel plating of primary tungsten powder," *Surf. Coatings Technol.*, vol. 203, no. 16, pp. 2333–2336, 2009, doi: https://doi.org/10.1016/j.surfcoat.2009.02.055.

[100] D. Easton, Y. Zhang, J. Wood, A. Galloway, M. O. Robbie, and C. Hardie, "Brazing development and interfacial metallurgy study of tungsten and copper joints with eutectic gold copper brazing alloy," *Fusion Eng. Des.*, vol. 98–99, pp. 1956–1959, Oct. 2015, doi: 10.1016/j.fusengdes.2015.05.033.

[101] C. J. Huang *et al.*, "Microstructures and wear-corrosion performance of vacuum plasma sprayed and cold gas dynamic sprayed Muntz alloy coatings," *Surf. Coatings Technol.*, vol. 371, pp. 172–184, 2019, doi: https://doi.org/10.1016/j.surfcoat.2018.09.058.

[102] A. A. K. M.M.Haque, "Investigation on Structure and Properties of Brass Casting," *J. Mater. Sci. Technol.*, vol. 24, no. 03, p. 299, 2008, [Online]. Available: http://www.jmst.org/EN/abstract/article_8182.shtml.

[103] A. C. Reardon, *Metallurgy for the Non-Metallurgist*. ASM International, 1993.

[104] *Casting, ASM handbook*, vol. 15. ASM International, 2001.

[105] Weldability, "Product information Sifbronze No 101." https://www.weldability-sif.com/media/pdfs/info/RO101501.pdf.

[106] T. Specimens, "ASTM Designation: D1708-10 Standard Test Method for Tensile Properties of Plastics by Use of Microtensile pecimens," vol. i, pp. 1–5, 2010, doi: 10.1520/D1708-10.2.

[107] L. Qian, M. Li, Z. Zhou, H. Yang, and X. Shi, "Comparison of nano-indentation

hardness to microhardness," *Surf. Coatings Technol.*, vol. 195, no. 2, pp. 264–271, 2005, doi: https://doi.org/10.1016/j.surfcoat.2004.07.108.

Previous publications

N. R. Hamilton, J. Wood, A. Galloway, M.B. Olsson Robbie, **Y. Zhang**. The metallurgy, mechanics, modelling and assessment of dissimilar material brazed joints. Journal of Nuclear Materials. Volume 432. Issues 13. Pages 42-51. 2013.

Y. Zhang, A. Galloway, J. Wood, M.B. Olsson Robbie, D. Easton, W. Zhu. Interfacial metallurgy study of brazed joints between tungsten and fusion related materials for divertor design. Journal of Nuclear Materials. Volume 454. Issues 13. Pages 207-216. 2014.

J. Wood, N.R. Hamilton, D. Easton, M.B. Olsson Robbie, **Y. Zhang**, A. Galloway. Thermal Autofrettage of Dissimilar Material Brazed. Journal of Materials and Design. Volume 67. Pages 405-412. 2014.

D. Easton, **Y. Zhang**, J. Wood, A. Galloway, M.B. Olsson Robbie, C. Hardie, Brazing Development and Interfacial Metallurgy Study of Tungsten and Copper Joints with Eutectic Gold Copper Brazing Alloy. Fusion Engineering and Design. Volume 98-99. Pages 1956-1959. 2015.

N. R. Hamilton, J. Wood, D. Easton, M.B. Olsson Robbie, **Y. Zhang**, A. Galloway. Thermal autofrettage of dissimilar material brazed joints, Materials and Design. Volume 67. Pages 405-412. 2015

D. Easton, J. Wood, S. Rahimi, A. Galloway, **Y. Zhang**, C. Hardie, Residual stress generations in brazed tungsten dissimilar joints, IEEE Transactions on Plasma Science. 44, 9, p. 1-6 6 p. 2016